Faculty of Natural Sciences
Supervisor: Prof Tapas Kumar Chatterjee
Academic Year: 2017

A Systematic Evaluation of Fault Seal Integrity in the southern Pletmos Basin, offshore South Africa: A 3D Multidisciplinary Modelling Approach

SANELISIWE MHLAMBI

UNIVERSITY *of the*
WESTERN CAPE

THESIS PRESENTED TO THE DEPARTMENT OF EARTH SCIENCES

IN PARTIAL FULFILLMENT OF THE REQUIREMENTS

FOR THE DEGREE OF MASTER OF SCIENCE

IN PETROLEUM GEOLOGY

Declaration of Authorship

I, SANELISIWE MHLAMBI, declare that this thesis and the work presented in it are my own and have been generated by me as the result of my own original research.

A Systematic Evaluation of Fault Seal Integrity in the southern Pletmos Basin, offshore South Africa: A 3D Multidisciplinary Modelling Approach

I confirm that:

1. This work was done wholly or mainly while in candidature for a research degree at the University of the Western Cape;
2. Where I have consulted the published work of others, this is always clearly attributed;
3. Where I have quoted from the work of others, the source is always given. Except for such quotations, this thesis is entirely my own work;
4. I have acknowledged all main sources of help;
5. None of this work has been published before submission

Signed: ……

Date: ……

Acknowledgements

The journey towards the completion of this research has been equally exciting and difficult. Many have participated in this huge effort and I would like to acknowledge them for helping me in various ways to make this possible.

First, I am very grateful to my supervisor Prof Tapas Kumar Chatterjee for giving me the opportunity to perform this research, as well as for his guidance and support during this project. Also, I would like to express my gratitude to the Petroleum Agency of South Africa (PASA) for providing the data used in this study, and for their co-operation.

I would like to give a special note of appreciation to Fritz Agbor for his help and support during this research and for his motivation and words of encouragement during the difficult times. I would also like to give him my appreciation for providing an excellent atmosphere and for many insightful discussions. Those sleepless nights in the computer labs have finally paid off!

I also want to express my sincere and endless gratitude to my mother Maria Judith Mhlambi for putting up with not seeing me – her favourite daughter – for months on end whilst I have spent thousands of hours working on this project. Her love, massive help and encouragement in difficult times have tremendously helped towards the completion of this work. Also, deepest thanks to the rest of my family for their boundless affection and support throughout these years.

Last, but certainly not the least, I would like to thank the Almighty God, for everything that has been given to me in this life.

"Ngiyabonga"

"Although the precise role of faults has never been systematically defined, much has been written that touches on the subject. One thing is certain: we need not try to avoid them."

Frederick G. Clapp (1929)

Abstract

The syn-rift succession encompasses the primary exploration target in the southern Pletmos Basin. Several fault-bounded structural traps that contain gas accumulations have been discovered within this succession. Likewise, ubiquitous residual gas shows have been encountered in most drilled wells. Yet, the impact of faults on fluid flow is poorly understood. Therefore, this study aspires to predict, and where possible, quantify fault seal integrity and sealing capacities of some of the major prospect-bounding faults.

A multi-disciplinary research strategy was employed in order to fulfil the study objectives. Fault mapping and geo-cellular modelling using geostatistical algorithms were undertaken to provide the basic geometric and structural input for more advanced fault seal analysis applications. Juxtaposition analysis was carried out to identify zones with a high probability to seal (or leak) and as the first-order tool for predicting fault seal potential. Threshold pressures, hydrocarbon column heights, cross-fault permeability and transmissibility were used to estimate the sealing capacities of the faults. In addition to juxtaposition and customary fault-rock properties, the study also analysed parameters that can be deemed to be representative of cross-fault fluid flow (i.e. effective cross-fault permeability and transmissibility; ECFP and ECFT). Finally, modelling of the geo-history facilitated the validation of the properties that underpinned fault seal analysis studies.

The Ga-Q and proposed Ga-K prospects along with their main bounding faults formed the foci of the fault seal analysis results. The analysed faults showed excellent initial sealing potential due to either favourable juxtaposition or shale gouge development. Nonetheless, predicted hydrocarbon column heights and threshold pressures were low suggesting that the seal integrity of the analysed faults is predisposed to failure. In addition, high predicted fault permeability and transmissibility values signify the presence of open and permeable fracture networks within the fault zones. Thus, it is proposed that the faults are very likely to have leaked during hydrocarbon migration and filling of traps resulting in empty or under-filled hydrocarbon reservoirs.

Keywords: Geo-cellular modelling; Fault-seal analysis; Fault seal potential; Sealing capacities; juxtaposition; Shale gouge; threshold pressure; hydrocarbon column heights; seal integrity; transmissibility

Table of Contents

List of Figures

List of Tables

1

Introduction

1.1. BACKGROUND AND RATIONALE

The Pletmos Basin is situated on the southern continental shelf of South Africa (Fig 1-1). Because of its complex tectonic history, the basin is characterised by reservoir sequences that are dismembered by faults. Geologic faults can bring both risk and reward in prospect generation and reservoir development. A critical issue is whether these faults are baffles, barriers or conduits for fluid flow.

Hydrocarbon exploration within the Pletmos Basin began in the late 60s. This led to the discovery of gas and condensate accumulations and the establishment of proven petroleum systems (Brown *et al.*, 1996; McMillan *et al.*, 1997; Roux, 1997). The Ga-A gas field (Fig. 1-1) is the largest hydrocarbon field that has been discovered within the basin and has previously produced at commercial rates. Likewise, the highly probable presence of multiple source rocks makes this a potentially attractive basin. However, exploration interest in this area has waned of late as most targeted traps were found to be water-bearing. In addition, studies by Roux (1997) in the northern part of the Pletmos Basin revealed that syn-rift gas accumulations may be breaching their seals due to a recent major uplift.

Practically all the syn-rift traps in the study area have fault-dependent closures and are thus not only reliant on the overlying top seal for hydrocarbon retention but on the fault seal as well. The overlying drift-onset unconformity and Cretaceous marine mudstones are both laterally extensive and of sufficient capacity to make up the top seal. Hence, fault seal integrity constitutes a critical issue to exploration risk in the basin.

While there has been significant research carried out in the basin, no work has been done to quantify the effects of faulting on the primary reservoir interval. Accordingly, to evaluate

whether fault seal failure played a role in the failed exploration efforts and to minimize fault risk associated with hydrocarbon exploration in the Pletmos Basin, here an attempt has been made to evaluate, for the first time, the fault seal attributes of the major prospect-bounding faults within the basin. The results from the analyses can provide a predictive model for future exploration in this area as the ability to identify fault-dependent leak points is a fundamental tool for prospect assessment.

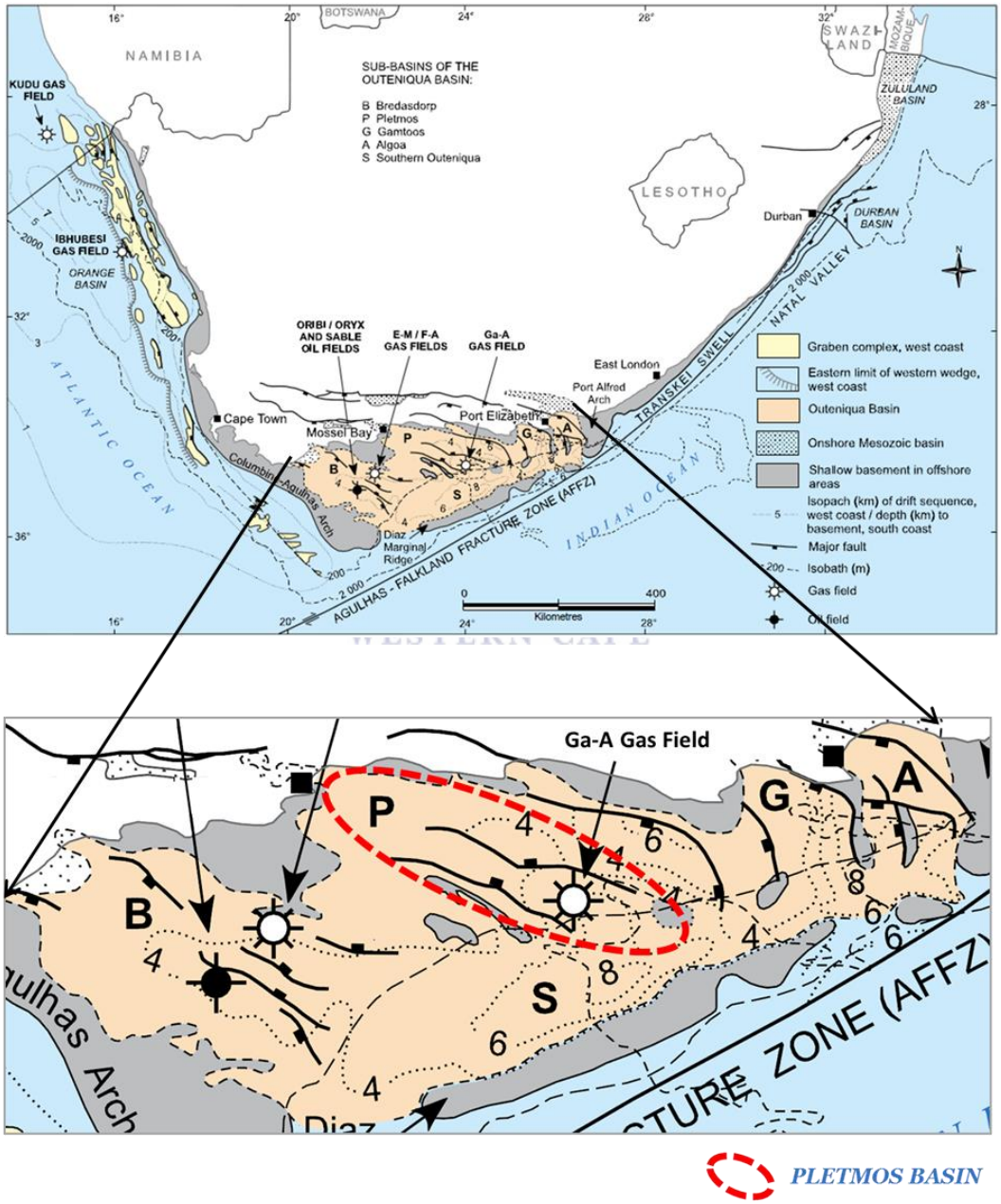

Figure 1-1: *The location of the Pletmos Basin and a close-up view. After Viljoen et al., 2010. The area of study comprises the southern Pletmos Basin and covers an area of approximately 1 025 km^2.*

1.2. STUDY OBJECTIVES

The prime objective of this thesis is to integrate seismic, well and core data in conjunction with structural geology and basin modelling techniques to predict and, where possible, quantify fault seal in the primary reservoir interval within the study area.

To narrow the aspects of the study that are investigated, the following research questions have been formulated;

1) What is the sealing nature of the prospect-bounding faults within the study area, i.e. are they baffles, barriers or conduits?
2) Did fault seal failure play a role in the failed exploration efforts within the study area?

Thus, the aims pursued to answer the research questions are to:

- Construct a detailed 3D geo-cellular model,
- Identify the potential leakage/seal points at reservoir juxtapositions and assign petrophysical properties along the faults,
- Obtain systematic relationships between the key parameters related to fault seal in the area, and from these make predictions regarding fault seal integrity and sealing capacities,
- Evaluate the effects of burial (temperature and stress) history on some of the key parameters controlling the sealing nature of the faults.

1.3. THESIS OUTLINE

The rest of this thesis is organised as follows. Chapter 2 begins with a brief review of the literature pertinent to the Pletmos Basin's structure and related basin geology, followed by a comprehensive review of literature concerning fault seal analysis. The data and the methods of investigation utilized in the study are explained in Chapter 3. Chapter 4 presents the results obtained from the data analyses, and the subsequent Chapter 5 discusses the principles, relationships and generalizations shown by the results. Finally, Chapter 6 discusses the theoretical implications of the study and possible applications and ends with a short summary regarding the significance of the work and any further work needed on the topic.

2

Literature Review

2.1. GEOLOGIC SETTING

2.1.1. Tectonics

2.1.1.1. The Outeniqua Basin

The Outeniqua Basin is a *circa.* 124 000 km^2 intra-cratonic rift basin which lies at the southernmost tip of Africa, where the plate margin experienced dextral shearing along the Agulhas Falkland Fracture Zone (AFFZ) (Fig. 2-1; Bate and Malan, 1992; McMillan *et al.*, 1997; Roux and Davids, 2009; Viljoen *et al.*, 2010); as opposed to elsewhere in southern Africa where the margins are generally extensional in style (McMillan *et al.*, 1997).

The Outeniqua Basin is believed to have formed because of extensional stresses before the commencement of Gondwana break-up in the Middle to Upper Jurassic (Fig. 2-1; McMillan *et al.*, 1997; Viljoen *et al.*, 2010), and extended onto what is identified today as the Falkland Plateau (Roux, 1997). Presently, sediments associated with rifting are confined in a series of rift sub-basins (Bredasdorp, Pletmos, Gamtoos, and Algoa) and their adjoining deep-water extension, the Southern Outeniqua (Fig 1-1; McMillan *et al.*, 1997; Roux, 1997). These sub-basins are separated by fault-bounded basement arches made up of the Ordovician Cape Supergroup, Cape Granite and Pre-Cambrian metamorphic rocks (van der Merwe and Fouché, 1992; McMillan *et al.*, 1997; Roux, 1997; Roux and Davids, 2009). Furthermore, the normal faults related to rifting are parallel to the compressional Permo-Triassic lineaments of the Cape Fold Belt (Roux, 1997). Whilst the fault systems commenced during the onset of basin-forming rifting around the time of Gondwana break-up, they maintained notable structural control during most of the basin's drift Cretaceous history (Brown *et al.*, 1996).

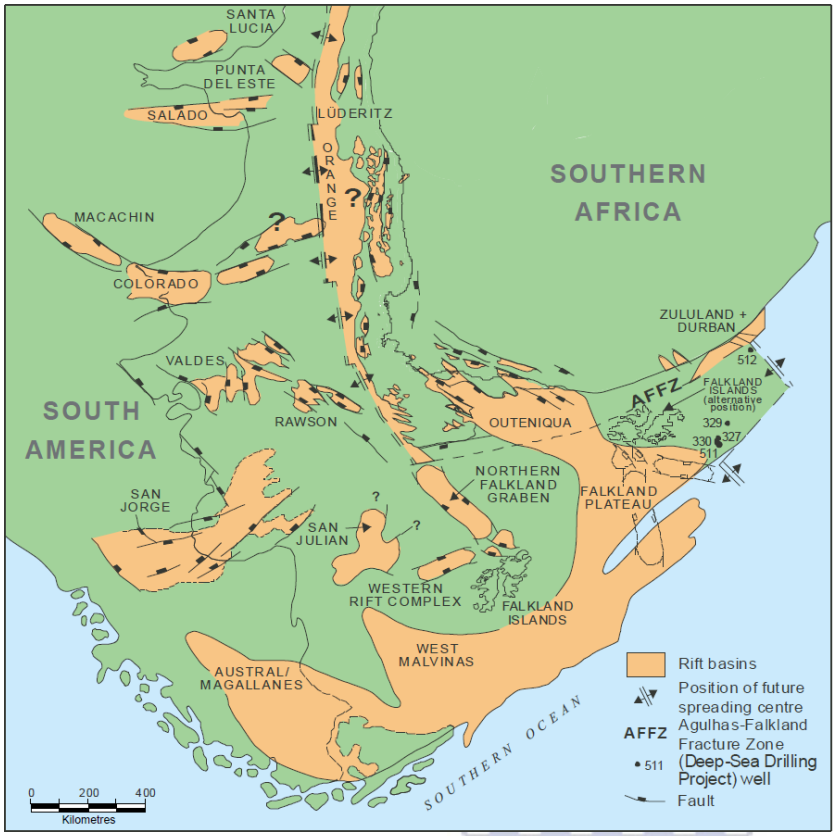

Figure 2-1: *The distribution of rift basins within southwest Gondwana before Gondwana separation (after Jungslager, 1999).*

2.1.1.2. The Pletmos Basin

The Pletmos Basin has an area of *circa.* 18 000 km^2 (Brown *et al.*, 1996; Broad *et al.*, 2006). It is delimited by the St Francis Arch to the East and by the Infanta Embayment to the West (Fig. 1-1) which form basement highs.

The basin is structurally complex, much more so than the other sub-basins of the Outeniqua Basin. The basin-bounding Superior Fault divides the basin into two major areas, and during the rift period markedly different sub-basins existed to the north and south of the fault (McMillan *et al.*, 1997). The other two major bounding faults, particularly the Pletmos Fault in the southwest, and the Plettenberg Fault in the northeast, define the limits of rift sedimentation (Fig. 2-2). McMillan *et al.* (1997) suggest that the maximum known displacement of the basement on the Plettenberg, Superior and Pletmos normal faults is roughly 5600 metres, 5000 metres and 2600 metres, respectively.

Furthermore, three stages of sedimentation are recognised in the Pletmos Basin: rift, transitional-early drift and late drift phases. The basin-wide unconformities Horizon D, 1At1 (drift-onset unconformity) and the mid Aptian 13At1 represent the onset of these episodes, respectively (McMillan et al, 1997).

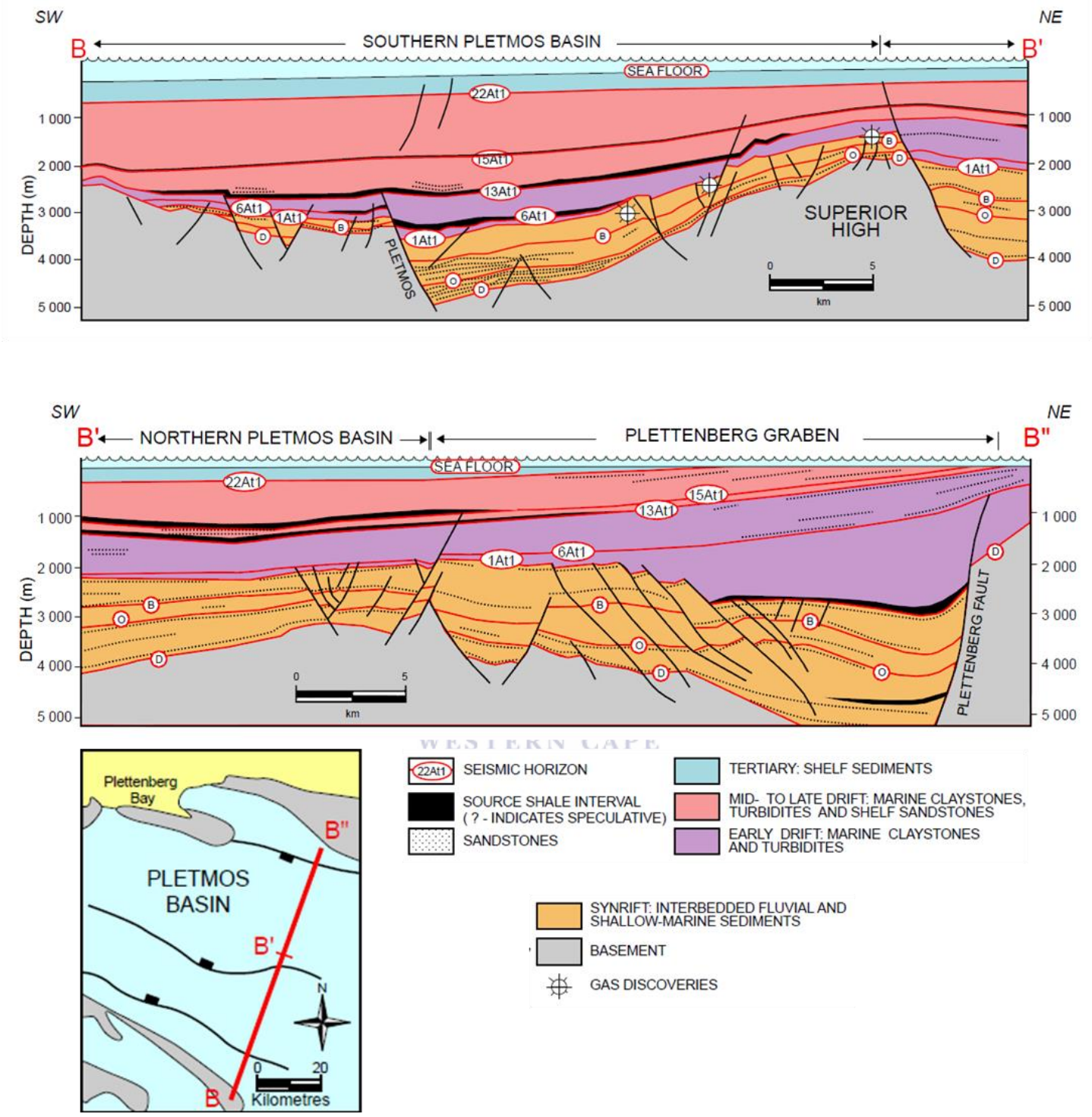

Figure 2-2: *Schematic section across the Pletmos Basin. Modified after Viljoen et al. (2010).*

The following sections will describe in detail the tectonic phases and depositional systems leading up to the present-day basin-fill configuration of the Pletmos Basin.

2.1.2. Stratigraphy and Basin Development

The sequence chrono-stratigraphy of the Pletmos Basin (Fig. 2-3) has been developed from that of Brown *et al.* (1996) and utilizes the geologic time scale of the International Union of Geographical Sciences (IUGS) of 2015.

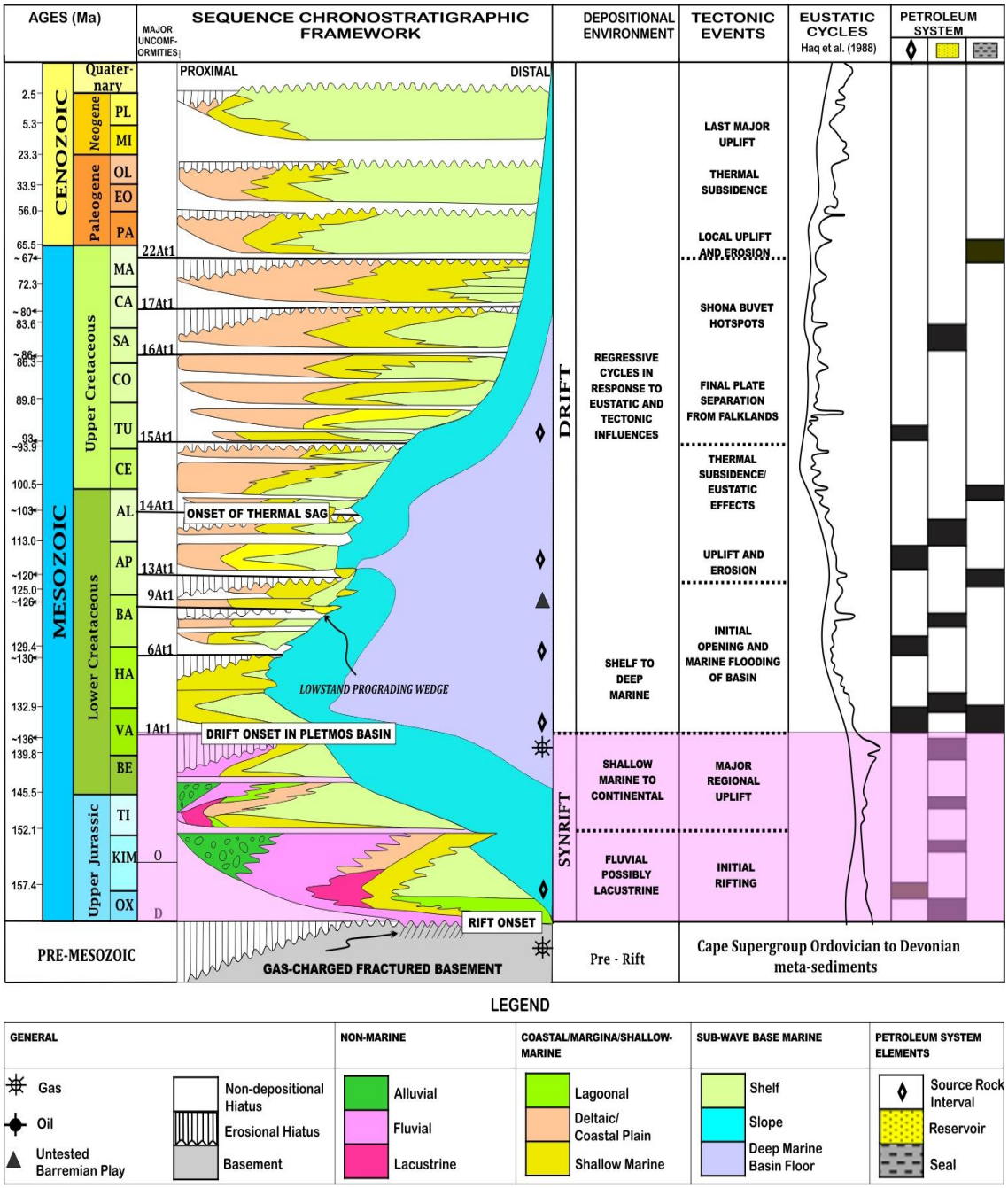

Figure 2-3: *Chronostratigraphic chart of the Pletmos Basin showing the major depositional and tectonic events in the basin and the prognosed petroleum system elements. Figure redrawn from Brown et al. (1996) and incorporates eustatic cycles by Haq et al. (1998). The modelled interval (D-1At1) is highlighted.*

The following sections discuss the Mesozoic sequence stratigraphy of the Pletmos Basin based on Fig 2-3, and define the tectonic phases and related depositional and erosional events during most of the basin's evolution.

2.1.2.1. Rift Tectonics and Syn-rift Sedimentation

It is widely accepted that the onset of rifting in the Pletmos Basin is linked to Gondwana break-up and began in the Middle to Upper Jurassic (Dingle *et al.*, 1983; Bate and Malan, 1992; van der Merwe and Fouché, 1992; McMillan *et al.*, 1997; Viljoen *et al.*, 2010). The resultant dextral trans-tensional stresses exerted north of the Agulhas Falkland Fracture Zone (AFFZ) (Fig 2-1) led to the initiation of the major North West to South East trending normal fault systems such as the Superior Fault (Fig. 2-2). The period of normal faulting and syn-rift deposition lasted until mid Valanginian (~136 Ma; Fig. 2-3) when extensional faulting generally ended. This terminated syn-rift deposition and introduced drift tectonics and deposition in the southern Pletmos Basin (McMillan *et al.*, 1997).

An extensive regional uplift event enhanced the subaerial erosion of the drift-onset unconformity (1At1) at ~136 Ma (Fig, 2-3), marking a major change in tectonic style from active rifting to thermal subsidence and drifting (Bate and Malan, 1992).

2.1.2.2. Post-rift Tectonics and Sedimentation

2.1.2.2.1. Transitional: 1At1 – 6At1 (136 – 130 Ma)

Following the onset of Post-rift tectonics in the basin, the first tectonic phase was characterized by significant but declining extensional stress, rapid but decreasing accommodation rates (subsidence), high sediment supply rates, aggradation grading upward into progradation, and increasing sporadic erosional impact of falling sea level, all ceasing in regional uplift and intense erosion of the late Hauterivian unconformity (6At1) at ~ 130 Ma (Brown *et al.*, 1996; Fig. 2-3). The main sediment depocentre was in the northern Pletmos Basin, where subsidence and some periodic uplift and erosion along the major rift faults continued to exert dominant tectonic control on sedimentation.

According to Brown *et al.* (1996) and McMillan *et al.* (1997), the present-day fault patterns of the rift lineaments and the irregularity thereof are indicative of strike slip movement along the AFFZ around 6At1 time. The consequential patterns created potential fault traps for hydrocarbons in the D-1At1 interval (McMillan *et al.*, 1997; Fig. 2-3). 6Atl symbolizes the

termination of large normal movement of the basin-bounding faults: Pletmos, Plettenberg and Superior, and ensuing strike-slip reactivation can be seen along the Superior Fault (McMillan *et al.*, 1997).

2.1.2.2.2. Early-drift: 6 At1 – 13 At1 (130 – 120 Ma)

The second tectonic phase was characterized by initial rapid subsidence and deposition. This was followed by declining rates of subsidence (accommodation space) probably due to renewed transpressional stress (Brown *et al.*, 1996), increased rates of sediment supply, cyclic progradation and aggradation, and cyclic increase followed by a reduction in the erosional impact of falling sea level, all coming to an end in regional uplift and intense erosion of the mid Aptian unconformity (13At1) at ~120 Ma (Fig. 2-3). During this time, depocentres were in the northern and southern Pletmos Basin (Fig. 2-2) and sedimentation occurred concurrently in each (McMillan *et al.*, 1997).

2.1.2.2.3. Late drift: Post 13 At1 (120 Ma – Present Day)

The Upper Cretaceous tectonic phases were primarily characterized by thermal subsidence with increasing extensional stress, declining sedimentation rates, long-term subsidence lasting about 10 million years following the divergence of the Falkland Plateau away from the African plate, progradation and aggradation, and moderate erosional impact of falling sea level, each episode terminated by a tectonically-enhanced erosional event (Brown *et al.*, 1996; McMillan *et al.*, 1997). Throughout this period, the Superior High had hardly any effect on sedimentation patterns (McMillan *et al.*, 1997).

The Cenozoic history of the basin is characterized by a degree of tilting, with the basin margins experiencing a major regional uplift at ~10 Ma (Davies, 1997). In the northern Pletmos Basin, based on geochemical analyses and petroleum systems modelling, this has been thought to have led to some gas accumulations breaching their fault seals (Roux and Davids, 2009).

2.1.3. Paleogeography and Depositional Systems

2.1.3.1. Syn-rift

D to 1Atl sediments (Fig. 2-3) are generally composed of inner to outer shelf sandstones and claystones with some fluvio-deltaic sediments north of the Superior Fault (e.g. Ga-H1 well location; Fig. A1). The variability in the lithologies reflects rapid changes in the environment of deposition during syn-rift times (McMillan *et al.*, 1997).

Thick late Oxfordian to Kimmeridgian-age sediments make up the early rift (Horizon D – O) basin-fill in the northern Pletmos Basin (Roux, 1997; McMillan *et al.*, 1997). In the southern Pletmos Basin, these sediments were deposited in a shallow marine environment ranging from inner shelf to transitional. Marine sedimentation became more argillaceous in the Late Kimmeridgian due to slight deepening of the basin (McMillan *et al.*, 1997). Directly overlying the early basin-fill are thick aggradational fluvial sediments. It is suggested by Roux (1997) that these sediments were directly sourced off the flanks of the basin and down the axes of the grabens, as can be seen in Fig. 2-4.

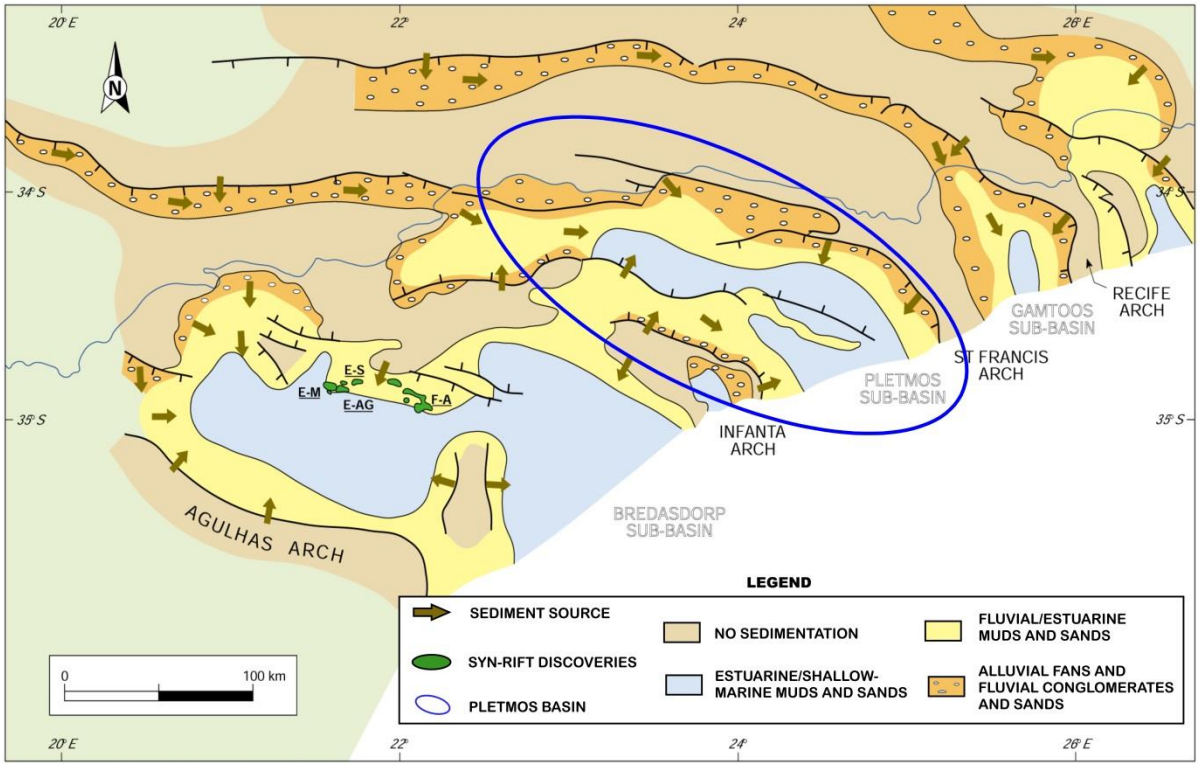

Figure 2-4: *Late Jurassic – Early Cretaceous (D-1At1) Paleogeography. After IHS Basin Monitor (2010).*

The Horizon O to 1At1 (late syn-rift) interval consists of fluvial, shallow marine, and shelf deposits of Kimmeridgian to Valanginian age. Marginal marine and tidally-influenced sandstones were best developed during this time with thicknesses and petrophysical properties (porosities and permeabilities) attaining a maximum in this interval (McMillan *et al.*, 1997). These sandstones are generally fine-grained and with varying amounts of argillaceous matrix, and are interbedded with claystones and siltstones. The amount of sand contained in the whole syn-rift sequence increases towards the Superior Graben (southern Pletmos) in a south-westerly direction (Roux, 1997) away from the sand-starved northern Pletmos Basin.

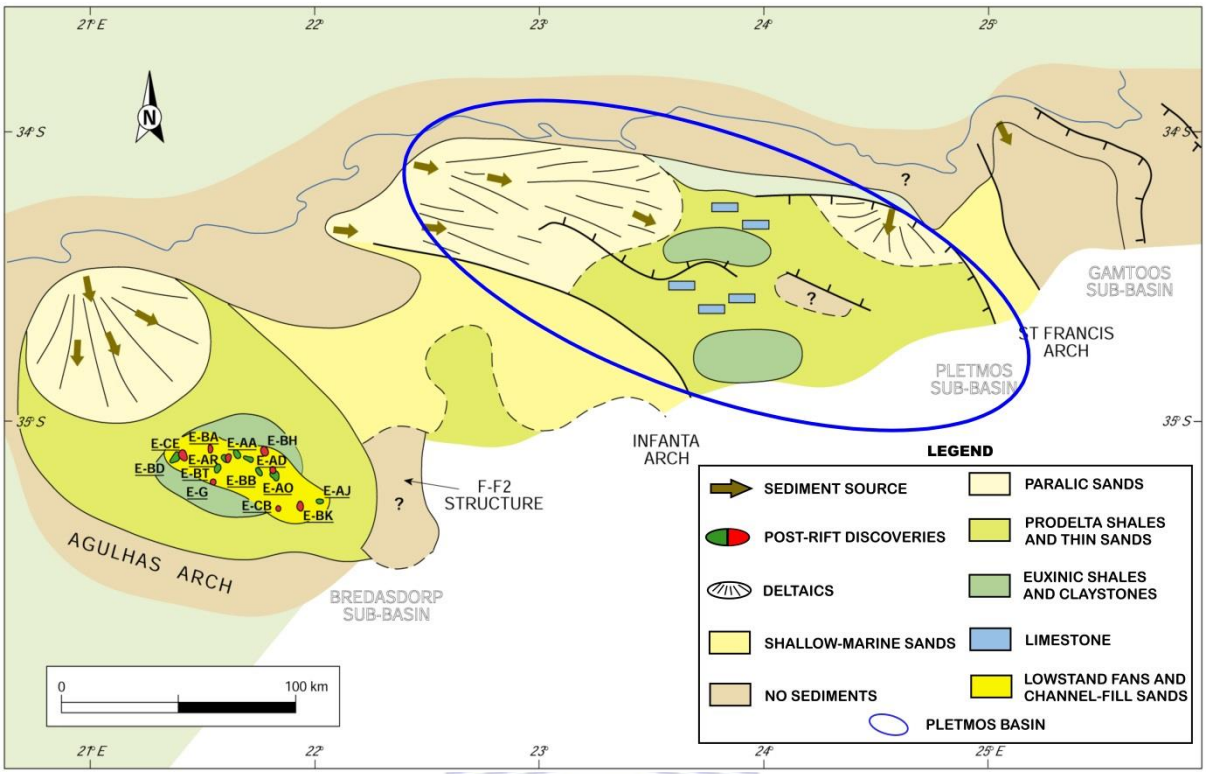

Figure 2-5: *Late Barremian – Early Aptian Paleogeography. After IHS Basin Monitor (2010).*

2.1.3.2. Post-rift

The onset of thermal subsidence at the mid Valanginian unconformity (1At1) resulted in deposition in mainly deep marine, poorly-oxygenated environments (McMillan *et al.*, 1997; Roux and Davids, 2009). The markedly deeper environment reflected by these sediments was due to abrupt subsidence of the basin (McMillan *et al.*, 1997). During the 1At1 and 6At1 transitional period, deep marine claystones and thin-bedded turbidites of late Valanginian to Hauterivian age were deposited (Roux, 1997). This marks depositional systems that were restricted and dominantly fan-deltaic (Brown *et al.*, 1996). However, the pre-6At1 and parts of the upper pre-1At1 sequences were severely eroded in the central and southern Pletmos Basin due to substantial uplift at 6Atl times. The most developed successions are consequently found along the northern margin of the Pletmos Basin (McMillan *et al.*, 1997).

The late Hauterivian to early Aptian (6At1 – 13At 1) period was characterized by high energy shelfal progradation from the northern margin of the basin (Fig. 2-5). Sediments deposited during this time comprise interbedded shelf sandstones and claystones (Roux and Davids, 2009). As suggested by Brown *et al.* (1996) depositional systems dominant during this period

were river- or tide-dominated embayment systems. The tectonic events leading up to the intense erosion of 13At1 are believed to have resulted in a period of relative sand starvation in most parts of the basin during this period. Post-13At1 to about 67 Ma, depositional systems evolved to open marine wave- and river-dominated systems (Brown *et al.*, 1996).

2.1.4. Key Petroleum System Elements

It has been documented that exploration wells drilled in the southern Pletmos Basin intersected gas accumulations within syn-rift sediments (Roux, 1997), particularly in the Ga-A gas field (Fig 1-1; Fig. 2-6). Summarized here are the key geologic elements of the existing syn-rift reservoirs in addition to petroleum system elements that are crucial to understanding fluid flow in the primary reservoirs. Figure 2-6 is a schematic map of the fault-dependent traps in the basin.

2.1.4.1. Reservoir Rocks

Thick late Jurassic marginal-marine and shelf sandstones that are generally interbedded, fine-grained, well-sorted with average porosities of about 10-24% provide good reservoirs in some places. Their fair to good permeabilities constitute economically significant reservoir facies that were formed during early to late Valanginian periods (IHS Basin Monitor, 2010). They were sourced from the basin flanks and down the south-easterly graben axes, and deposited in early depocentre areas (Roux, 1997). They attained maximum thicknesses of ~100m, with porosities that can be as high as 25% and permeabilities that range between ~10 and 100mD mainly in the Superior High area (Maier, 1990; Bate and Malan, 1992; Brink *et al.*, 1994).

2.1.4.2. Charge

Davies (1997) provided a detailed description of the source and reservoir components of the Bredasdorp Basin. In assuming a more regional approach, he proposed that the petroleum systems of all the south coast basins be named the ‘Outeniqua Petroleum System’. Thermal maturity modelling suggests that hydrocarbon generation in the Outeniqua Basin peaked at around Upper Cretaceous times (~80Ma) (Davies, 1997). Correlations of source-specific and maturation-dependent indicators in hydrocarbon samples with those of their presumed source rocks indicate two phases of charge (Davies, 1997; Roux and Davids, 2009); primarily in the Palaeocene (~60 – 50Ma) and the Late Plio-Pleistocene (0 – 10Ma).

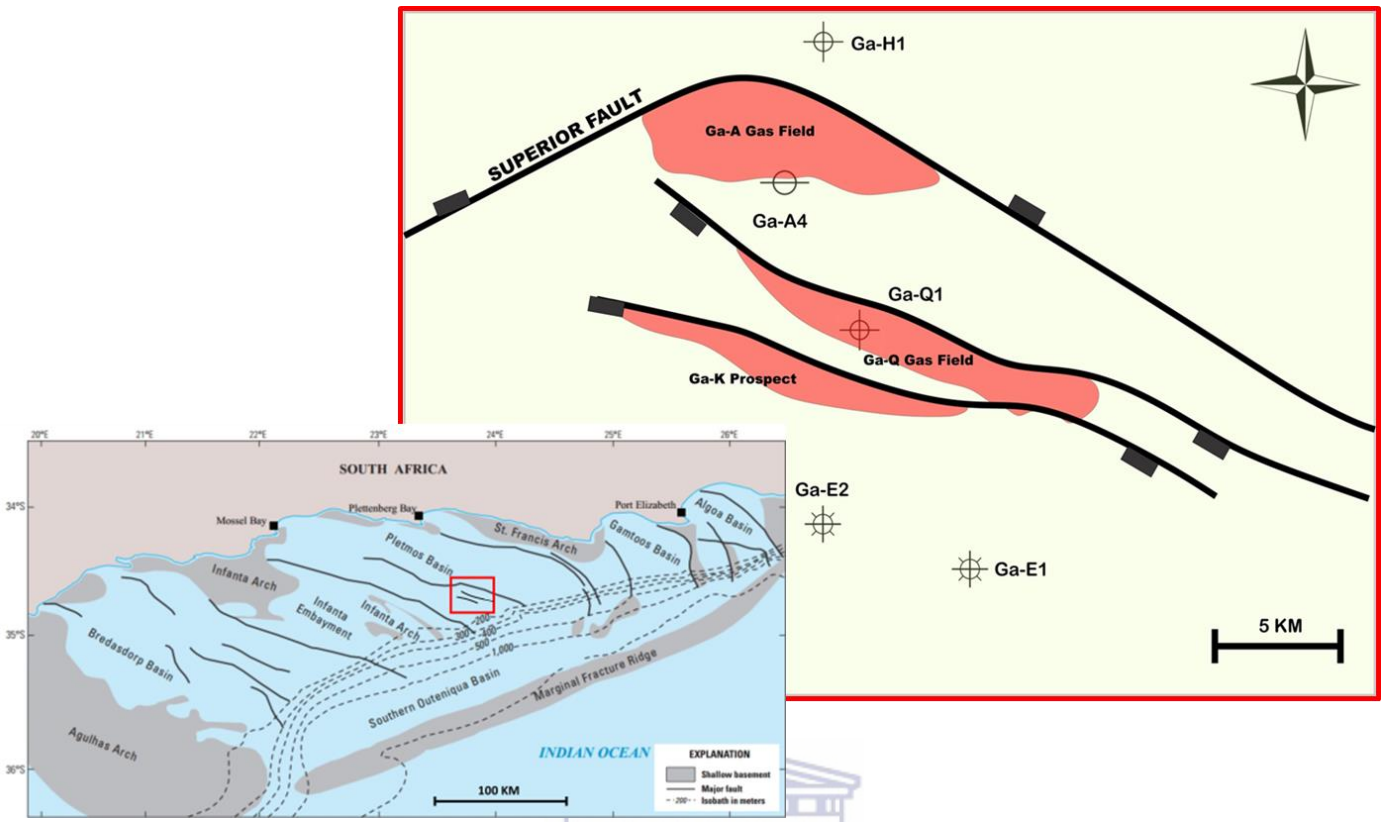

Figure 2-6: *Schematic diagram showing the previously producing fields in the southern Pletmos Basin. The proposed Ga-K prospect (Roux, 1997) is also shown. Figure redrawn from that of Roux (1997). Map insert after Brownfield (2016).*

2.2. FAULT-SEAL ANALYSIS – AN OVERVIEW

Having discussed the geological context in the previous sections, the following sections provide a comprehensive review of literature regarding fault seal analysis.

A seal can be defined as a low-permeable to impermeable rock or immobile fluid, such as tar, with a capillary entry pressure great enough to obstruct fluid flow or trap hydrocarbons. Typical seals include bottom, top, lateral and fault (Fig. 2-7). For purposes of this study, the following discussion only focuses on fault seal.

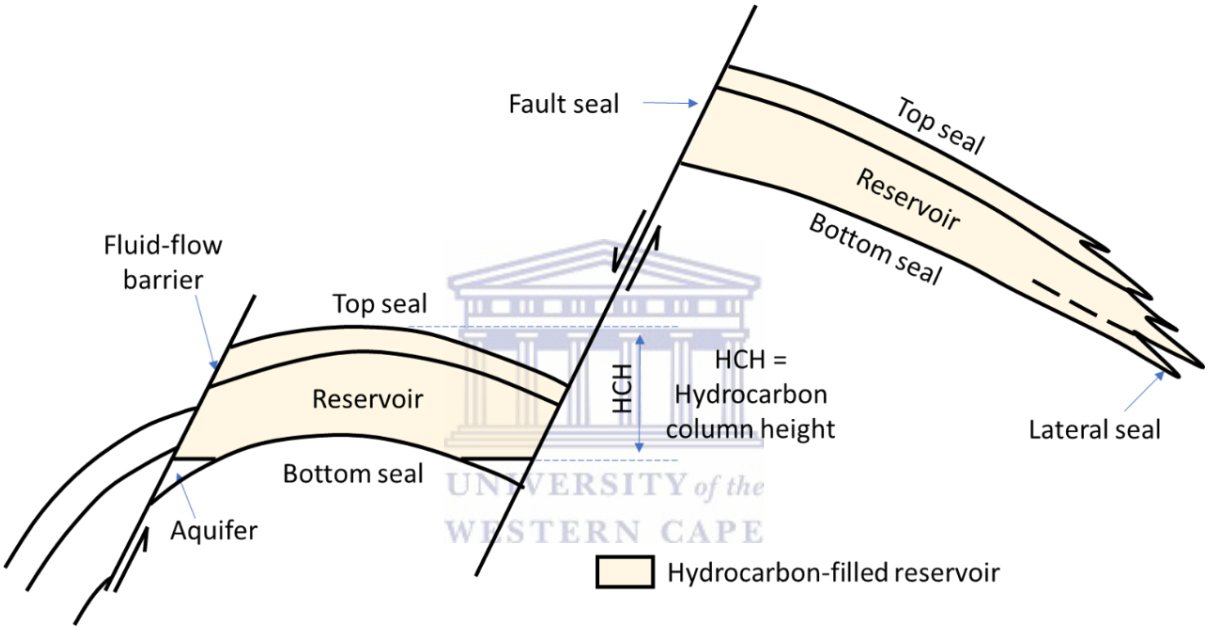

Fig. 2-7: Some typical seals; HCH is the hydrocarbon-column height that the weakest seal will hold. Modified after Sneider *et al.*, 1997.

Within sedimentary basins, faults play a central role in hydrocarbon entrapment and migration. Faults can be conduits, baffles or retarders (barriers) for fluid flow. Thus, in assessing fault-bound prospects, fault seal potential is an important risk to consider (Allan, 1989; Bouvier *et al.*, 1989). Fault seal risk is difficult to evaluate and is often associated with great uncertainty. Hence, in the last three decades there has been significant research and debate within literature regarding the controls of fault seal integrity (Allan, 1989; Bouvier *et al.*, 1989; Knipe *et al.*, 1997; Fisher and Knipe., 1998; etc.). The key research disciplines relevant to the assessment of fault seal integrity in the southern Pletmos Basin are discussed below.

2.2.1. Classification of Fault-Seal

While there has not been a global consensus reached on the fault seal classifications, two types of fault seals have already been documented: juxtaposition seals and fault rock seals (Knipe, 1992a; Knott, 1993; Knipe *et al.*, 1997; Cerveny *et al.*, 2004).

2.2.1.1. Juxtaposition Seals

The occurrence of this class of fault seal is due to the relative movement between the hanging wall and the footwall of the faults. This may lead to juxtaposition between stratigraphic units with completely different lithologies and/or petrophysical properties, as suggested by Allan (1989). Figure 2-8 presents the three principal cases that may result from the lithology contact relations along a fault.

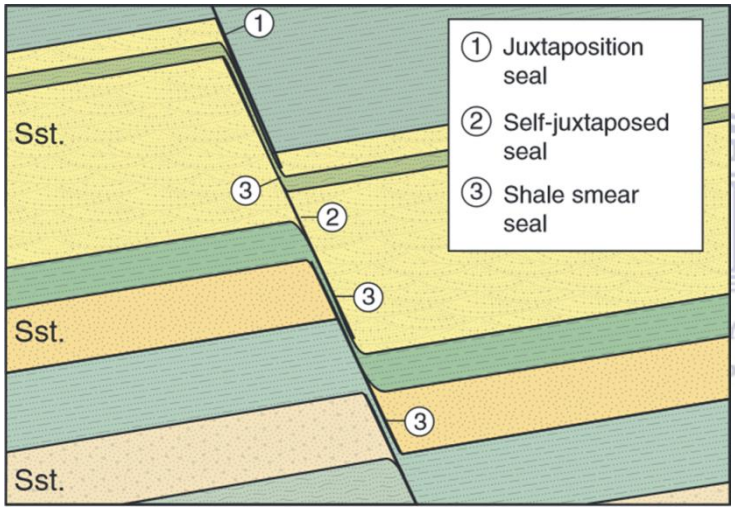

Figure 2-8: *Seal types that may arise from juxtaposition of different stratigraphic units along a fault. After Fossen (2010).*

The term 'juxtaposition seal' most accurately describes cases where permeable sandstone units are completely juxtaposed against impermeable shale causing a retardation of cross-fault fluid flow regardless of the fault-rock properties (Fossen, 2010; 1 in Fig. 2-8). This class of fault seal is often assessed by means of creating fault plane cross-sections that depict the reservoir sands on both sides of the fault (also called Allan maps; Allan, 1989).

Furthermore, Knipe (1997) proposed an updated technique in which juxtaposition as a function of lithology and offset can be visualized, i.e. the triangle juxtaposition diagrams. By making use of these diagrams, one can make an initial judgement and prediction of fault-seal properties at any point along the fault plane, particularly when looking for possible leak zones.

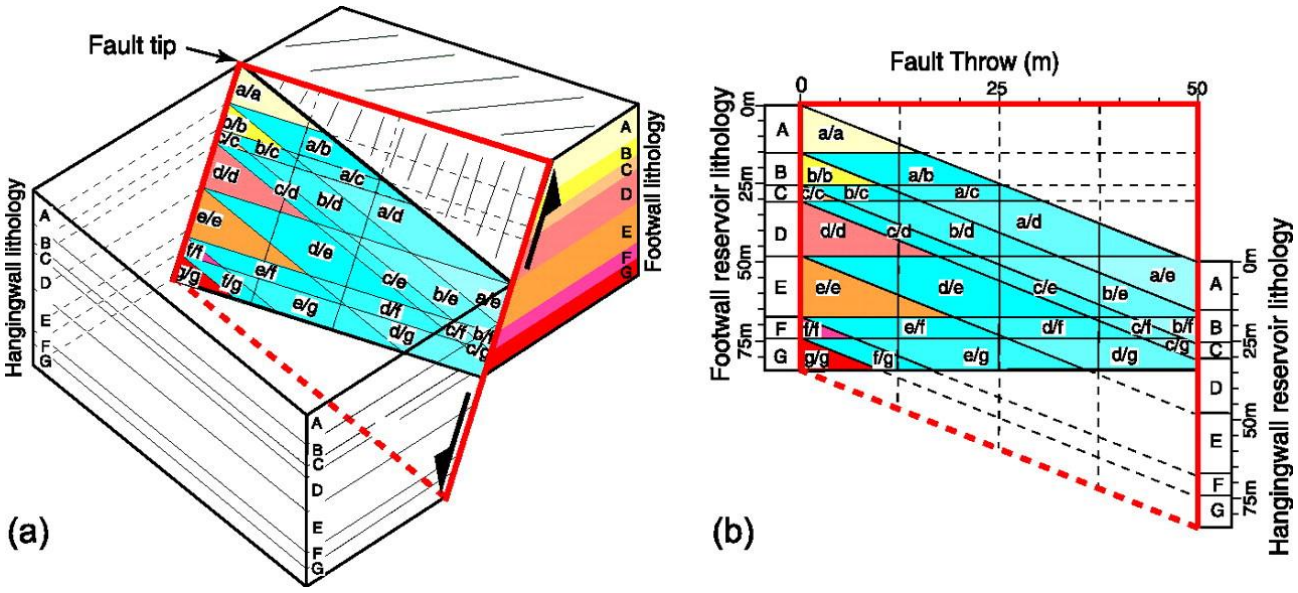

Figure 2-9: *The concept of creating a triangle juxtaposition diagram.* ***a)*** *Block diagram displaying upthrown beds as horizontal layers and downthrown beds as diagonal. The synthetic fault is indicated by the red trapezoidal shape. The synthetic fault plane is illustrated in* ***b)****. Adapted from Porter et al. (2000).*

Figure 2-9 is a schematic diagram denoting the occurrence of the juxtaposition seals along a synthetic fault. As per example, the first three lithologies: A, B and C in Fig. 2-9 are mudstone, sandstone and mudstone, respectively. If the hanging wall moves downward relative to the foot wall, the different units from the two sides will juxtapose against each other. For example, if the mudstone layer (A) of the hanging wall juxtaposes against the sandstone layer (B) of the footwall (a/b), a juxtaposition seal (1 in Fig. 2-8) occurs; If B of the hanging wall juxtaposes against B of the footwall (b/b), either a self-juxtaposed seal or shale smear seal (2 and 3 in Fig. 2-8) occurs as sandstones possess higher permeabilities and lower capillary entry pressures than mudstones (Porter et al., 2000).

2.2.1.2. Fault-Rock Seals

Notwithstanding, other lithological contact relationships along a fault may result in varying fluid flow effects in porous reservoirs. For example, where sand is juxtaposed against sand with no shale smear between sand layers (2 in Fig. 2-8), the fault transmissibility is entirely controlled by the physical properties of the fault zone (e.g. amount of shale smear along fault, fault zone thickness and the deformation mechanisms of the fault rock) (Fossen, 2010). Conversely, where two different sand layers that are stratigraphically intercalated with shale layers are juxtaposed, the shale layers may smear out to form a continuous membrane (3 in Fig.

2-8). In such cases faults may still seal hydrocarbons despite the absence of juxtaposition seal. In these circumstances, it is the fault itself that provides an effective seal (Lindsay et al, 1993; Knipe, 1997; Yielding *et al.*, 1997).

Studies such as Yielding *et al.* (1997) and Bretan *et al.* (2003) have demonstrated that with faulting within mixed sand and shale siliciclastic successions, there is usually a relationship between the seal capacity and clay content. Depending on the clay content and the continuity of the smears, multiple predictive algorithms for determining the seal potential of a fault have been proposed (Lindsay *et al.*, 1993; Yielding *et al.*, 1997; Pei et al., 2015; Fig. 2-10). Where there is a single shale layer and a single fault, the shale smear factor (SSF) is the ratio of the fault throw to the shale layer thickness (Lindsay *et al.*, 1993; Fig. 2-10(a)). Where there is a likelihood of clay mixing due to the presence of more than one source of clay or shale, the combined contributions must be considered. This is known as the Shale Gouge Ratio (SGR) (Yielding *et al.*, 1997; Fig. 2-10(b)). Estimation of the Clay Smear Potential (Fig. 2-10(c)) is the third method of characterizing clay smear. It is related to how far a continuous shale layer can be smeared before it breaks (Bouvier *et al.*, 1989; Fulljames *et al.*, 1997).

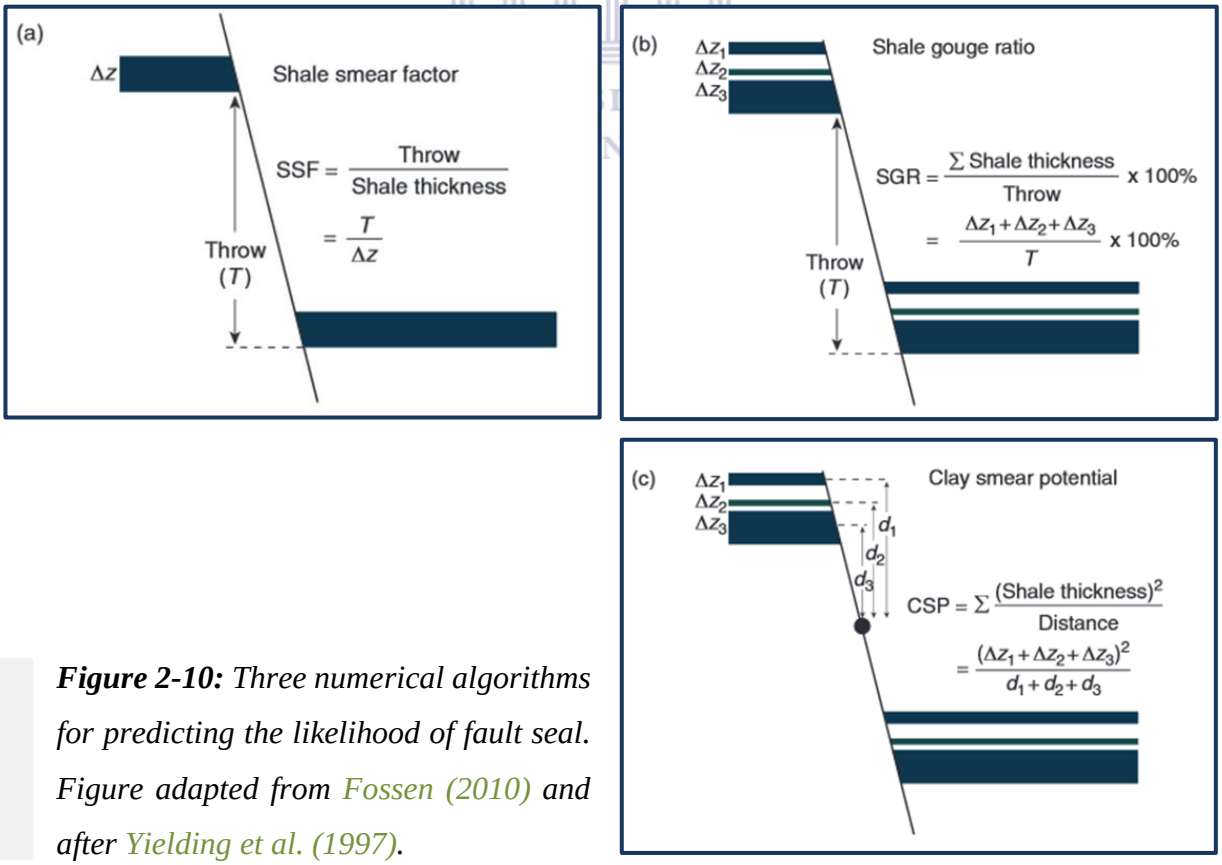

Figure 2-10: *Three numerical algorithms for predicting the likelihood of fault seal. Figure adapted from Fossen (2010) and after Yielding et al. (1997).*

The abovementioned algorithms are often calibrated against across-fault pressure data based on laboratory measurements (Sperrevik *et al.*, 2002) or otherwise on known hydrocarbon column heights (i.e. the vertical measure of the reservoir or trap containing hydrocarbons) (Bretan *et al.*, 2003). Bretan *et al.* (2003) calibrated SGR values against pressure data for a global dataset of fault-related traps. The relationships derived have been used to compute the capillary entry pressure of a fault zone (FZP) for a given SGR value by the equation;

$$FZP\ (bar) = 10^{(\frac{SGR}{27} - C)}$$

Where; C=0.5 for burial depths less than 3km, C=0.25 for burial depths between 3 and 3.5km and C=0 for burial depths greater than 3.5km.

Capillary leakage across a fault takes place when the buoyancy pressure of the hydrocarbon column exceeds the minimum FZP (Bretan *et al.*, 2003). This allows the computation of the maximum buoyancy pressure that can be sustained by a fault before the occurrence of capillary leakage (i.e. threshold pressure). Thus, the most crucial fault property in fault seal analysis is the capillary threshold pressure of the fault rock which is controlled by the size of the pore throat (Yielding *et al.* 1997; Ottesen Ellevset *et al.* (1998); Manzocchi *et al.* 2010). The smaller the pore throat, the higher the capillary threshold pressure required before migration into a fault zone will occur and the greater the fluid column that can potentially be supported by a given fault-related trap before leakage (Bretan *et al.*, 2003). Generally, the strongest seal has threshold pressures greater than 1373 psi (>94 bar) and can hold hydrocarbon columns greater than 1500m, assuming that the fluid is 35^0 API oil and saline water. On the other hand, the weakest seals have threshold pressures ranging between 69 – 137 psi (≥4.75 to <30 bar) and can hold oil columns between 15 and 30m (Beaumont and Foster, 1999).

2.2.2. The Effects of Burial (Temperature/Stress) History

The interplay between temperature and stress (confining pressure) history can lead to fault rocks with dissimilar physical properties (Fisher and Knipe, 2001), even when generated from host rocks with identical clay contents. Therefore, it is imperative to account for the temperature and stress history of the fault rock in addition to the clay content when analysing fault-seal properties (Pei et al., 2015). Knipe (1992b) suggests that the variation of petrophysical properties, fault seal mechanisms and resultant sealing behaviour, depends not only on the processes described above, but on the geo-history as well (Ottesen Ellevset *et al.*, 1998; Fig. 2-11).

2.2.2.1. Temperature History

Notably, high SGR values may not necessarily correlate to high fault seal potential. Similarly, self-juxtaposed sands with low SGR may still seal because of other fault-rock properties. For example, at great burial depths (>3km), the fault rocks may be subject to in-situ quartz cementation, cataclasis and enhanced pressure solution (Fig. 2-11) which have excellent seal potential (Walderhaug, 1996). The rate of quartz cementation increases as a function of temperature (Fisher and Knipe, 2001; Fisher *et al.*, 2009) and becomes rapid at temperatures above ~90 ^{0}C.

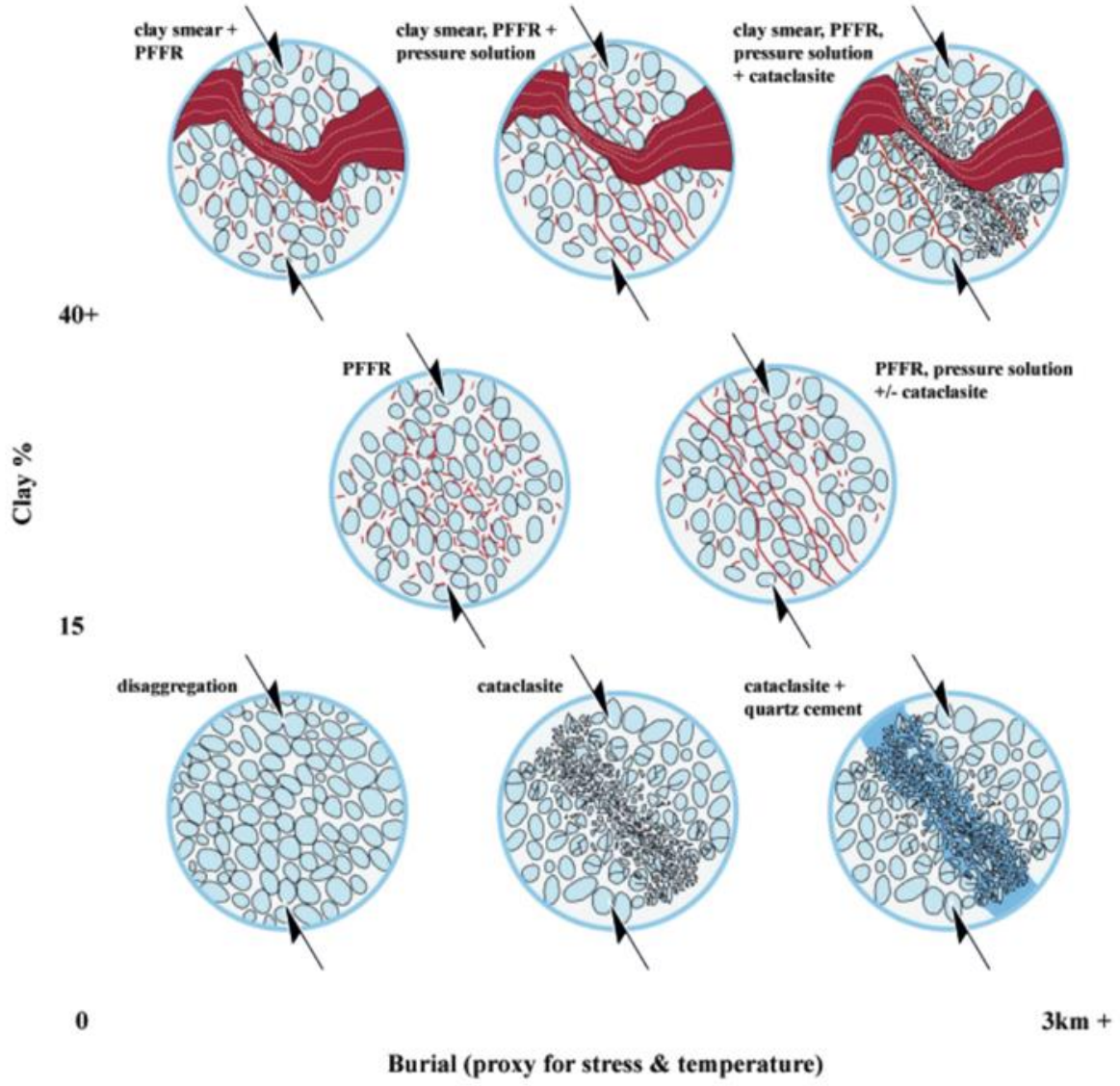

Figure 2-11: *Tentative illustration of how the different fault rock types relate to clay/phyllosilicate content and depth (representative of the temperature and confining pressure). After Jolley et al. (2007).*

2.2.2.2. *Stress History*

Experimental studies such as Handin *et al.* (1963) and Scott and Nielson (1991) attempted to identify the effects of vertical stress (confining pressure) on the behaviour of faults in sandstones. They put forward that at low confining pressures, sandstones tend to deform by brittle faulting, whereas at high confining pressures they tend to experience ductile deformation. Further, studies such as Crawford (1998) and Fisher and Knipe (2001) stipulate that the permeability and grain size of fault rocks within fault zones tend to decrease with increasing temperature and stress.

On the other hand, studies such as Wiprut and Zoback (2000) in the North Sea and Castillo *et al.* (2002) in the Timor Sea have revealed that changes in the stress field can cause weakening of the fault-seal integrity resulting in underfilled or completely breached hydrocarbon traps. These studies have also shown that fault-seal integrity is strongly influenced by the state of stress resolved on the reservoir-bounding faults. Thus, if a fault is critically stressed with reference to the present-day stress field, it is highly probable that the fault will slip, by that means recreating fault zone permeability that permits leakage of hydrocarbons. Leakage could be sporadic depending on the degree and rate of fracture healing, and on the recurrence rate between reactivated slip events (Castillo *et al.*, 2002).

3

Methodology

The overall purpose of this study was to formulate an understanding of fault seal integrity in the southern Pletmos Basin using different modelling strategies. The specific research questions were formulated in the first chapter. These are restated:

1) What is the sealing nature of the prospect-bounding faults within the study area, i.e. are they baffles, barriers or conduits?

2) Did fault seal failure play a role in the failed exploration efforts within the study area?

This chapter describes the data used in this study. It also outlines the methodology in a systematic manner and deploys the data analysis procedures that were decided to be most suitable for addressing the formulated research questions. Not only does it present the practical aspect of geo-cellular modelling and fault seal analysis, but it also discusses the theoretical fundamentals.

3.1. DATA COLLECTION AND PREPARATION

The main datasets utilized in this study were provided by the Petroleum Agency South Africa (PASA) and comprised the following:

- 3D seismic data spanning some area of 1 025 square kilometres acquired in 2000.
- Well data (Table A1). Five wells were chosen for this study. These are: Ga-H1, Ga-A4, Ga-Q1, Ga-E1 and GA-E2. The locations of these wells are shown in Figure 2-6. These wells were chosen because of their locations in potential fault compartments and they comprised comprehensive log suites including: Gamma Ray (GR), Neutron (NPHI), Density (RHOB), Sonic (DT), and Resistivity (ILD, LLS, LLD, and MSFL).
- Checkshot Data.
- Temperature Data - Static Borehole Temperatures (SBHT).

- Conventional core analysis results were used to gather petrophysical data which included core porosity, core permeability-air and core permeability-Klinkenberg. Other petrophysical data were derived from well log data and will be explained in the following sections. Note that core data was only available for two wells (Ga-E2 and Ga-Q1).
- Well reports were used to gather and evaluate general information about the wells.

It is worth noting that the Ga-Q1 well, was chosen for its favourable position between two of the major prospect-bounding faults (herein named Fault F1 and F2) within the study area. The well is located 2km and 1km from F1 and F2, respectively (Fig. 2-6) and was drilled to test structural closure on the southern downthrown side of Fault F2. Expected hydrocarbons were gas and condensate with a reasonable possibility for oil. However, this was never actualized. Thus, using it as the control well for fault seal analysis would allow testing whether the analysis would correctly replicate the poor result, to understand why the well failed to meet expectations and if failure can be attributed to fault seal.

3.2. DATA PROCESSING AND INTERPRETATION

3.2.1. Petrophysical Interpretation and Evaluation

Composite well log data from five wells were interpreted. Well log correlations (Fig. A2 and Fig. A3) were created and aided in determining the direction of thickness, establishing the lateral continuity of lithological units and in visually assessing the structural configuration. The basic analysis procedure used in this study involved the following steps, whose descriptions are provided below;

3.2.1.1. GR-derived Volume of Shale (VSh) Calculation

The VSh log was processed from the GR log using the following equation;

$$Vsh = \frac{GR - GRmin}{GRmax - GRmin}$$

Where; GR = Gamma Ray log, GRmin and GRmax were established at the minimum and maximum GR value, respectively and were determined by visual inspection.

3.2.1.2. Lithology and Rock Type Determination

The descriptions of conventional core found in the well reports for the selected wells served as a guide to aid in interpretation of the lithofacies. Three key facies were interpreted on the two

logs believed to represent depositional heterogeneity (GR and VSh). Three facies were deemed acceptable for the reservoir interval as modelling more facies types would result in an unwieldy model.

A discrete facies log was created for one of the wells and supervised neural networks were used to automatically determine the lithofacies classifications based on the combinations of the log responses. The supervised neural network is trained with interpreted data and therefore uses pattern recognition to carry out the interpretation (Anggraini and Puspa, 2008). The resultant facies interpretation for some of the wells is shown in Figure 3-1.

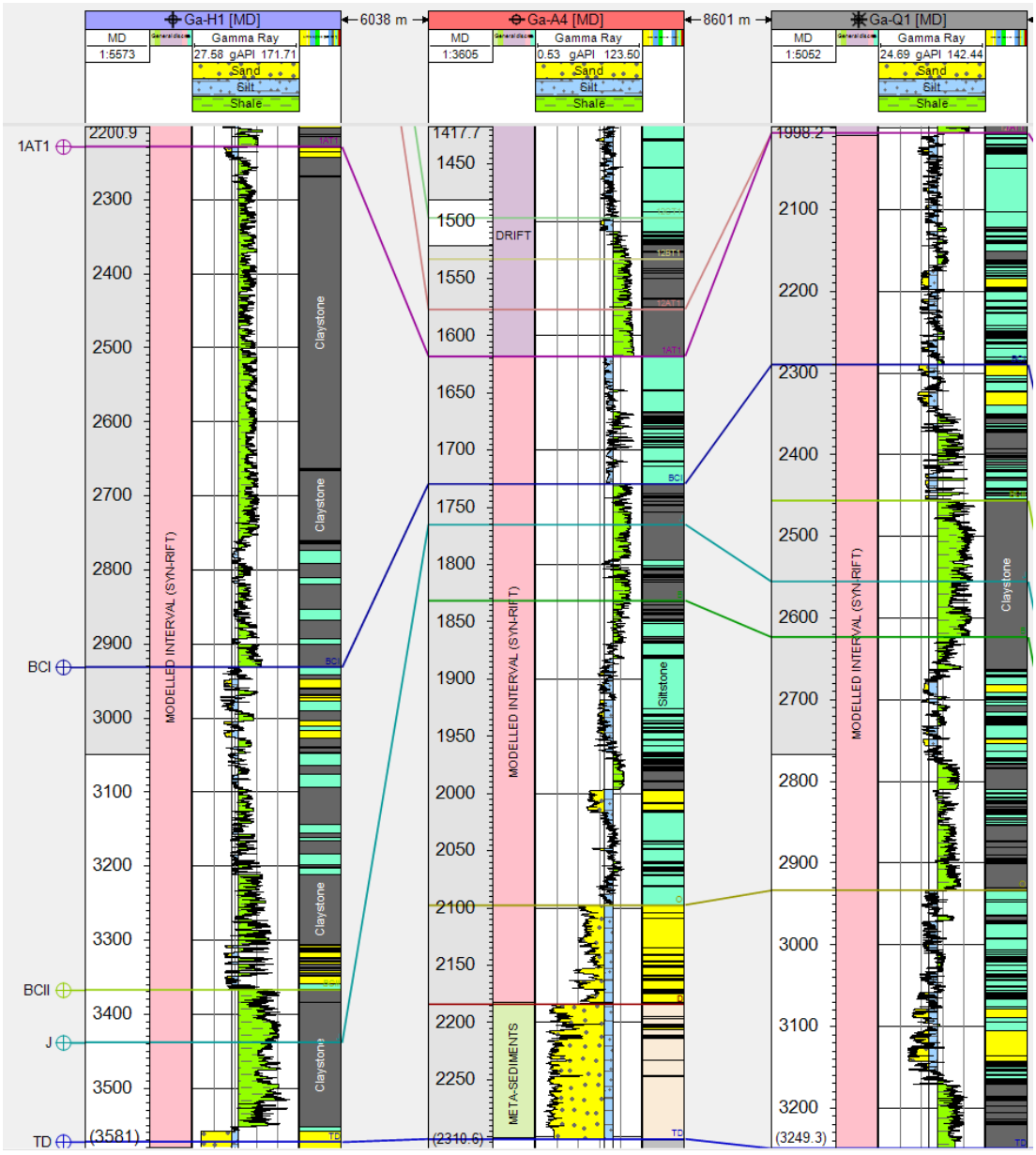

Figure 3-1: *Facies log correlation across three of the wells in the study area.*

3.2.1.3. Computation of Total and Effective Porosity

The porosity was calculated using a neutron-density log combination. Since it is believed that the syn-rift reservoirs are mostly gas reservoirs, the formula used for total porosity is;

$$\Phi nd = \sqrt{\frac{\Phi d^2 + \Phi n^2}{2}}$$

Where; Φnd = neutron-density porosity (total porosity), Φd = density-derived porosity, Φn = neutron porosity.

$$\Phi d = \frac{\rho matrix - \rho log}{\rho matrix - \rho fluid}$$

Where; ρmatrix = matrix density (depending on lithology), ρlog = the density log reading, ρfluid = fluid density.

The effective (shale-corrected) porosity (Φe) - defined as the amount of porosity in a system that can contribute to movable hydrocarbon saturations - was computed from the total porosity and VSh logs using the formula;

$$\Theta e = \Theta nd(1 - VSh)$$

The effective porosity is important because the presence of clay minerals can inhibit permeability and may contain a considerable amount of bound water. Figure 3-2 is a cross-plot between the effective porosity and VSh using the cut-offs defined in Table A1.

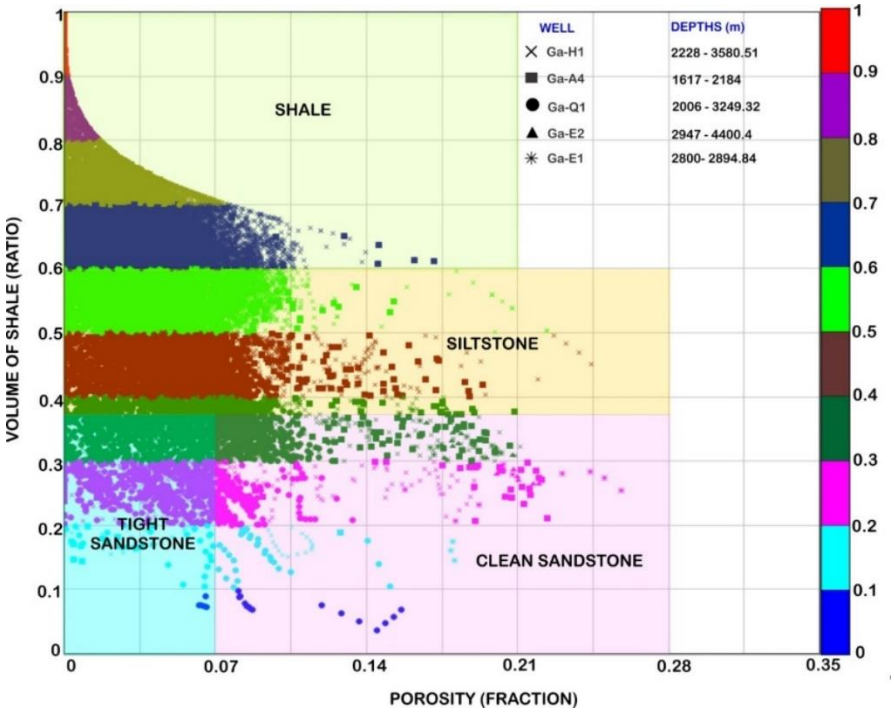

Figure 3-2: *Cross-plot of volume of shale and effective porosity. Note the cut-offs defined for siltstone may as well be for shaly sandstone as this classification is not dependent on the grain size.*

3.2.1.4. Permeability Estimation

Permeability was estimated from a relationship between core porosity and core permeability data using a log transform equation. The permeability estimates were based on the regression of core permeability (on a logarithmic scale) against porosity (Fig. 3-3) for the sandstones in the zone of interest. Due to the presence of tight sands within the interval of interest, the Klinkenberg-corrected permeability was used, as it approximates very well to the permeability of the rock samples measured with liquid flowing through the pore spaces (Rushing *et al.*, 2004).

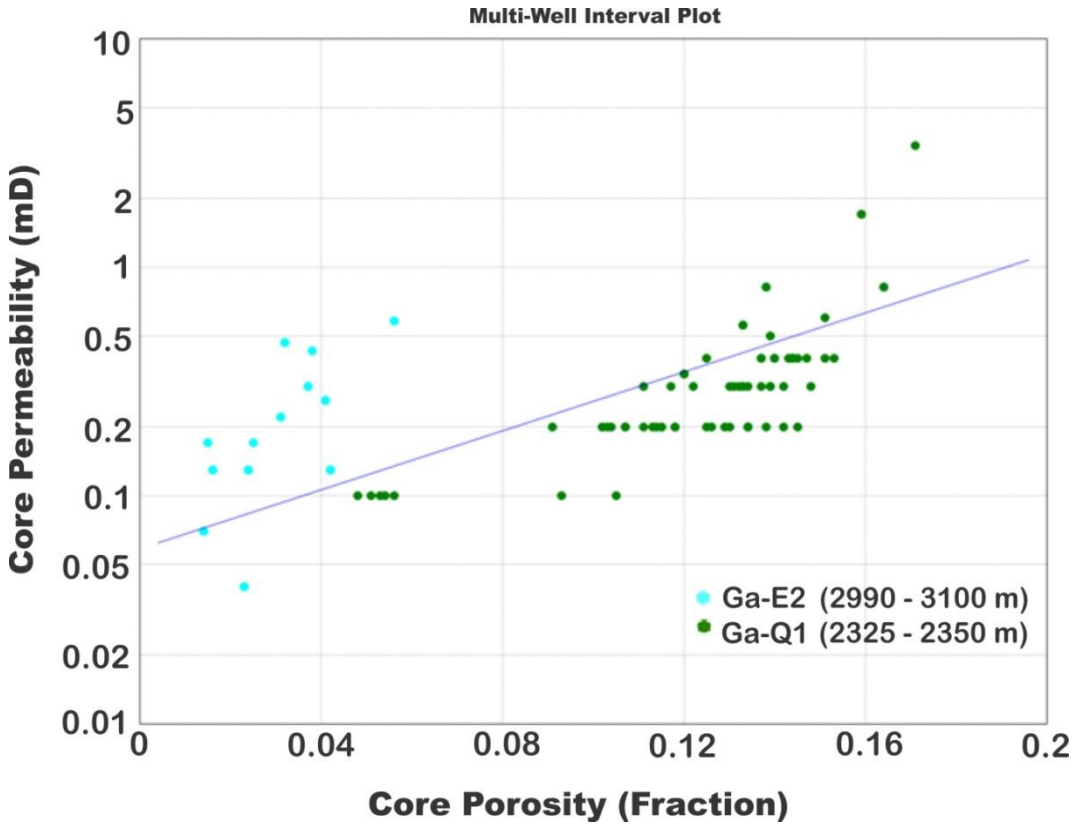

Figure 3-3: *Core porosity – core permeability transform.*

Figure 3-3 shows a clear trend with a degree of scatter associated with other factors controlling the permeability. It is clear from this figure that the permeability of the 'reservoir' sands (using a porosity cut-off of 7%) is extremely well controlled by the porosity, whereas the compact (tight) sandstone facies have a more dispersed cloud.

Note, however, that the drawback of the simple transform created from the core data is that it underestimates the presence of extreme values. For this reason, it may not effectively capture the unique permeability trends which vary from the trends observed in the porosities (Caers,

2005). Nonetheless, the resultant permeability curve matched the core values as can be seen in Figure 3-4 below.

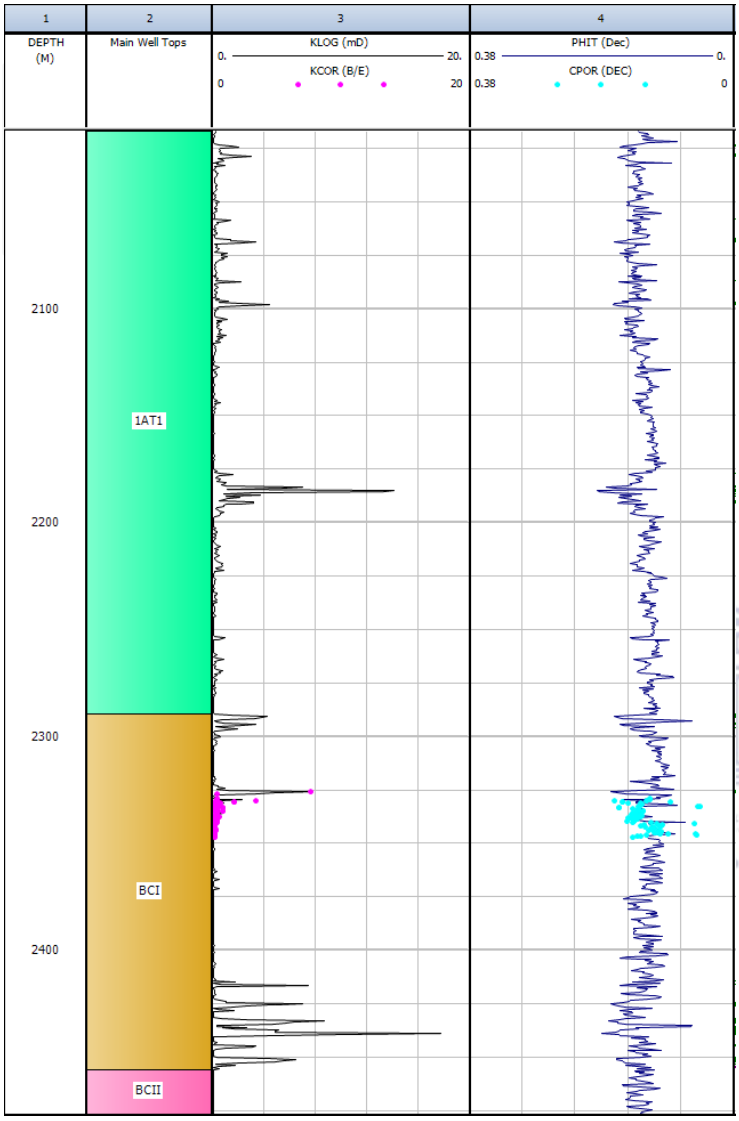

Figure 3-4: *Calculated permeability and porosity curves for the cored zone within the interval of interest. A good match is established between the core samples and the resultant curves. Note however that despite this match, a large uncertainty exists in the computed petrophysical logs because of core data scarcity.*

3.2.2. Seismic-to-Well Tie

To establish a relationship between seismic reflections and stratigraphy prior to seismic interpretation, an integrated seismic-to-well tie was created (Fig. 3-5).

The process involved the generation of a synthetic seismogram through the following steps;

- Sonic log conditioning and de-spiking – Since the log may be acquired in several runs and its sections may be influenced by casing, cycle skipping and so on, this step is necessary to remove erroneous data.
- Sonic calibration aimed at reconciling seismic (Check-shot) times and integrated sonic times for any given depth in a well.

- Multiplication of the sonic and density logs to give an acoustic impedance (AI) log.
- Conversion of the AI log into a log function of two-way-time – the reflection coefficients (RC) calculated using the formula:

$$RC = \frac{(AI_{n+1}) - AI}{(AI_{n+1}) + AI}$$

  Where AI is the acoustic impedance of the top layer and AI_{n+1} is that of the bottom layer.
- Convolution of the reflectivity curve with a convolutional wavelet. For some of the wells the wavelet was extracted from the reference seismic survey with an average frequency of 25 Hertz and for others a theoretical (Ricker) wavelet was used.

The ties across the drift-onset unconformity (1At1) and Horizon D were of the utmost importance in this study as they comprise the top and base of the interval of interest, respectively. The comparison of the synthetic traces with the reflections from the 3D dataset shows a good visual match for the main events and therefore, there is a high level of confidence in the tie. Hence, manipulating the traces to better align them with the real seismic data was kept to a minimum. Finally, the tie was applied through activating the synthetic seismogram as the calibrated time-depth relationship (TDR) curve.

3.2.3. Seismic Interpretation

The principal aim of seismic interpretation was to formulate a geological conceptual model based on the available data. This, together with the hypothetical depositional model and regional geologic knowledge constitute the main inputs when trying to predict the three-dimensional spatial heterogeneity of physical properties between wells based on available sparse data.

3.2.3.1. Fault and Horizon Interpretation (Time-domain)

Seismic interpretation involving fault and horizon interpretations was carried out for structural characterisation of the study area and it was geared towards the establishment of the physical and other properties that are important for fluid flow of the major fault systems.

The faults were particularly important in defining the geometry of the fault array. They were picked on seismic lines that reflect the ‘true dip’, or in other words perpendicular to the fault strike, as they permit for a clear view of the reflection terminations likely to represent faulting. Where neither the crossline nor inline directions were in true dip to a fault, the fault was mapped

on an arbitrary line, as required. Depending upon the geology and the scale of geometry for the individual faults, faults were mapped according to different diagnostic criteria. These are:

1. Traditional methods – TWT offsets, changes in reflection character and dip, and reflection terminations.
2. Non-traditional methods – Data 'attribute' variations such as amplitude dimming and coherency edges.

Further, minor faults were also mapped in the interval of interest as these would have an impact on the local fluid flow and therefore should be incorporated in the model. This is because the model was not constructed with the aim of calculating hydrocarbon volumes (in which case small faults would not make much of a difference to the outcome).

Horizons were manually traced across the seismic survey with the aid of the seismic-to-well tie (Section 3.2.2.) and regional geologic knowledge to capture a valid fault-horizon interpretation. The main structural influence on flow is the geometrical arrangement of sand to sand juxtaposition windows across the fault, as pointed out by Jolley *et al.*, 2007, and this depends on the cross-fault correlation of seismic horizons.

3.2.3.2. Velocity Modelling (Time-Depth Domain Conversion)

A comprehensive description of geology requires that any interpretation derived from reflection seismic data, recorded in the time domain, be placed accurately in the 3D depth domain, using velocity information to accomplish this transformation.

The velocity model was constructed using a standard layer-cake approach using the TDR obtained in the seismic-to-well tie process and a constant velocity function $V=V0=Vint$ for the individual layers (Fig. B1). The process began from a datum (mean sea level) and progressed downwards, horizon by horizon, node by node; each node corresponding with the intersection of one surface with one fault pillar.

The well adjustments (using well tops) were carried out within the model itself to ensure that the information from the correction will be maintained and can be used when converting objects with no well correction. The final depth-converted faults and regional horizons can be seen on Fig. 3-6.

A)

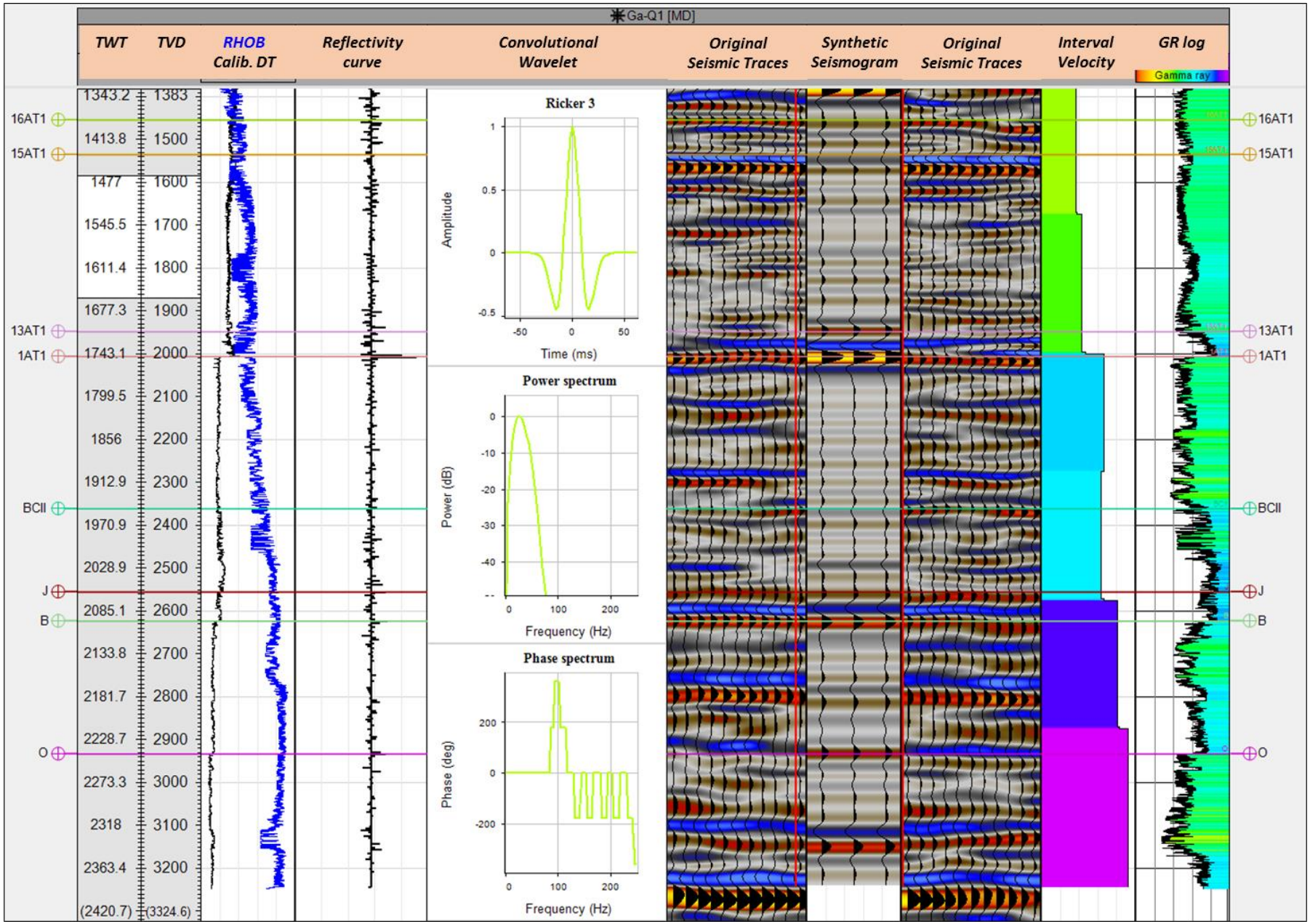

B)

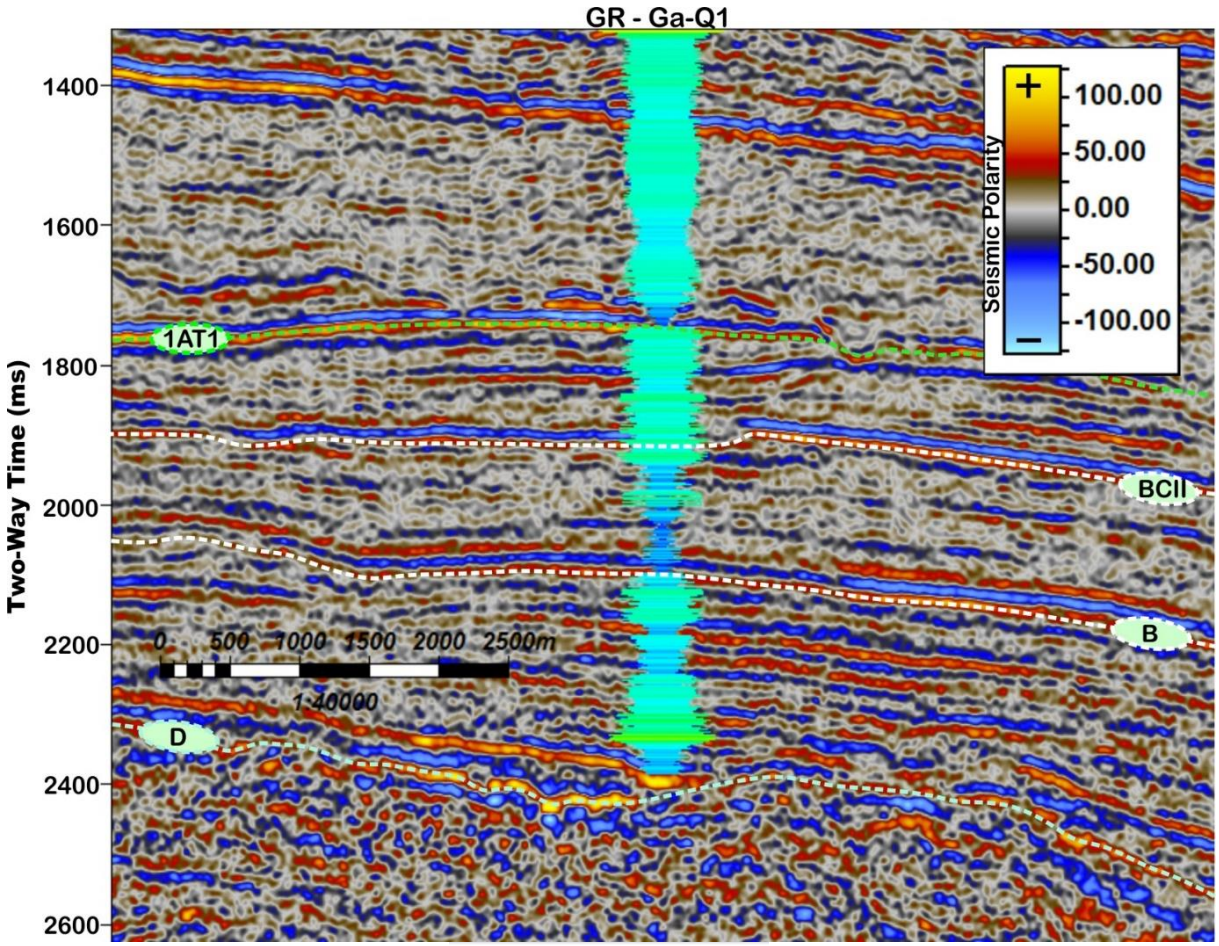

Figure 3-5: a) *Main variables used and produced in the generation of an integrated seismic-to-well tie, listed from left to right: two-way time (TWT), true vertical depth (TVD), density (RHOB; blue) and calibrated sonic (DT; black), reflectivity curve (RC), convolutional wavelet, original seismic traces displayed as two panels on either side of the resultant synthetic seismogram, interval velocity, gamma ray (GR) log;* ***b)*** *Full stack seismic section intersecting well Ga-Q1 with its key markers displayed. The 1At1 marker is picked as a peak and the seismic response at the top of the syn-rift sequence produces a high amplitude.*

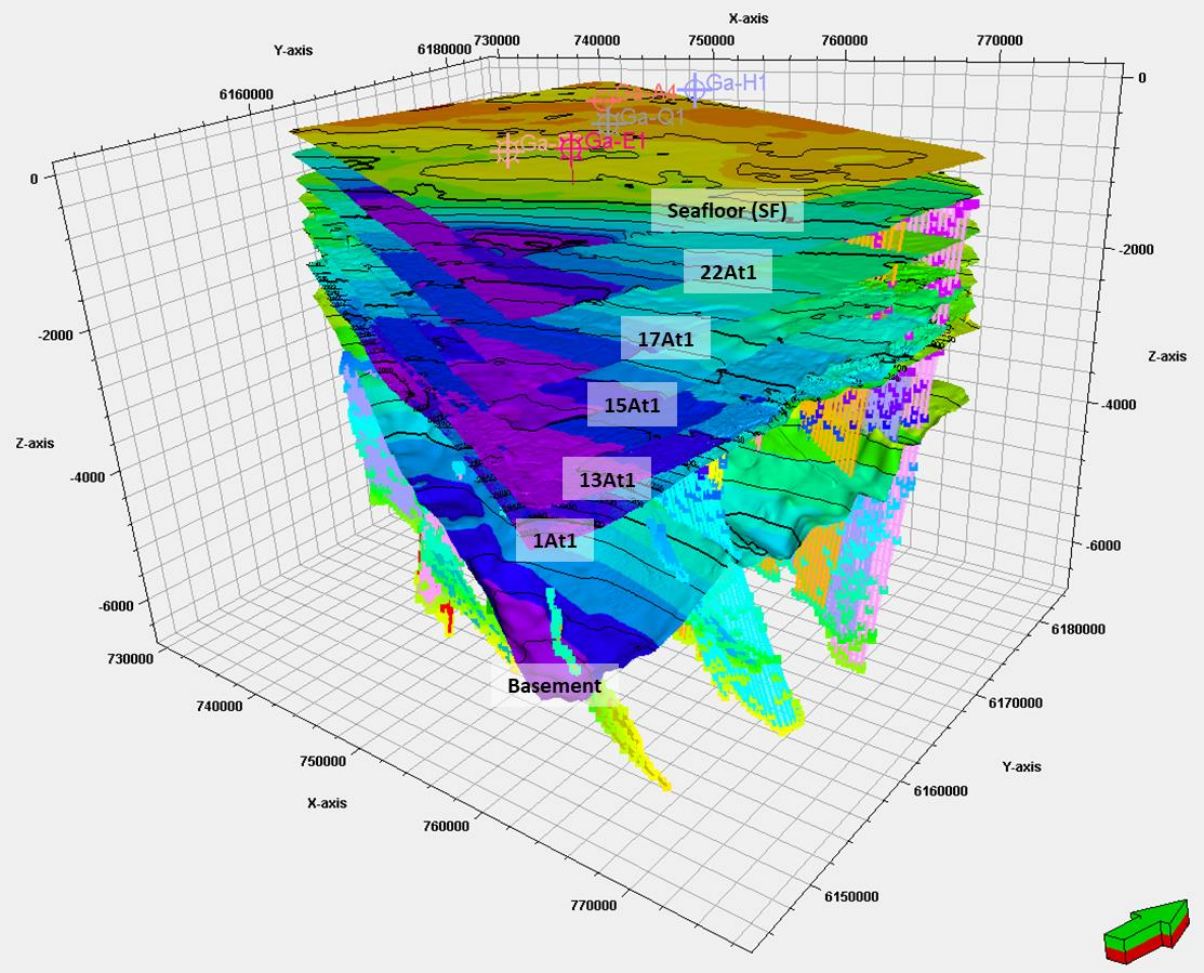

Figure 3-6: a) *Regional depth-converted seismic horizon and fault interpretations.*

3.3. GEO-CELLULAR MODELLING

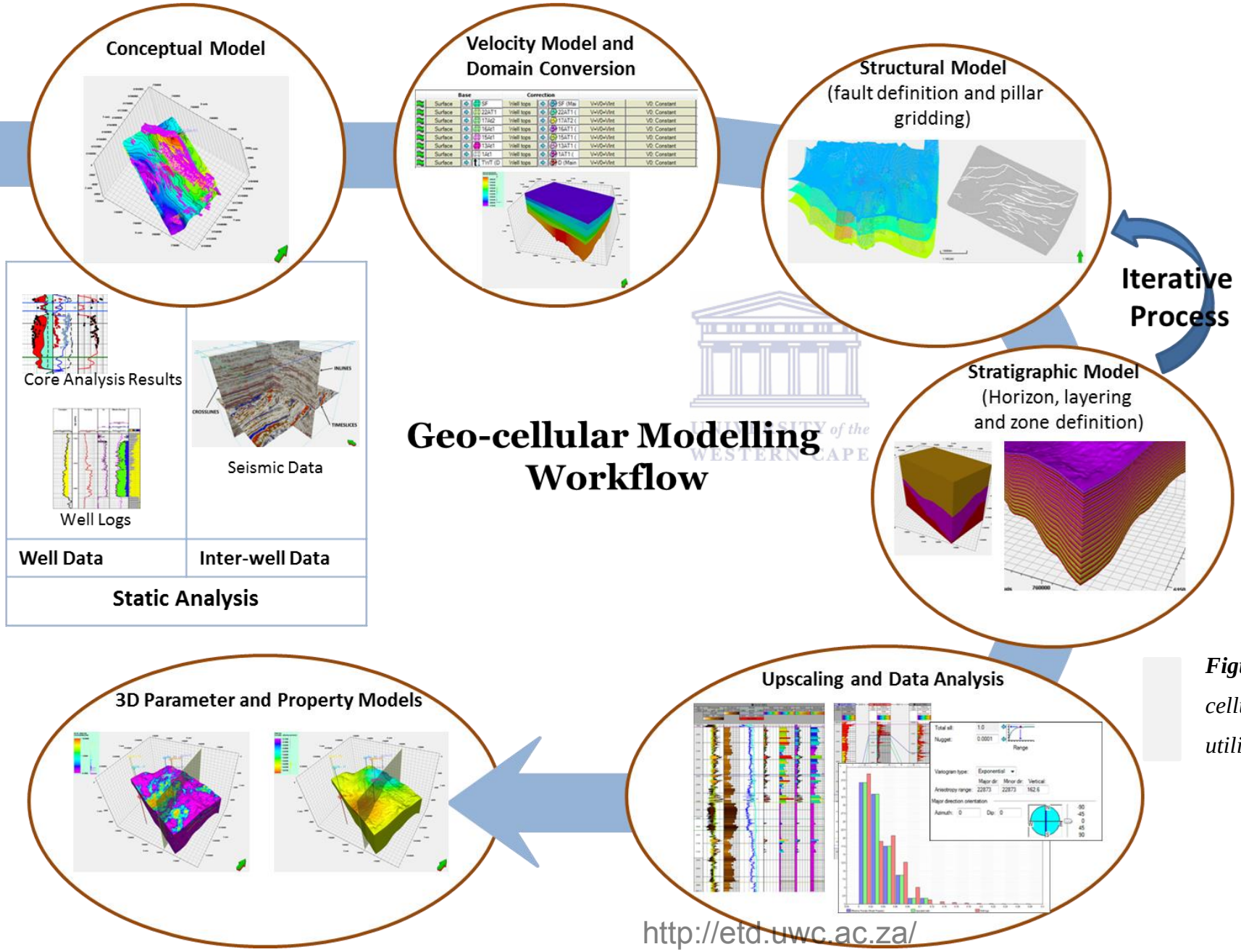

Figure 3-7: *Simplified geo-cellular modelling workflow utilised in this study.*

3.3.1. 3D Structural and Stratigraphic Framework

The structural framework was a sub-modelling phase that represented the overall geometry of the reservoir interval and was the backbone to designing a 3D grid that contains all the geological/petrophysical information and the generated reservoir properties. It included two main elements, the depth-converted structural surfaces and faults and defined the topographical relationships between those and the interpreted well data (Gomes *et al.*, 2004). Depth markers that define the correlation of the reservoir units along the well trajectories were also incorporated as input.

The process involved two key stages: 1) fault definition and pillar gridding, 2) horizon definition, layering and zoning (Fig. 3-7), via the use of some reliable coded commercial mapping and geostatistical gridding algorithms. Uncertainty was quantified using geostatistical simulations that are Gaussian-based (Gomes *et al.*, 2004).

1) Fault Definition and Pillar Gridding

During this process, a stratigraphic vertical coordinate system was modelled in order to restore the existing structure of the layer to its natural correlation style prior to geological deformation. As indicated by Deutsch (2002), an appropriate grid system within each of the layers defined by the structure model is needed for the population of petrophysical properties. Since the number of cells or resolution is a balance between required detail and CPU resources (MacLennan and Deutsch, 2006), the maximum grid cell dimensions were dictated by the minimum sizes of the features to be resolved. These were: 100m (i) x 100m (j).

2) Horizon, Layering and Zone Definition

Particularly, depth-converted seismic horizons were the main input for defining the geometry of the main bounding surfaces, in addition to the orientation, extension and throw of faults, and the broad shape of the structure.

Since grid cell dimensions are defined by three indices (i, j and k), layering and zone definition were the two last steps in defining the vertical resolution (k) of the 3D grid by setting the number of desired cell layers. A hundred were set for the zone of interest as this ensured that a cell thickness of 10 - 40 m was maintained.

3.3.2. Upscaling and Data Analysis

3.3.2.1. Upscaling

This process involved the coarsening up of the processed discrete facies and continuous petrophysical logs which are innately fine-scaled. Averages of the samples were calculated over distance increments and the resultant averages were then populated into the model. In this way, the process is a means of reducing the resolution of the logs in preparation for model simulation. The most important aspect to consider was maintaining the heterogeneity of the fine-scale data.

The 'most of' averaging method was used for facies upscaling. The method selects the discrete value most represented in the log and assigns it to the upscaled property. The arithmetic averaging method was used for the petrophysical properties: VSh, porosity and permeability. Normally permeability is upscaled using either the geometric or harmonic method depending on whether it has spatial correlation. Here, the arithmetic method was chosen. As a rule of thumb, the arithmetic method is used when flow is along the main permeability changes (i.e. due to horizontal bedding or overall laminar layering). Thus, this was the most appropriate method since the interest lies on the across-fault (horizontal) fluid flux.

Once the raw data were upscaled, a series of data analysis procedures were performed. These were essentially quality control processes.

3.3.2.2. Data Analysis

The data analysis process was used for detailed property analysis before interpolating them across the grid volume using geostatistical algorithms. The first step involved visual quality checks of the upscaled cells. Different tools were used for discrete and continuous properties. For the discrete facies property, this was performed to ensure that the interpreted facies succession is preserved. For the continuous properties, the aim was to ensure that the vertical property variations were preserved. For this study, it was imperative to model realistic well to reservoir connectivity; hence this process was also to ensure that high porosity/permeability streaks in the raw data were preserved.

Furthermore, statistical quality checks were also performed on the upscaled logs. Discrete data analysis was performed to analyse the facies proportion, facies thickness, calibration between continuous properties and facies within the zone of interest, and to model a variogram. Further,

continuous data analysis was performed to define data transformations and to generate variograms. This study made use of the exponential variogram model for all property modelling to constrain the 3D geo-cellular model to local data representative of the geologic knowledge. The data transformation prepared the data for the geostatistical modelling algorithms as it allowed for spatial trends in the data to be extracted prior to property modelling to ensure stationarity. The extracted trends were later reapplied to the modelled property to ensure their preservation. Figure 3-8 roughly illustrates the upscaling and data analysis procedure and results.

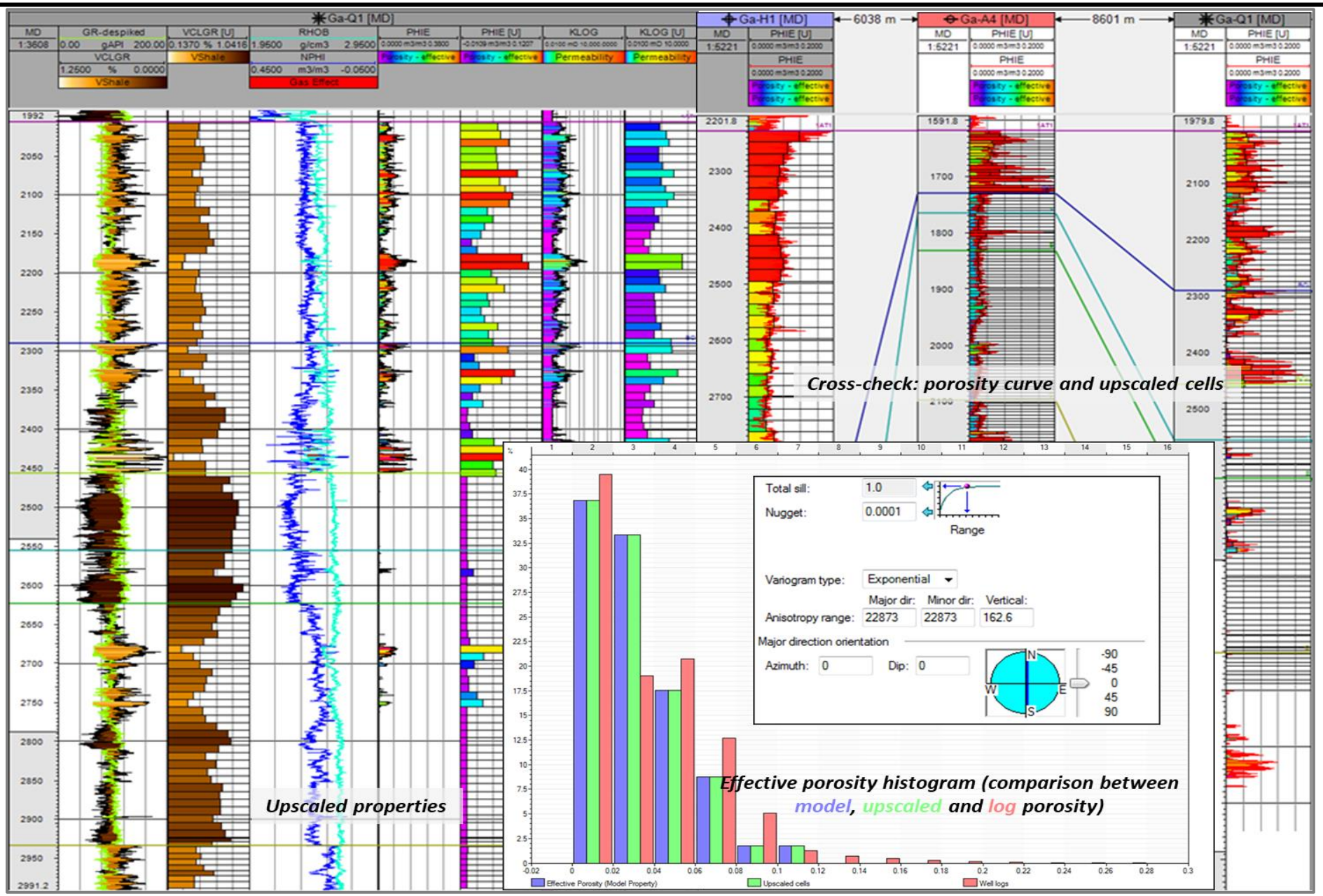

Figure 3-8: *Broad depiction of the upscaling and data analysis processes.*

3.3.3. 3D Parameter and Property Modelling

3.3.3.1. Facies Modelling

During this stage, a variety of facies modelling techniques which can be broadly grouped into cell-based and object-based modelling were available on Petrel. Some of the key approaches available on Petrel are: object modelling (OM), sequential indicator simulation (SIS), truncated Gaussian simulation (TGS) and multi-point facies simulation (MPS). Due to uncertainty in the facies distribution and heterogeneity in the syn-rift succession, the SIS technique was used. This technique is a cell-based technique mostly applicable in cases where there are difficulties in inferring reliable shapes for object-based modelling (Deutsch, 2002; MacLennan and Deutsch, 2006). Further, SIS allows a stochastic distribution of the properties using the predefined histogram (Fig. 3-8). Directional settings, such as variogram and extensional trends (Fig. 3-8) are also honoured.

3.3.3.2. Petrophysical Property Modelling

The rock types were the main considerations during petrophysical modelling. The reason for this is that the spatial distribution of petrophysical properties often shows significant differences in first and second order summary statistics due to different lithological or facies types (Bridger *et al.*, 2013).

The volume of shale, porosity, and permeability models were built using the sequential Gaussian simulation (SGS) technique within each facies type and layer. The SGS approach honours well data, input distributions, variograms and trends (Fig. 3-8). The mean and variance are given by Kriging. It acts in the same manner as the SIS algorithm except it simulates continuous properties instead of discrete properties.

Having established a geo-cellular model (populated with facies and petrophysical properties) for the interval of interest, the likelihood of fluid flow communication across the mapped faults was investigated. The analysis was carried out using two main processes: 1) juxtaposition mapping (Juxtaposition Seal) and 2) generation of fault-rock properties (Fault-rock Seal); each process having its own operations as outlined in Figure 3-9 and discussed below.

3.4. FAULT-SEAL ANALYSIS

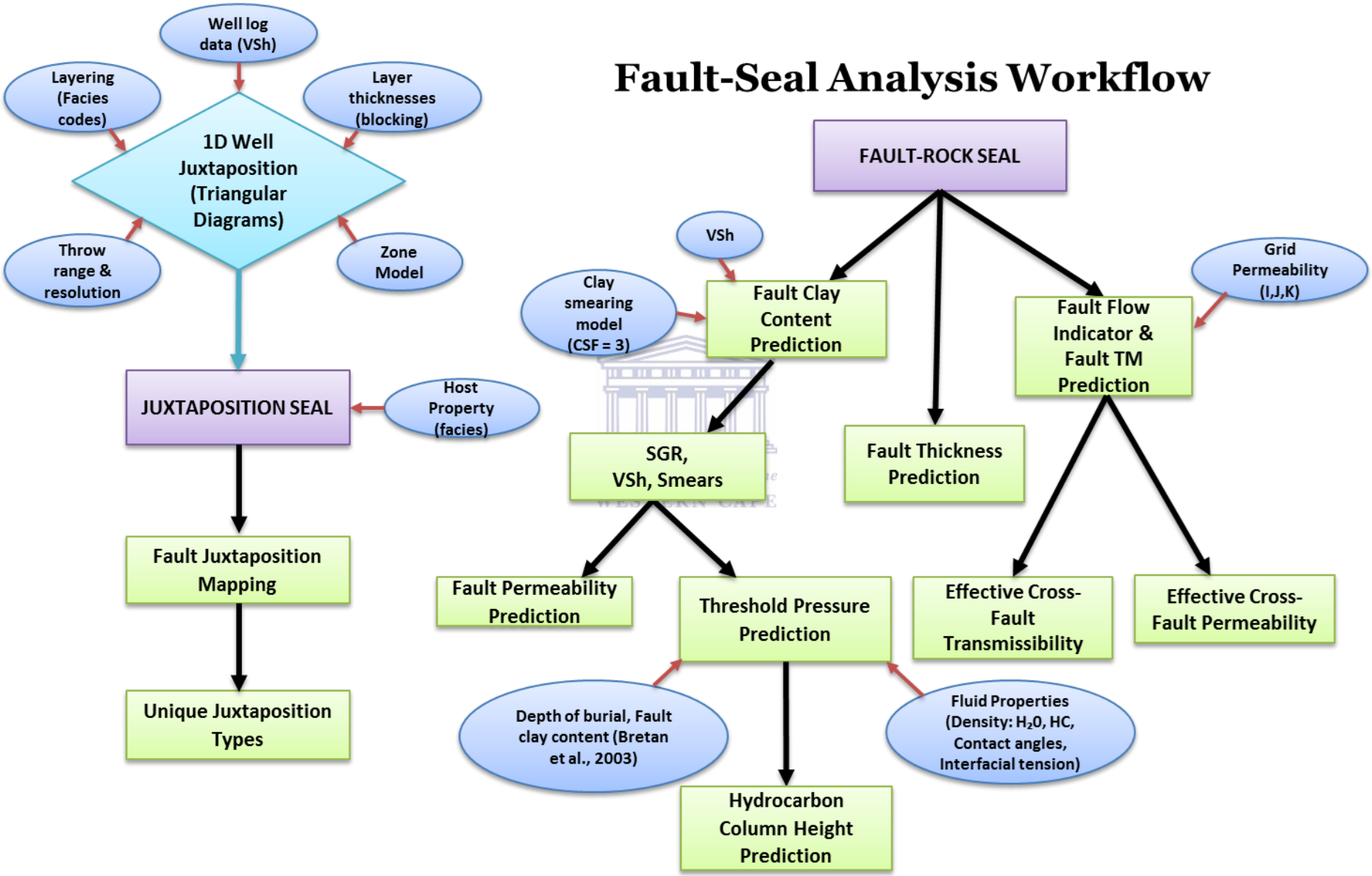

Figure 3-9: *Summary Fault-Seal Analysis workflow utilized in this study*

3.4.1. Juxtaposition Seal

3.4.1.1. 1D Well Triangle Juxtaposition Diagrams

This operation was used as a rapid analysis of the likely impact of faulting and to assess the key offsets on faults that can induce seal or fluid flow from reservoir units. The triangle juxtaposition diagrams produced in this process provide a quick-look self-contained fault seal analysis tool using well curves, as pointed out by Porter et al. (2000). To define the stratigraphy in the 1-D juxtaposition model, the VSh log (continuous well property) was used. To convert from the continuous log property to discrete stratigraphic facies types, a discrete facies template with specific facies codes was created on Petrel based on the VSh cut-offs provided in Figure 3-2.

To define the stratigraphic interval of interest for the creation of the 1-D juxtaposition models, the layer thicknesses were incorporated into the workflow. Moreover, to capture the variability in the VSh well log, the minimum layer thickness was set to 1 metre. Also incorporated into the workflow were the throw range and the zone model. The minimum throw was set at 0m and the maximum was set at full stratigraphic offset for the interval of interest. This reduced the total grid size while keeping the stratigraphic resolution required.

3.4.1.2. Fault Plane Juxtaposition Mapping

This operation was used to map the 3D distribution of discrete (facies) property juxtapositions for the faults within the geo-cellular grid. From this, the number of unique juxtaposition types that occur across the faults for the facies property was determined. These were classified and produced as a fault-rock property and therefore will be presented and discussed as such in Chapter 4. Lastly, critical windows along the fault that may impact across-fault fluid flow were extracted.

3.4.2. Prediction of Fault-Rock Properties

3.4.2.1. Fault Clay Content (VSh, SGR and Smears)

Both clay mixing, and clay smearing algorithms were performed during this operation. These were based on the fault throws and the VSh grid property distributions. The clay mixing model chosen was Shale Gouge Ratio (SGR) developed by Yielding *et al.* (1997) and the clay smearing model chosen was Clay Smear Factor (CSF). Based on the assumption that the fault

throws in the area are three times the shale layer thicknesses in interval of interest, a CSF of 3 was assigned; this means that a continuous shale bed can be offset by three times its original thickness before breaking down (Section 2.2.1.2; Fig 2-10(a)).

3.4.2.2. Fault Permeability Prediction

The generated fault-rock clay content variations acted as a proxy for the assignment of fault permeability estimations. As noted by Knipe *et al.* (1998), this allows better capture of the key variations in fault permeability for fault rocks that have undergone different faulting, burial and thermal histories.

3.4.2.3. Threshold Pressure Prediction

It is worth noting that a fault may not be open or closed to fluid flow in a complete sense (Berg 1975; Schowalter 1979). So, permeability alone is not the best criterion for assessing seal and flow-barrier behaviour. As studies such as Yielding *et al.* (1997), Ottesen Ellevset *et al.* (1998) and Manzocchi *et al.* (2010) pointed out, fluid flow will only occur once a fault has reached (and exceeded) a certain value (threshold pressure). Cross-fault pressure differences that are below this threshold value render the fault sealing.

Two methods for the threshold pressure calculation were available for this operation;

1) User-defined look-up function – based on local core-calibrated data
2) Global equations – used in the absence of core-calibrated data.
   Options include Sperrevik *et al.* (2002) and Bretan *et al.* (2003).

Due to the lack of core-calibrated data, this study utilized the latter calculation method. The Bretan *et al.* (2003) approach was selected for this process as it required less input parameters than the other available option and therefore is prone to fewer errors in the computation of the threshold pressure for the zone of interest. The requisite input parameters were the maximum burial depth of the reservoir interval and the predicted fault clay content.

The data were then used, in conjunction with fluid properties from Bolas *et al.* (2005), to estimate the potential hydrocarbon column height support across the faults. This operation was carried out to determine the potential differential hydrocarbon column heights of the faults assuming a relationship between fault clay content distribution and clay to threshold pressure relationship. This process was in essence seal capacity estimation (Watts, 1987).

3.4.2.4. Fault Thickness Prediction

Likewise, the flow rate is also a function of the thickness of the fault rock. Thus, the combination of the threshold pressure, the fault-rock permeability and fault-zone thickness is the main control of the sealing or retardation capacity of a fault (Ottesen Ellevset *et al.*, 1998).

The fault-rock thickness and its variations on individual faults are related to the length of and displacement along the fault, and the lithology of the faulted rock (Childs *et al.*, 2007). The prediction of this property was carried out using the displacement to thickness ratio; from the amount of displacement that has occurred on the fault. This method of fault zone thickness prediction of sub-surface faults has been addressed by Childs *et al.* (1997) and Walsh *et al.* (1998). Fault zones encompass portions where volumes of deformed rock are bounded by two or more slip surfaces; and portions where single slip surfaces accommodate the entire displacement. The separation between the outermost slip surfaces minus the thickness of undeformed lenses defines the thickness of the fault zone (Manzocchi *et al.*, 1999). Compilations of fault outcrop data from studies such as that of Robertson (1983) and Hull (1988) demonstrate an approximately linear relationship between fault zone thickness (t_f) and displacement.

Data compiled by Hull (1988), and data from faults in interbedded sandstone and shale successions in Western Sinai (Knott *et al.* 1996), from the Moab fault in SE Utah (Foxford *et al.* 1998) and from faults in a Westphalian sandstone/shale succession from Lancashire, UK (Walsh *et al.* 1998) are summarized in Figure 3-10. Likewise, synthetic thickness values generated using the relationship: $t_f = D/66$, are plotted for several displacements, to define a median thickness value. When displacements are over about one metre, the data populate closely the envelopes defined by the outcrop studies. Thus, the equation above tends to underestimate the thickness of smaller faults. However, fault displacements less than a metre are hardly ever incorporated in production flow simulation models, therefore there was no need to estimate accurately their thickness for this application.

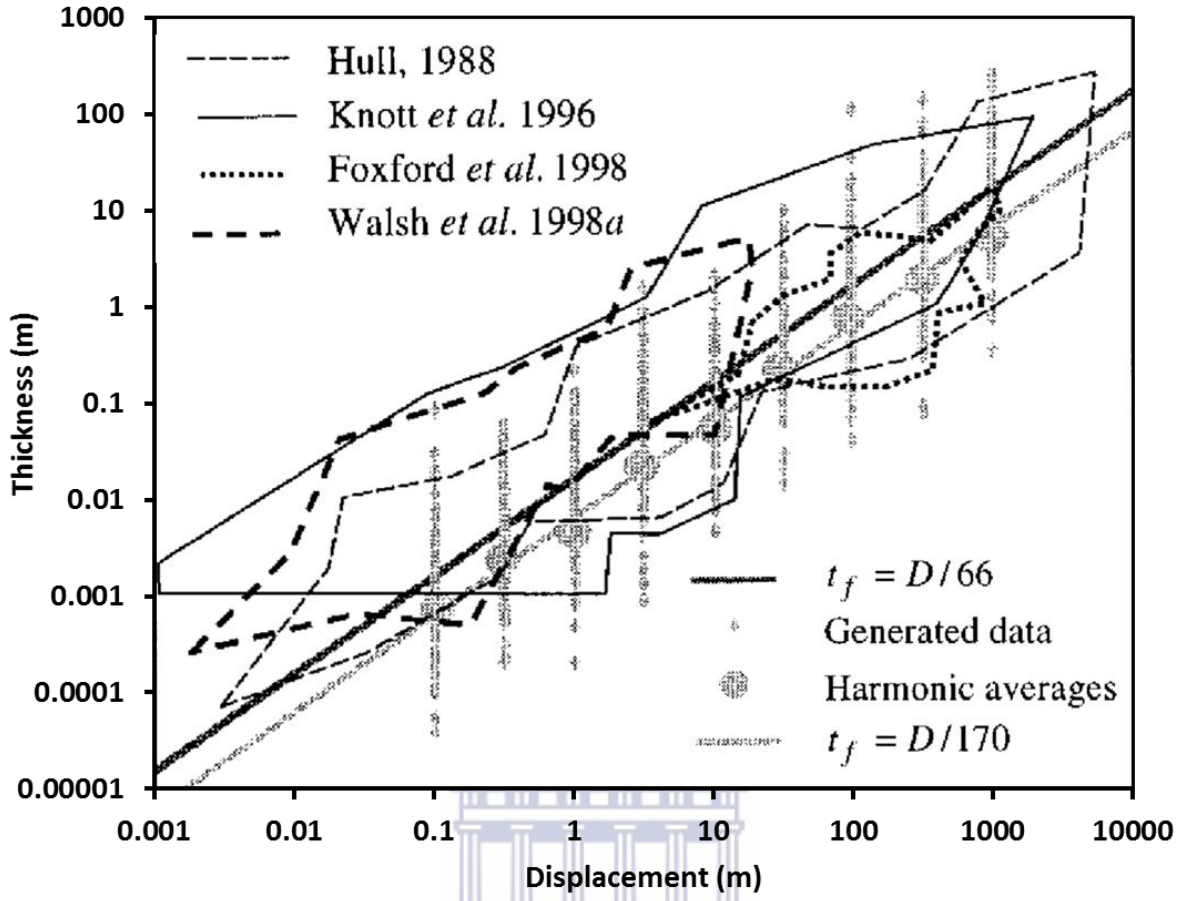

Figure 3-10: *Log thickness vs. log displacement. Summaries of outcrop data are given as envelopes encompassing measurements from a variety of sources as indicated. 200 log-normally distributed thickness data (small circles) have been generated at numerous displacements with median value following the relationship $t_f = D/66$. The harmonic averages of these data (large circles) follow the relationship $t_f = D/170$. Modified after Manzocchi et al. (1999).*

3.4.2.5. Fault Flow Indicators

As a basis for understanding reservoir communication across the faults, the fault transmissibility multiplier distributions across the fault planes were determined using the combination of the predicted fault-rock permeability values, the fault-rock thickness estimates, host rock (matrix) permeability and grid cell dimensions of the geo-cellular model (Manzocchi *et al.*, 1999).

Subsequently, the potential flow indicators such as effective cross-fault permeability (ECFP) and effective cross-fault transmissibility (ECFT) were computed. The ECFT and ECFP are compound parameters that incorporate the widths of the hanging wall, fault and footwall host

rock (Freeman *et al.*, 2010). For this reason, they are known to remove the influence of the user-defined spatial grid geometry. Jolley *et al.* (2010) suggest that these parameters provide a more robust correlation with cross-fault fluid flow than host- or fault-rock permeabilities and transmissibility multipliers alone.

3.4.3. Burial (Temperature/Stress) History Modelling

Integrated basin modelling was achieved for the study area to quantify maximum burial depth and temperature with the PetroMod1D 2014.4 software package. The software uses a forward modelling, event-stepping approach. As follows, the simulation begins with the deposition of the oldest sediment layer and continues with younger strata in decreasing chronological order, event by event, until the present-day sediment-fill geometry is attained.

The first step involved the definition of a comprehensive present-day stratigraphic column of the studied section, including lithologies, depositional ages, petrophysical data and thicknesses of all sedimentary units. This is commonly referred to as a conceptual model and is based on the sequence of events, i.e. sedimentation, erosion, non-deposition (hiatus) and tectonic events. These are obtained from available data and regional knowledge, as previously mentioned.

For the definition of the complete thermal regime of the basin from a single well perspective (1D), thermal boundary conditions were necessary. The two core input parameters were the basal heat flow [HF (mW/m2), lower thermal boundary] and the paleo water depth [PWD (m), upper boundary]. The HF values were based on regional studies by Goutorbe *et al.* (2008) and were affected by local tectonic events (Fig. 3-11). The PWD values were derived from Brown *et al.* (1996) and used to calculate the sediment water interface temperature [SWIT (^{0}C)] using functions of Wygrala (1989). Moreover, the contribution from internal radiogenic heat was automatically computed based on the defined sedimentary lithologies and their average abundance of radioactive minerals such as uranium, thorium and potassium.

Compaction rates were empirically modelled and were used to derive an algorithm which calculates changes in porosity with depth of burial using default PetroMOD values.

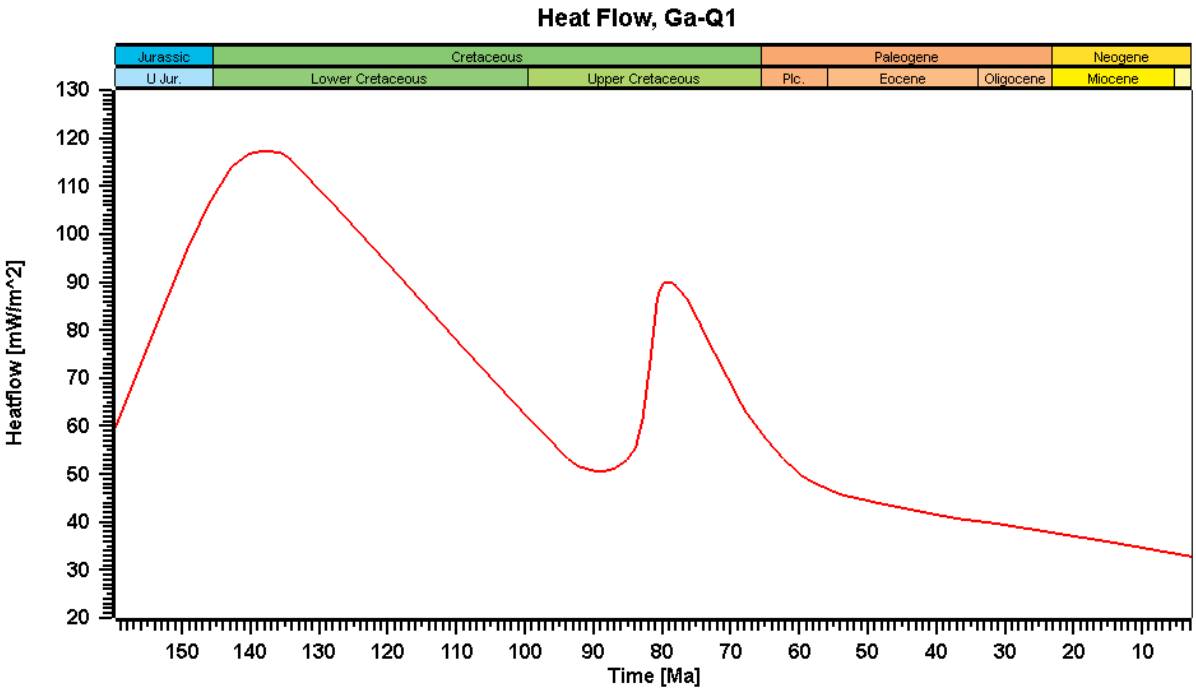

Figure 3-11: *The basal heat flow model used as input in the base case 1D basin modelling simulation showing the incorporation o f a rifting event during the Upper Jurassic-Lower Cretaceous in which the rifting heat flow has a maximum of 115 mW/m^2. The second peak is related to the Shona-Buvet hotspot event and has a maximum heat flow of circa. 90 mW/m^2. Note the heat flow model is calibrated to present day heat flow measurements (Goutorbe et al., 2008) and the overall heat flow trend likely diminished consistent with a McKenzie-type decay, i.e. exponential decrease (McKenzie, 1978) to a present-day value of circa. 35mW/m^2.*

4

Results

This chapter presents the results of the analyses in five sections. Section one presents the interpretations of the complexly-faulted subsurface configuration of the study area. The spatial variations of geological properties within the structural framework are presented in the second section. Section three introduces the fault seal analysis results by presenting the 1D triangle juxtaposition diagrams which served as quick-look guide for what to expect in the succeeding fault-rock property analysis results presented in the fourth section. Lastly, the fifth section presents the basin modelling results.

4.1. STRUCTURAL ANALYSIS

Figure 4-1 is a representative interpreted seismic section and corresponding schematic diagram that best reflect the structural configuration of the mapped area.

The most prominent feature apparent in Figure 4-1 is the thinning of stratigraphic units above the Superior High and the overall thickening of strata towards the south. The top of the rifted Pre-Mesozoic Basement is mapped as Horizon D with Cape Supergroup and older rocks below. Above Horizon D are Oxfordian to Valanginian sediments which onlap onto the basement in the south and show an increase in thickness towards the same direction. Further, the second rifted landscape is mapped as the late Valanginian 1At1 and faults associated with this phase extend down through the entire syn-rift package and in some places, displace Horizon D. The shallow normal faults above the early Aptian unconformity (13At1) can be inferred to have formed due to Post-rift tectonics.

A)

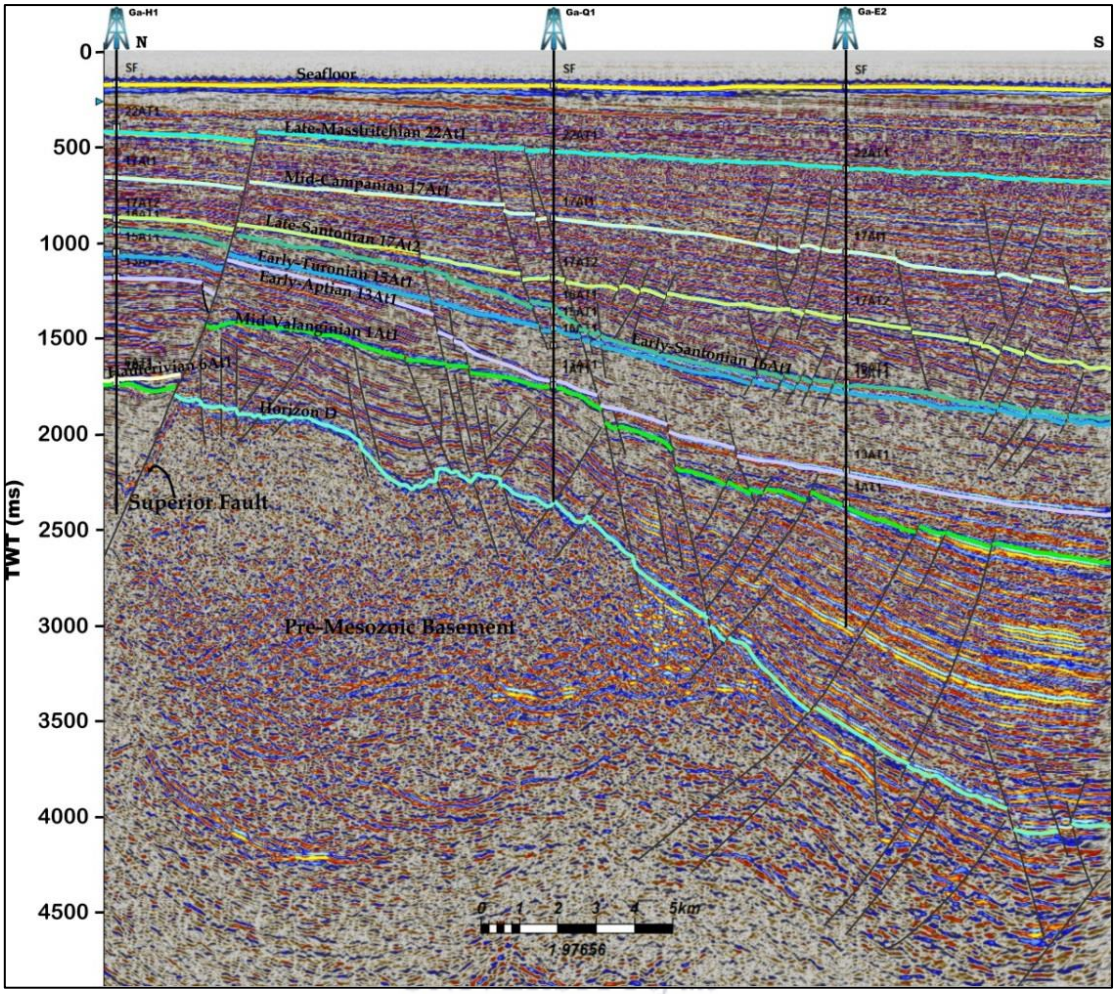

B)

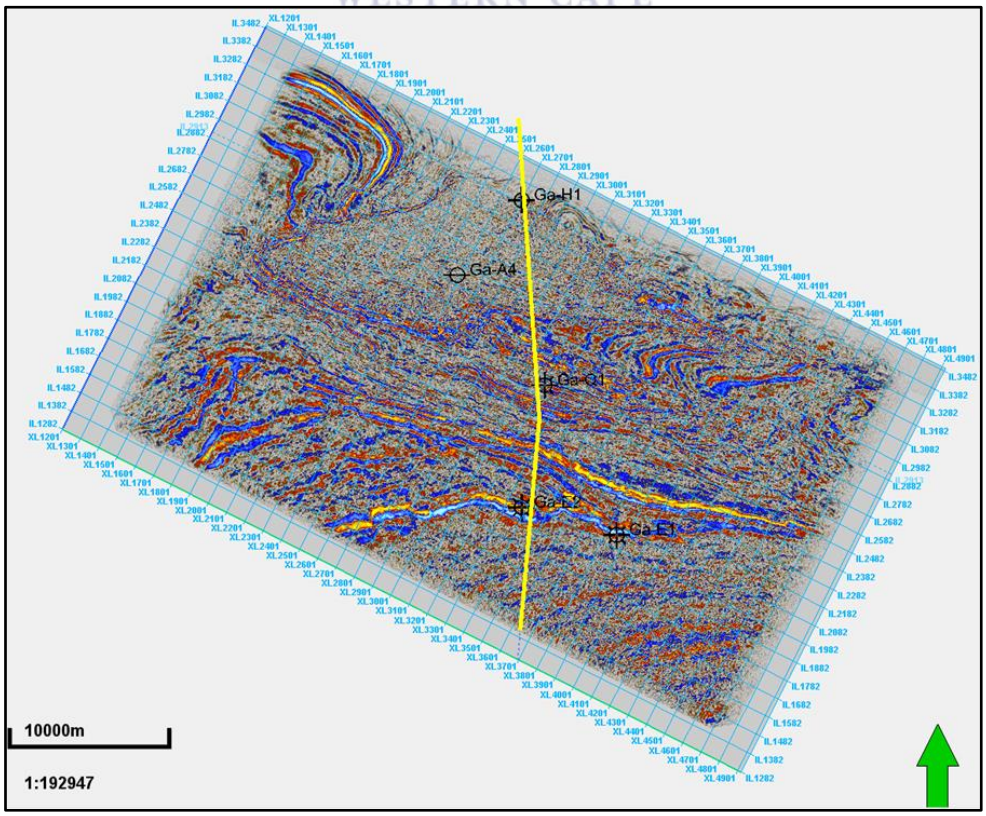

C)

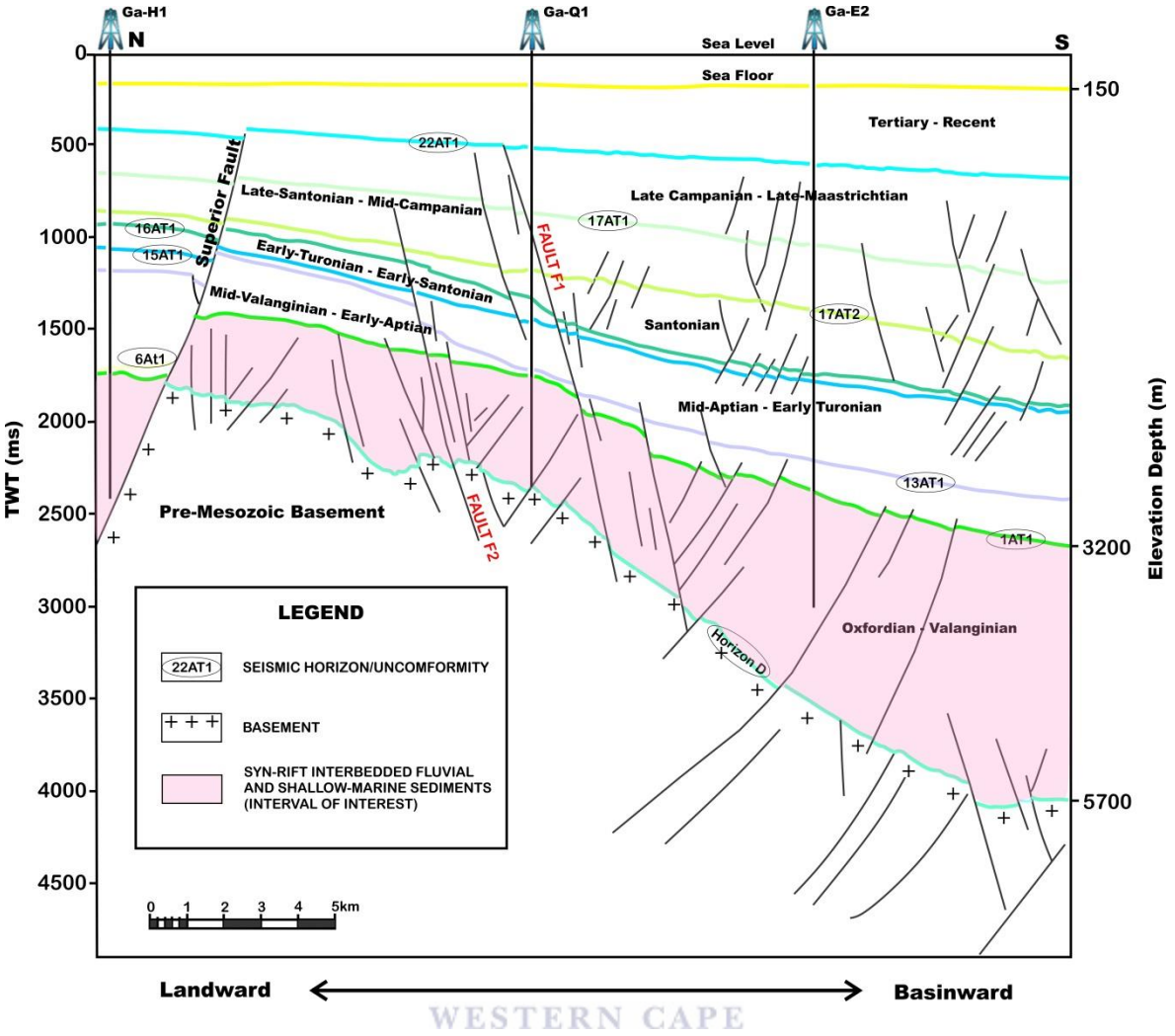

Figure 4-1: a) *Interpreted N-S oriented arbitrary seismic profile extracted from the 3D seismic survey; the time slice* ***(b)*** *has been placed for location, and* ***c)*** *schematic cross-section showing typical faulting and stratigraphy. The interval of interest has been highlighted.*

Most of the mapped faults in the area trend in a NW-SE direction and are generally normal in nature. The major basin-bounding Superior fault is interpreted to be listric and believed to have formed because of reactivation of Pre-rift compressional lineaments during the first rift period, as discussed in Chapter 2. The associated faults are a series of antithetic and synthetic faults and predominantly show increasing offsets with depth. Late reactivation of the basin is inferred from the minor folding and fault offsets of the early drift/post-rift sequences. Furthermore, structure-contour maps were produced depending on the interpretations for the interval of interest. The maps are one of the most important tools for structural characterization of this interval as they represent the full 3D form of the mapped top and base horizons (Fig. 4-2).

A)

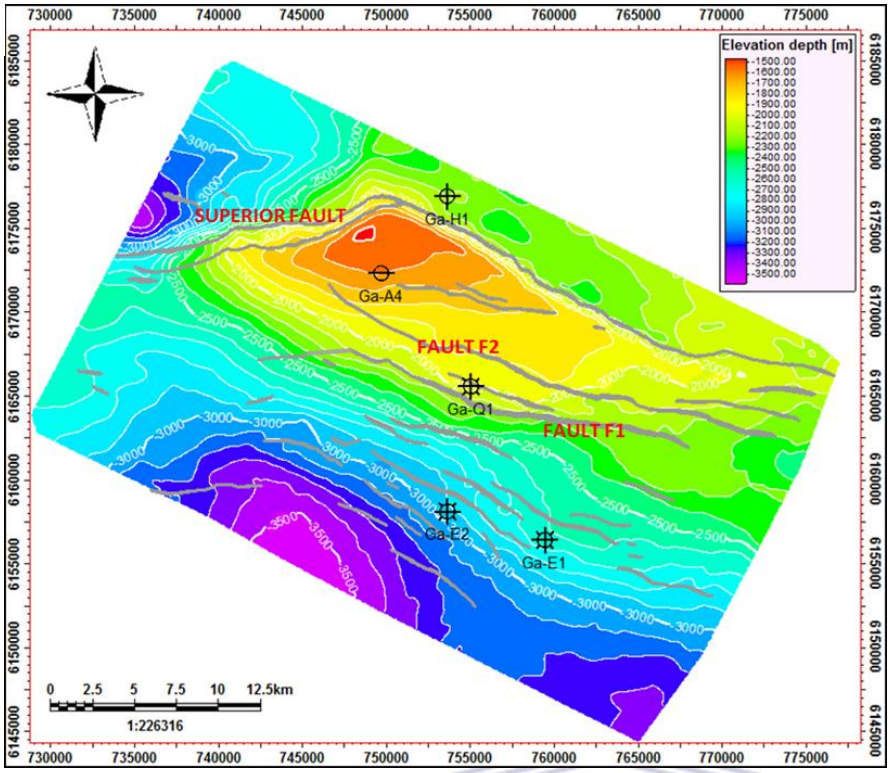

B)

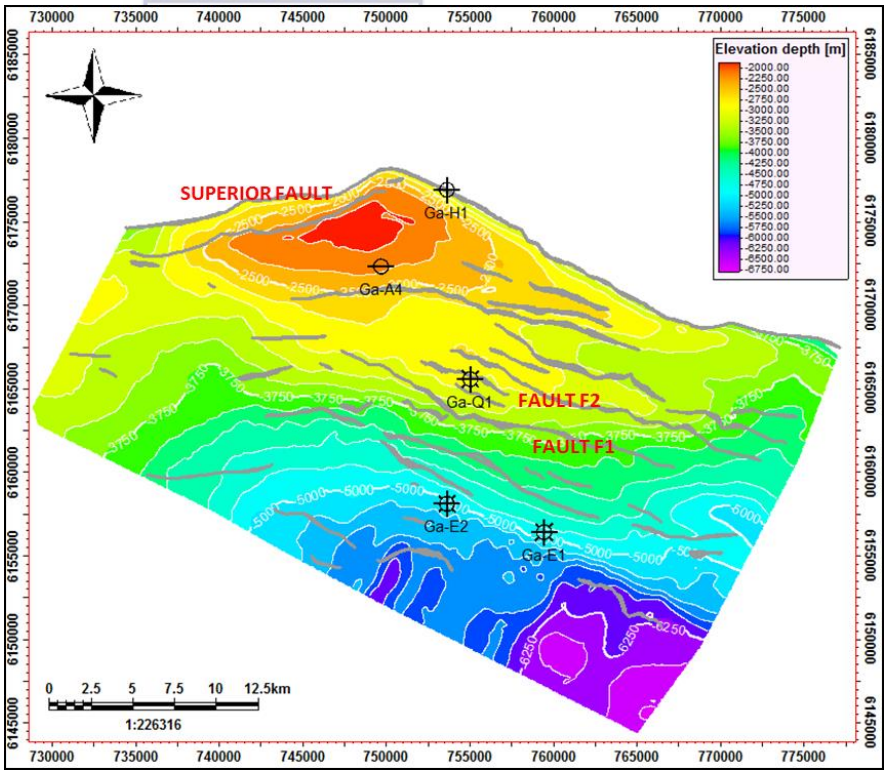

Figure 4-2: *Depth-structure maps for* ***a)*** *1At1 and* ***(b)*** *Horizon D. The key faults have been labelled.*

The structure-contour maps (Fig. 4-2) show the Superior Fault towards the north and a couple of sub-parallel faults which have been named F1 and F2. The two faults lie on either side of the Ga-Q1 well towards the centre of the mapped area and are both dipping southwards (see Fig. 4-1). The *circa.* 22 km long Fault F2 bounds the Ga-Q1 non-commercial gas discovery in the north and Fault F2 bounds the proposed Ga-K prospect on the updip section and extends for approximately 23 km (Roux, 1997; see Fig. 2-6; Fig. 4-3). The other faults are minor synthetic and antithetic faults which only extend up to ~25% of the entire length of the mapped area.

A)

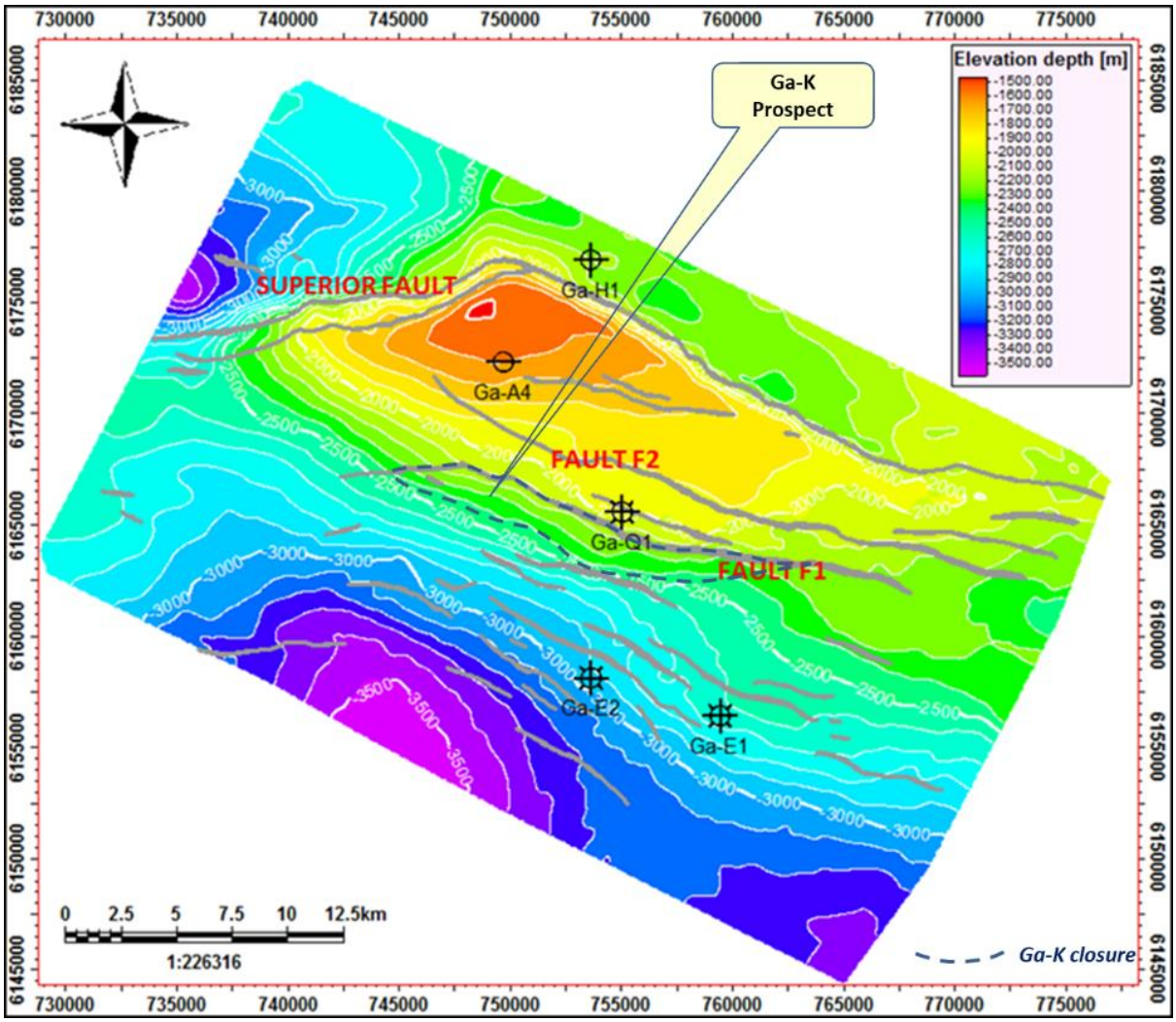

B)

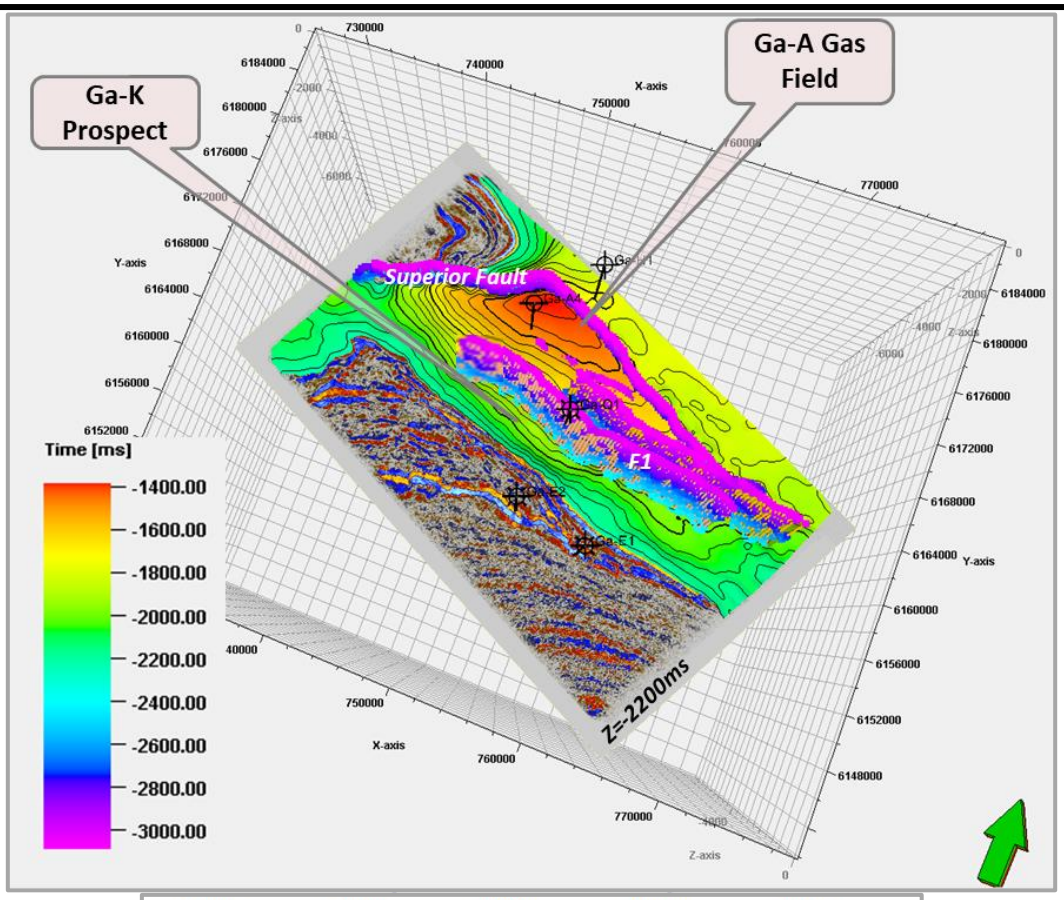

C)

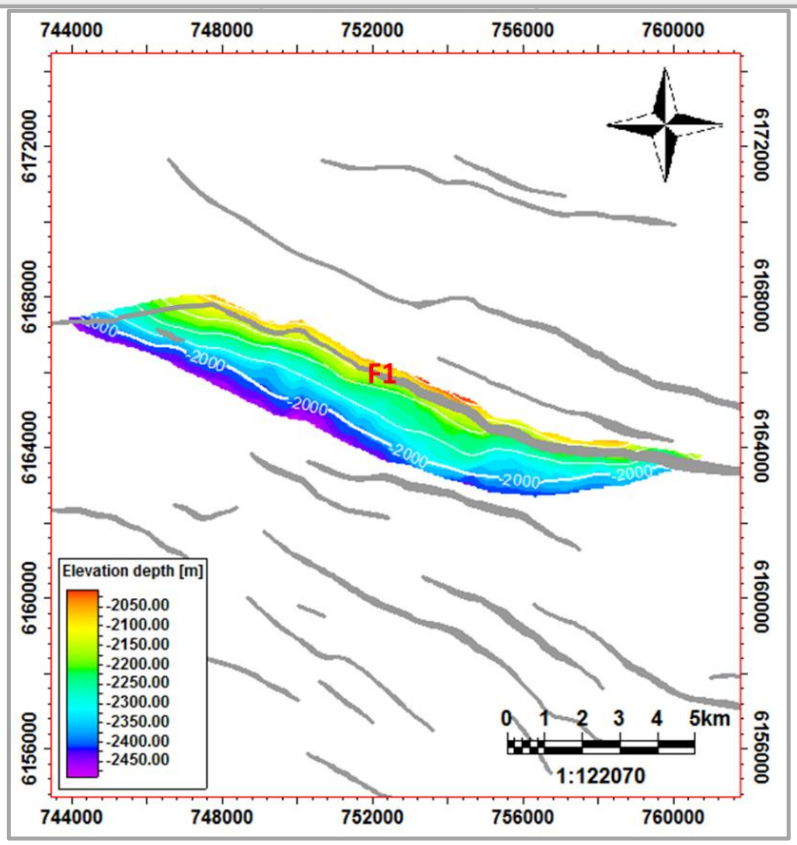

Figure 4-3: a) *Top 1At-1 map with the Ga-K prospect superimposed* ***b****) perspective view showing the Ga-A gas field and the Ga-K prospect and the major bounding faults* ***c****) Ga-K prospect map.*

4.2. GEOLOGICAL CHARACTERIZATION

4.2.1. Structural and Stratigraphic Framework

Presented below is the tectono-stratigraphic framework, or otherwise the 'container' within which the geological properties were populated.

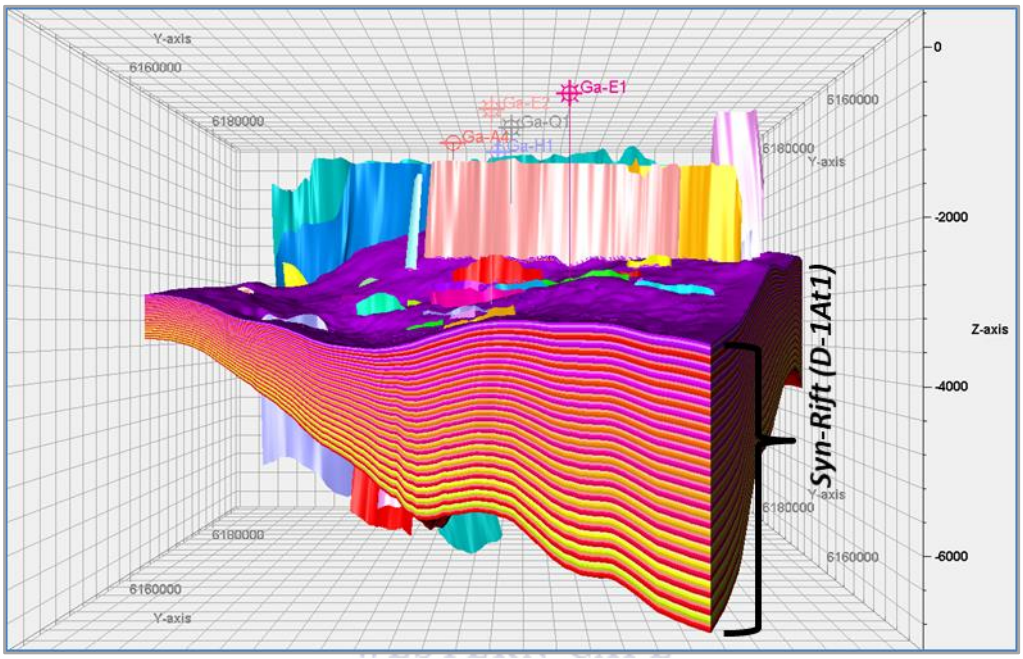

Figure 4-4: *Tectono-stratigraphic framework for the syn-rift zone (view directly from the south). Note that a hundred grid layers were created to model rapidly varying host rock properties within the stratigraphic succession.*

4.2.2. Parameter and Property Models

So far, the 3D structural and stratigraphic model (Fig. 4-4) has depicted the structural configuration and internal layering of the interval of interest. However, at this point the grid is still empty. Accordingly, presented here are the simulated facies and petrophysical models. The study wells are included for perspective.

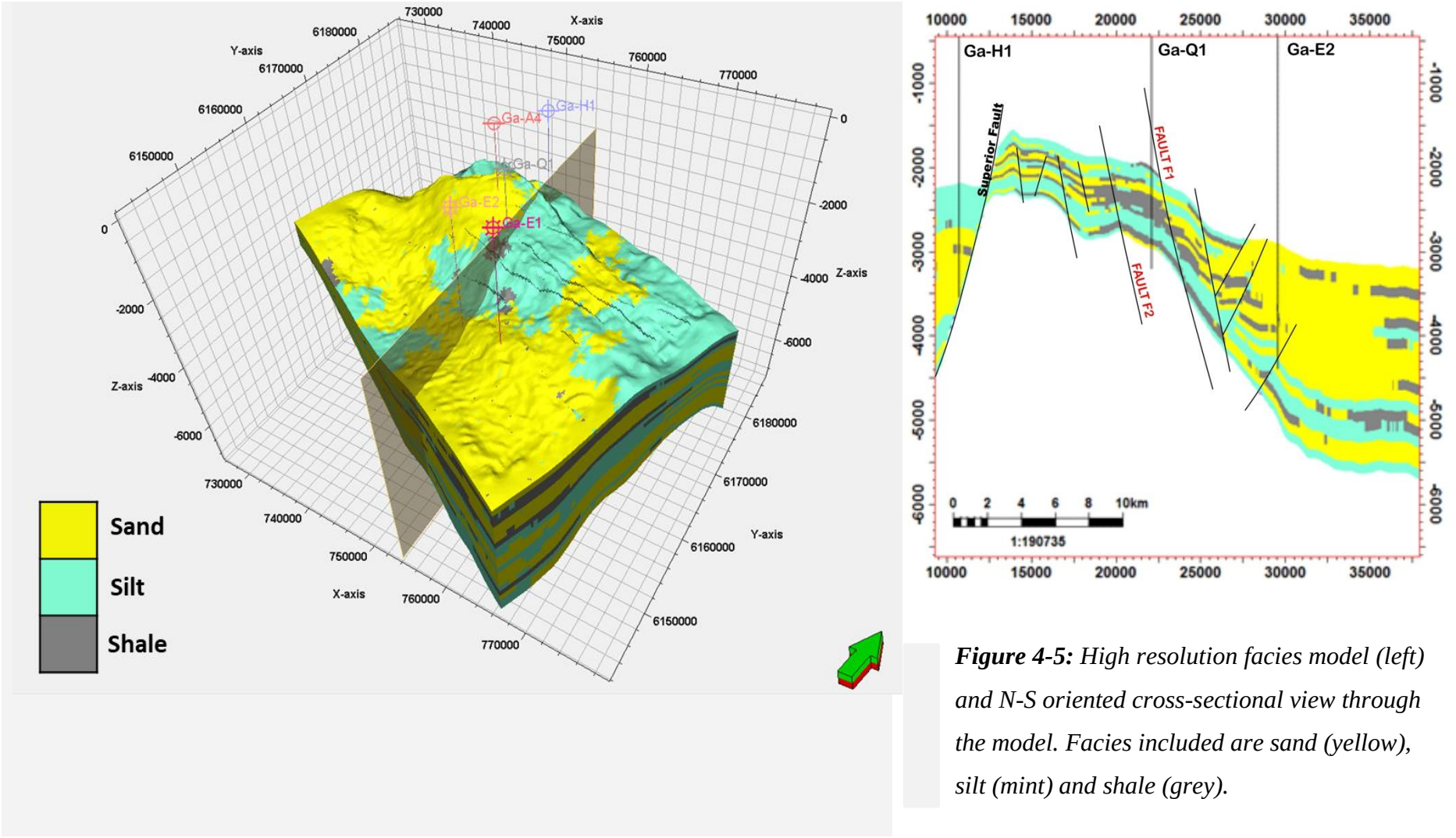

Figure 4-5: *High resolution facies model (left) and N-S oriented cross-sectional view through the model. Facies included are sand (yellow), silt (mint) and shale (grey).*

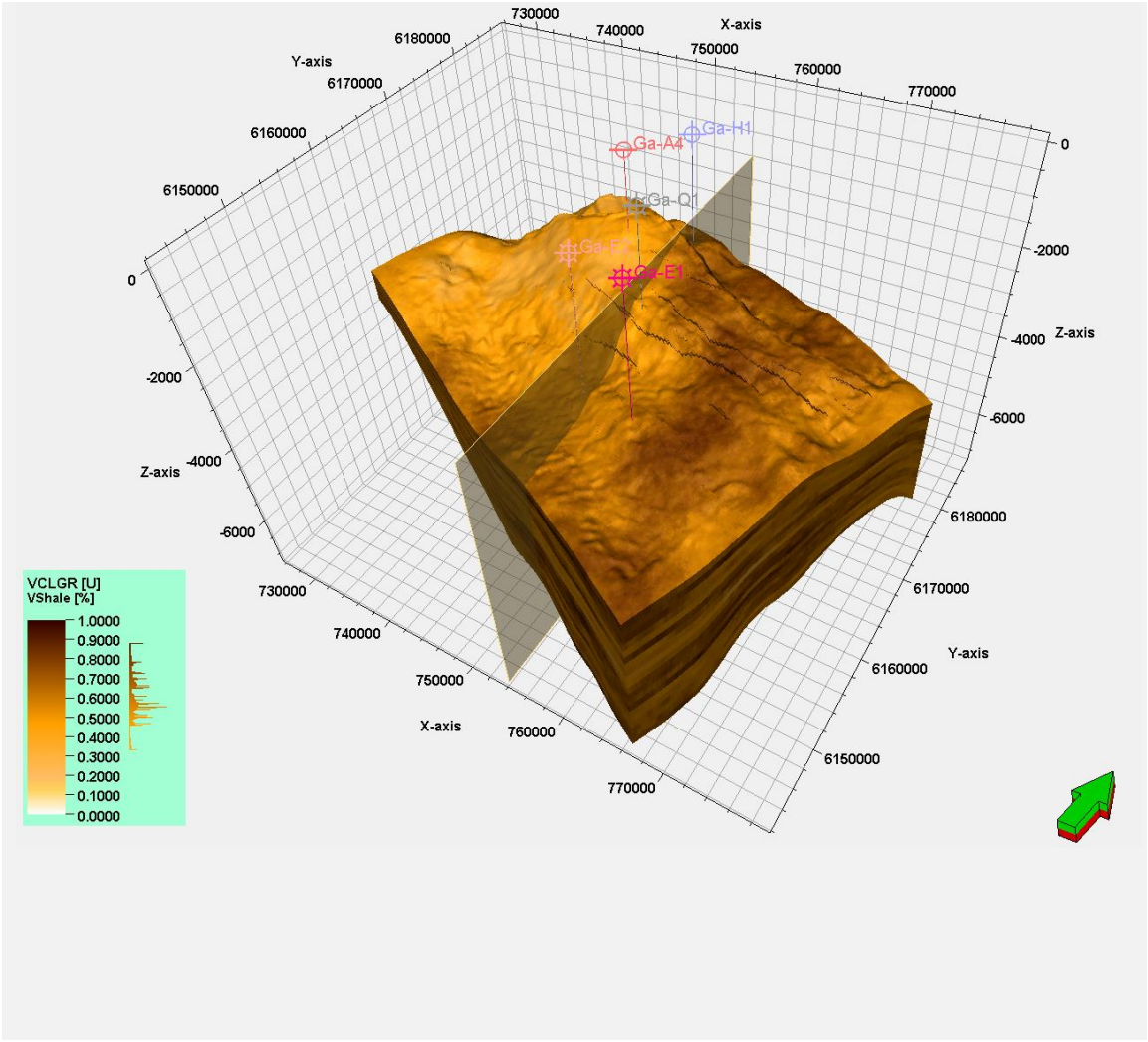

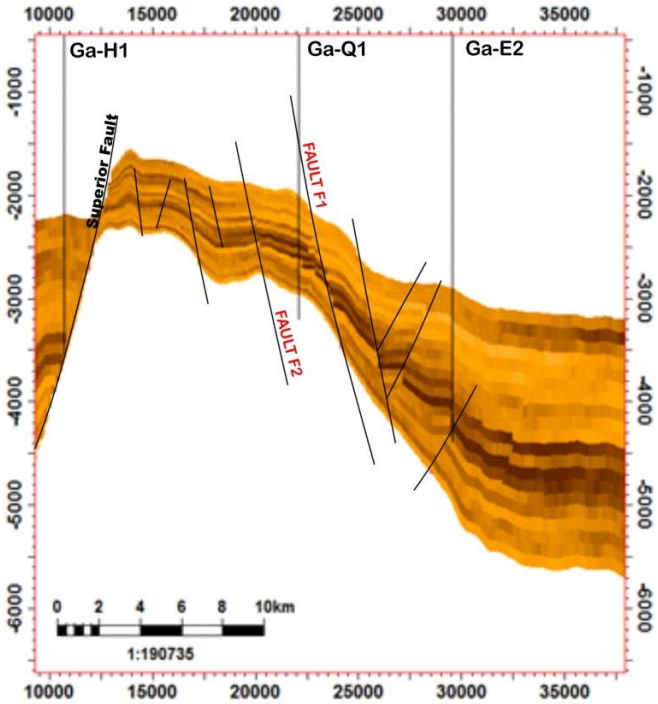

Figure 4-6: *Volume of shale model and N-S oriented cross section (right). The darker colours correspond to shale facies and the lighter colours to the sandstone facies.*

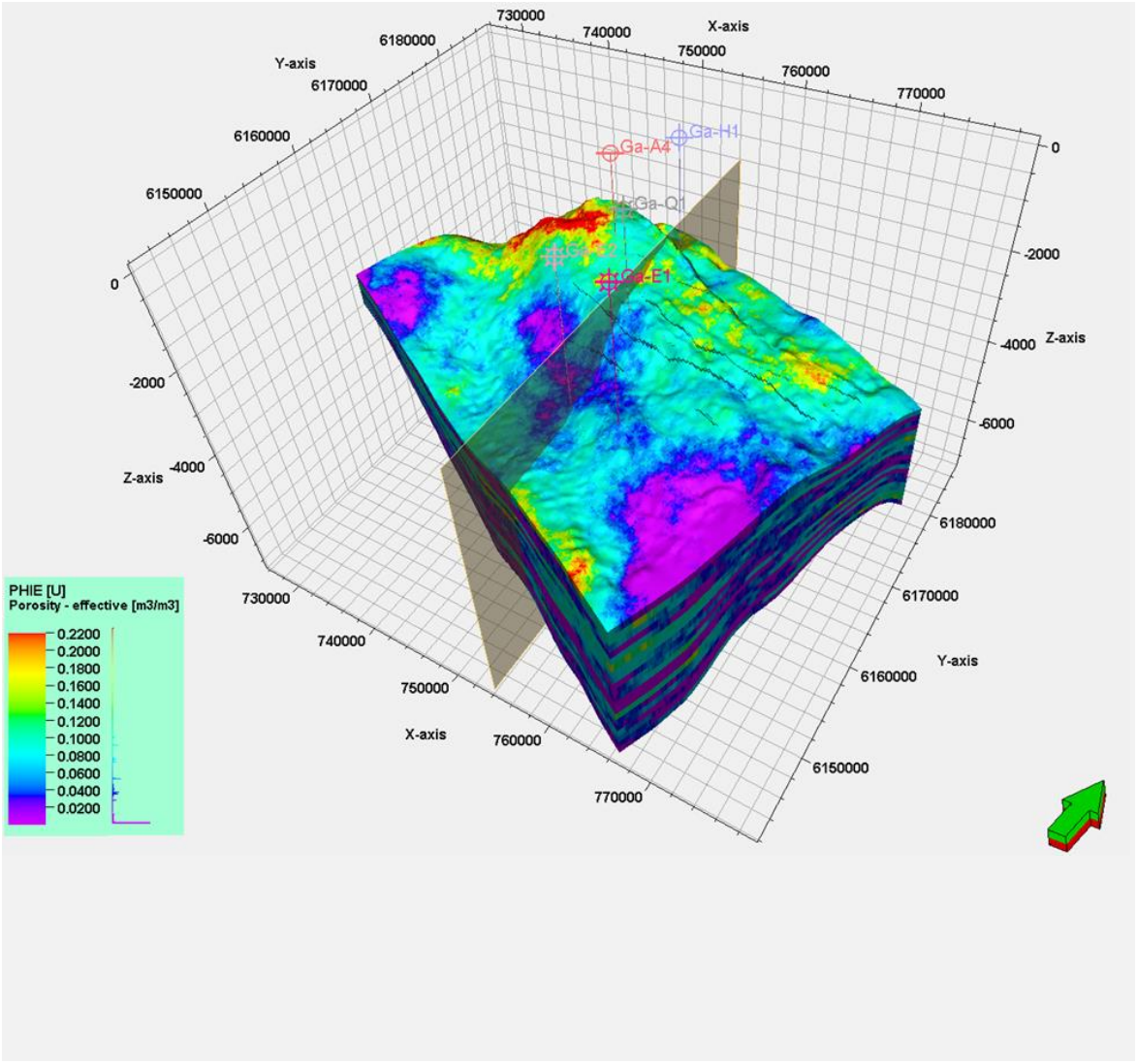

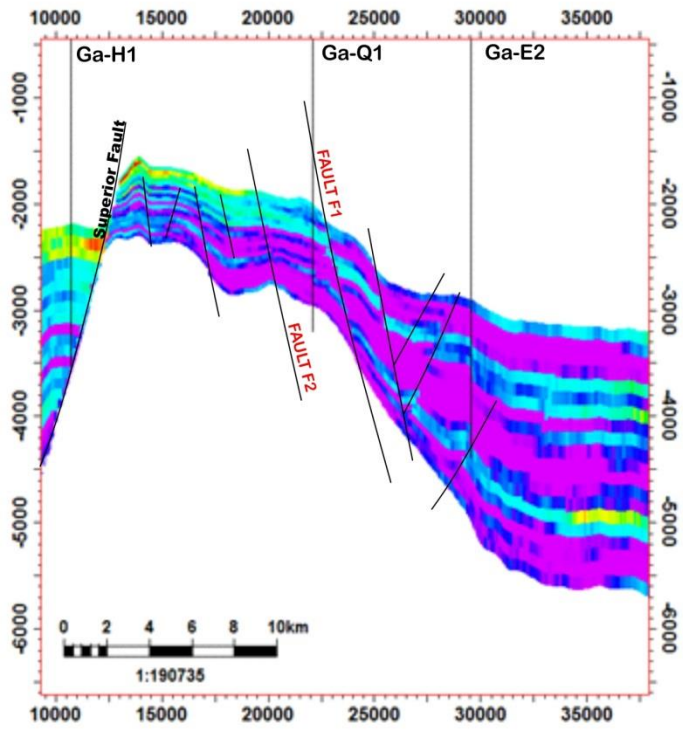

Figure 4-7: *High resolution porosity model (left) and N-S oriented cross-sectional view through the model. Porosity values range from 0 (purple) to 0.22 (22%) (red).*

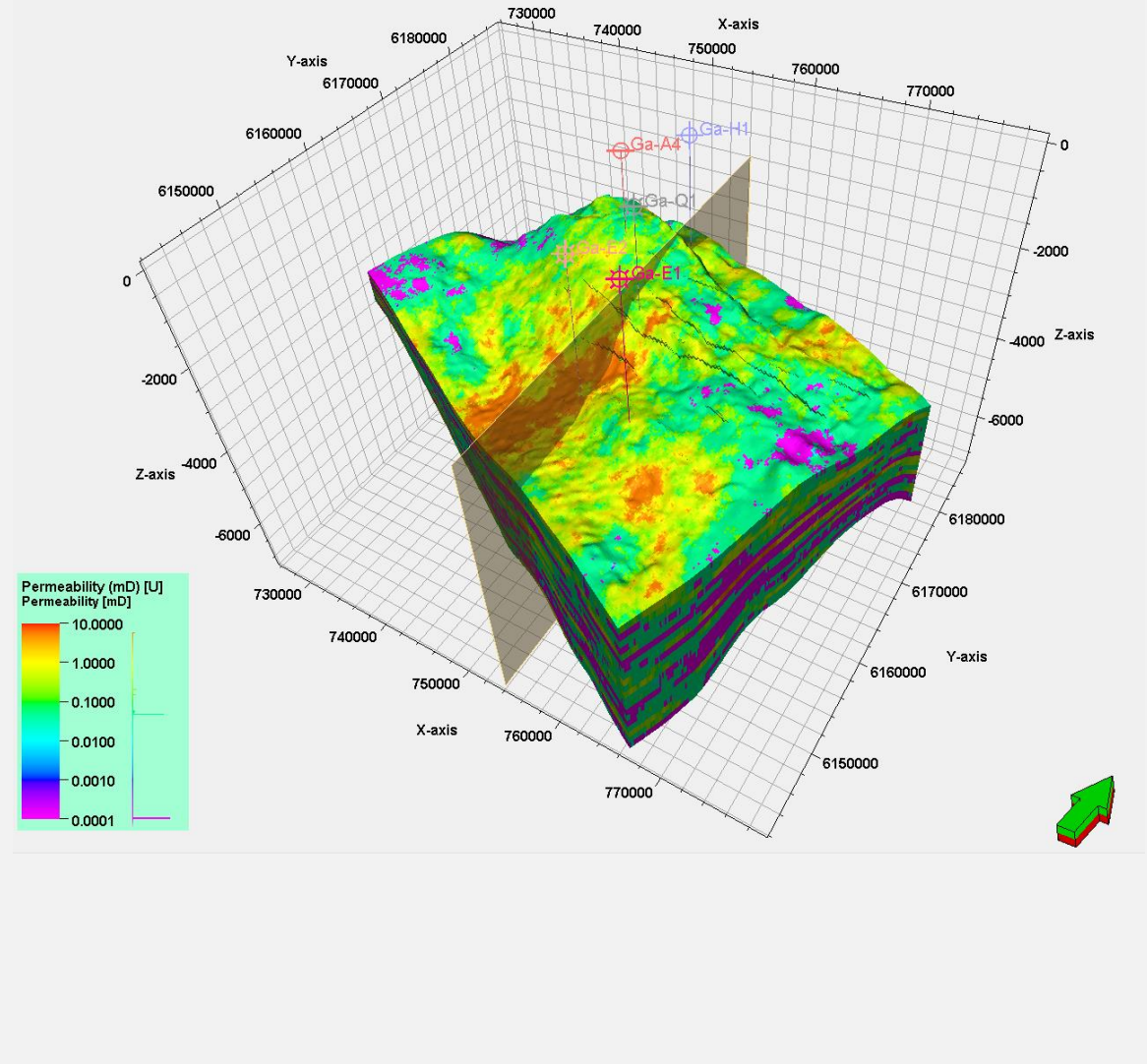

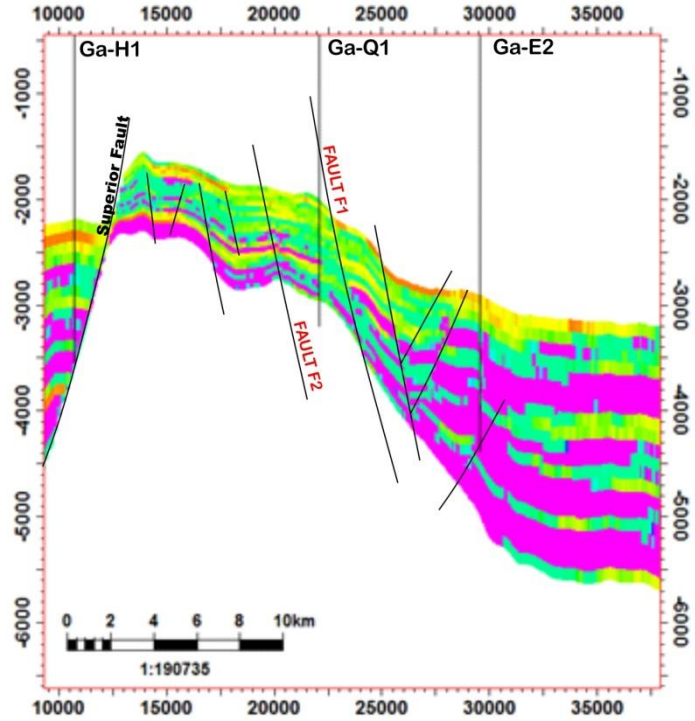

Figure 4-8: *High resolution model and cross section view through it (right). Permeability values range from 0.0001 (purple) to just less than 10 mD (dark orange).*

The facies model conditioned to well observations using Sequential Indicator Simulation (SIS) is presented in Figure 4-5. The term facies in this case is interpretive and refers to the lithology and rock type. Three facies types were identified based on their wireline log signatures and core descriptions (Chapter 3).

The facies model illustrates the geometry of the different rock bodies within the syn-rift reservoir interval. Based on statistical analysis, the modelled interval is predominantly sand (~50%) with some silt (~37%) and minor shale (~13%). Particularly of interest is the sand. The reason being that it is the most likely to have better porosity and permeability properties. The sand is thickest in the southern portion of the area and becomes thinner towards the north above the Superior High, as represented in the cross-sectional view (Fig. 4-5). The shale and silt layers are the thinnest units, but the silts are rather laterally extensive across the mapped area.

Figure 4-6 presents the Volume of Shale (VSh) model for the interval. The delineated volume of shale ranges between ~35% and 85% with the lower end corresponding to the sandstone facies (Fig. 4-5). Moreover, the established sandstone zones (Fig. 4-5) contain the vast majority of higher porosity cells (Fig. 4-7) compared to the other facies types. Average porosities in sand within the modelled area are approximately 11%.

Nonetheless, around the well-constrained areas in Figure 4-8, intuitively it is clear that the permeability largely depends on the porosity and is closely related to the different facies types.

4.3. 1D WELL TRIANGULAR JUXTAPOSITION MODELS

As aforementioned, the initial assessment involved the creation of triangle juxtaposition diagrams (Fig. 4-9). The diagrams deliver an estimation of the host rock lithology juxtaposition as a function of the fault throw.

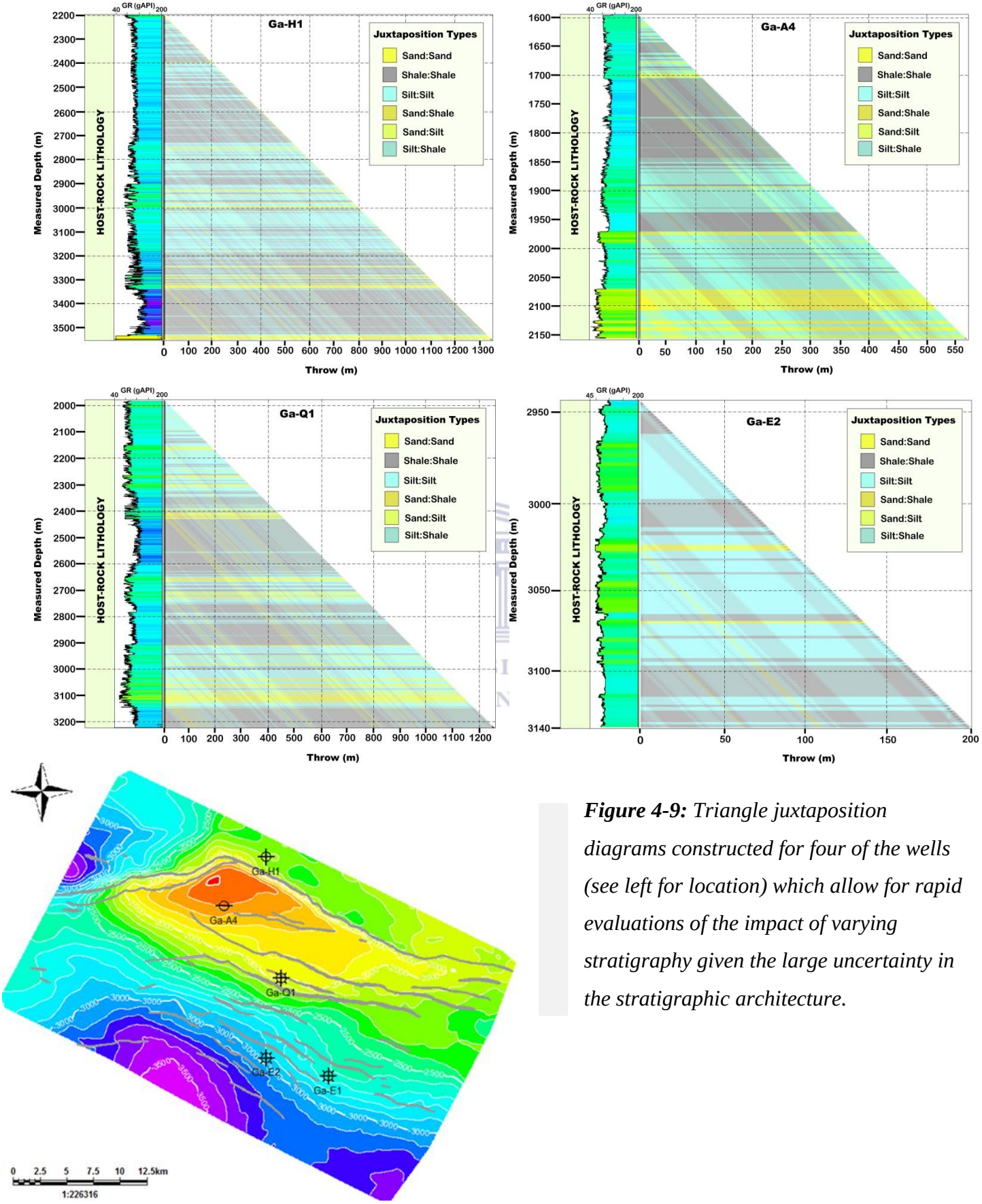

Figure 4-9: *Triangle juxtaposition diagrams constructed for four of the wells (see left for location) which allow for rapid evaluations of the impact of varying stratigraphy given the large uncertainty in the stratigraphic architecture.*

There are six key juxtaposition types likely to occur within the interval of interest as illustrated by Fig. 4-9. It can also be deduced that the interval is characterized by complex stratigraphic layering; intercalated layers of sand, silt and shale. The diagrams also serve as a tool to identify depth ranges of potential leakage/sealing points expected along the faults in the area. For instance, Ga-Q1 shows the possibility of self-juxtaposed (sand-sand) windows at around 2300 m, 2700 m and 3100 m depths.

Having displayed the key juxtapositions present within the interval of interest, the following section will present the fault plane maps created to describe the faults in the geo-cellular model on the basis of the fault rock physical properties.

4.4. FAULT ROCK PROPERTIES

Fault rock physical property analysis was carried out in order to quantify the petrophysical properties of the mapped faults within the area of study. To avoid a cumbersome presentation this section simply presents the fault plane maps along two of the main prospect-bounding faults (F1 and F2).

4.4.1. Potential Fault Seal Integrity

Fig. 4-10 a) shows the juxtaposition display of facies along the faults, based on the stochastically simulated facies model. The dark blue zones show the sand-sand juxtapositions; these have been extracted in Fig. 4-10 b). What stands out on Fig. 4-10 b) is that the sand-sand juxtaposition windows, the so-called leaky points are predominantly concentrated on the top half of the fault planes. Moreover, the extracted juxtaposition windows are in line with the expected locations based on the 1D triangle diagrams (Fig. 4-9) with respect to the measured depth. Where this does not apply, the discrepancy can be attributed to lateral facies changes within the syn-rift interval.

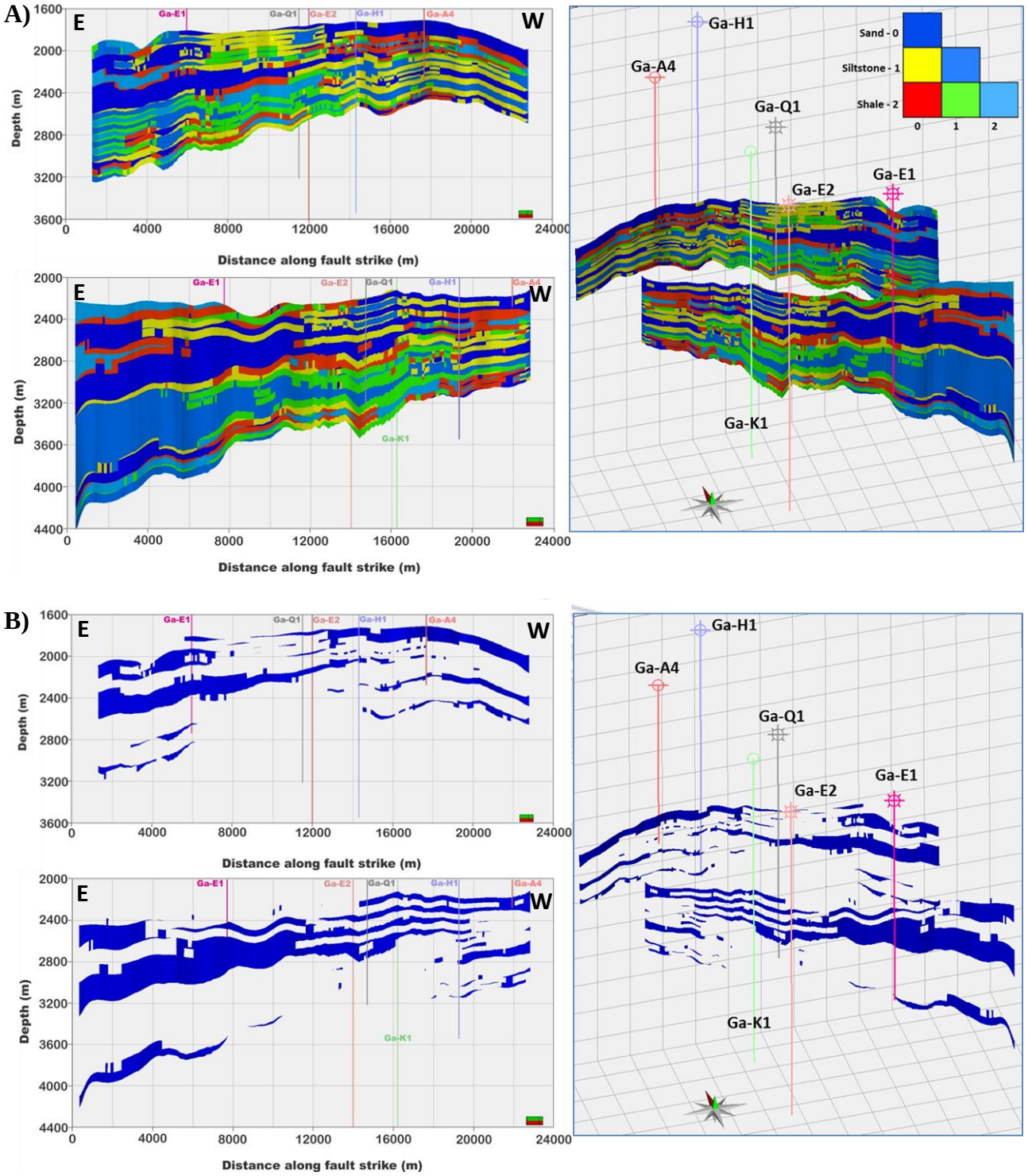

Figure 4-10: a) *Facies Juxtaposition diagram; the fault face has been colour coded according to the unique colours for the specific juxtaposition types developed (see detailed explanation of colour triangle in Appendix C.,* ***b)*** *self-juxtaposed windows extracted along the fault. The vertical lines are the projections of the study wells. Uncertainty increases away from the wells.*

A more accurate way of estimating the leakage potential is the derivation of the Shale Gouge Ratio (SGR) along the fault planes. Figure 4-11 presents clay content distribution based on the VSh model, smearing and clay mixing models. The property has been colour-coded according to the SGR. Orange and yellow colours indicate low SGR and blue colours indicate high SGR. It is evident that for the most part, the highest SGR values correspond to shaly zones within the interval and vice versa.

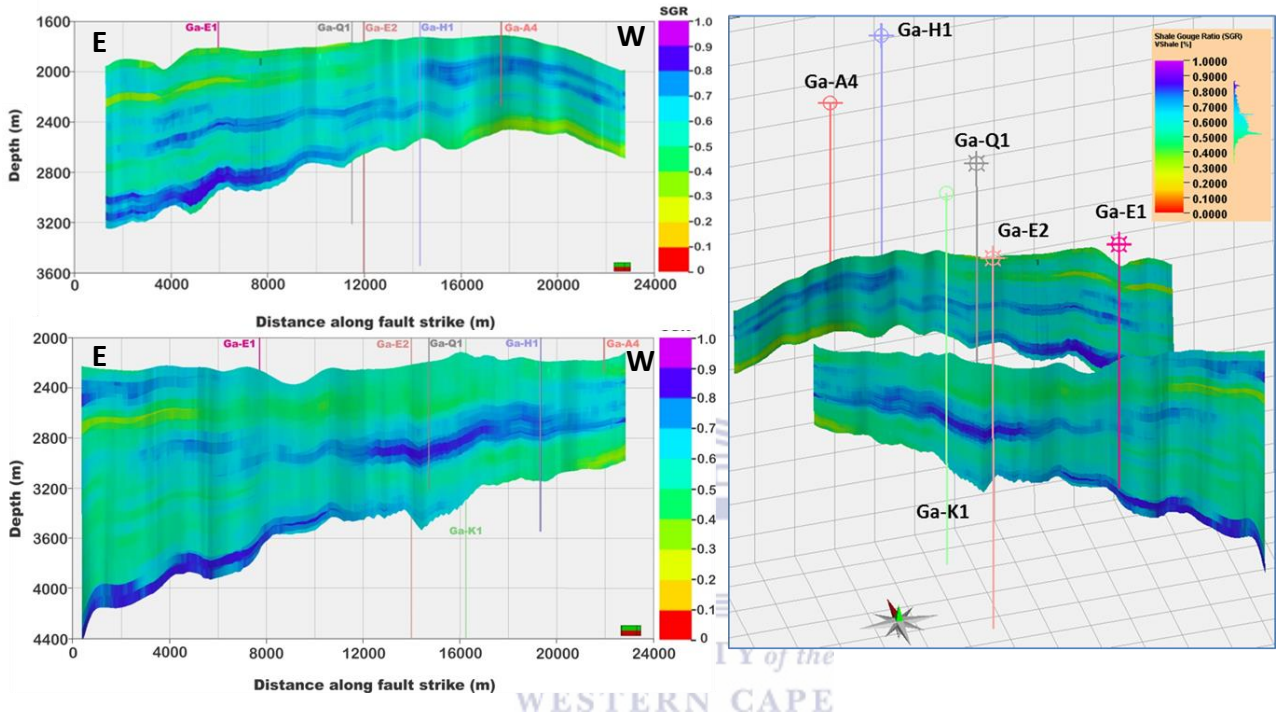

Figure 4-11: *Fault clay distribution defined by the Shale Gouge Ratio.*

4.4.2. Factors Limiting Hydrocarbon Accumulation - Seal Capacity

The threshold pressures calculated from a global trend are presented in Figure 4-12 a). Figure 4-12 b) presents the resultant hydrocrabon column heights and Figure 4-12 c) presents the contact depths – that is, the theoretical hydrocarbon contact depth at every cell along the fault plane.

A)

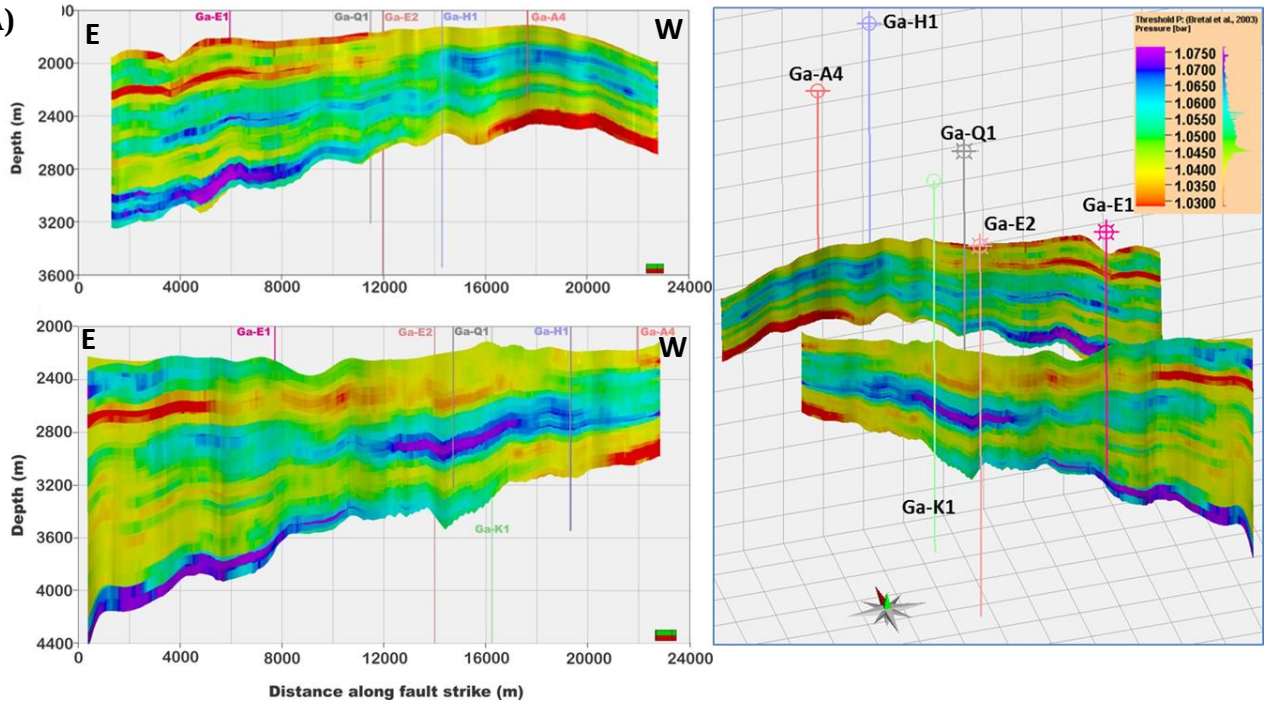

B)

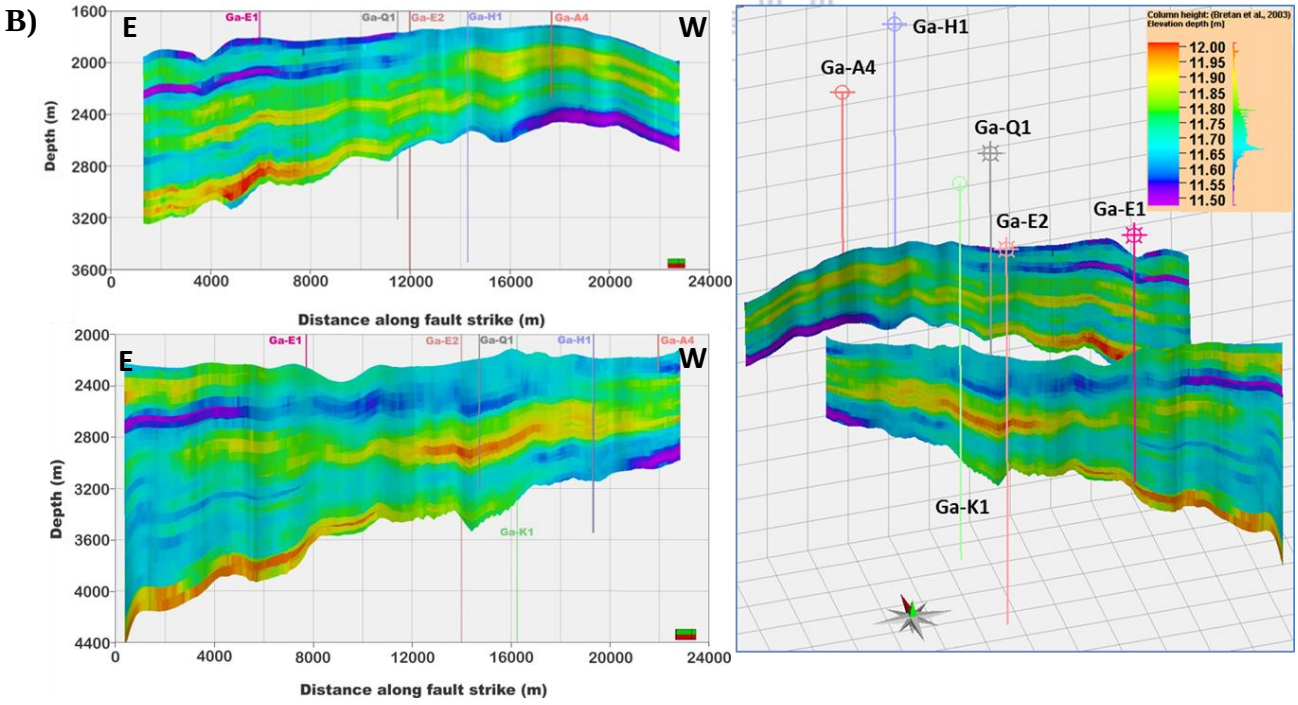

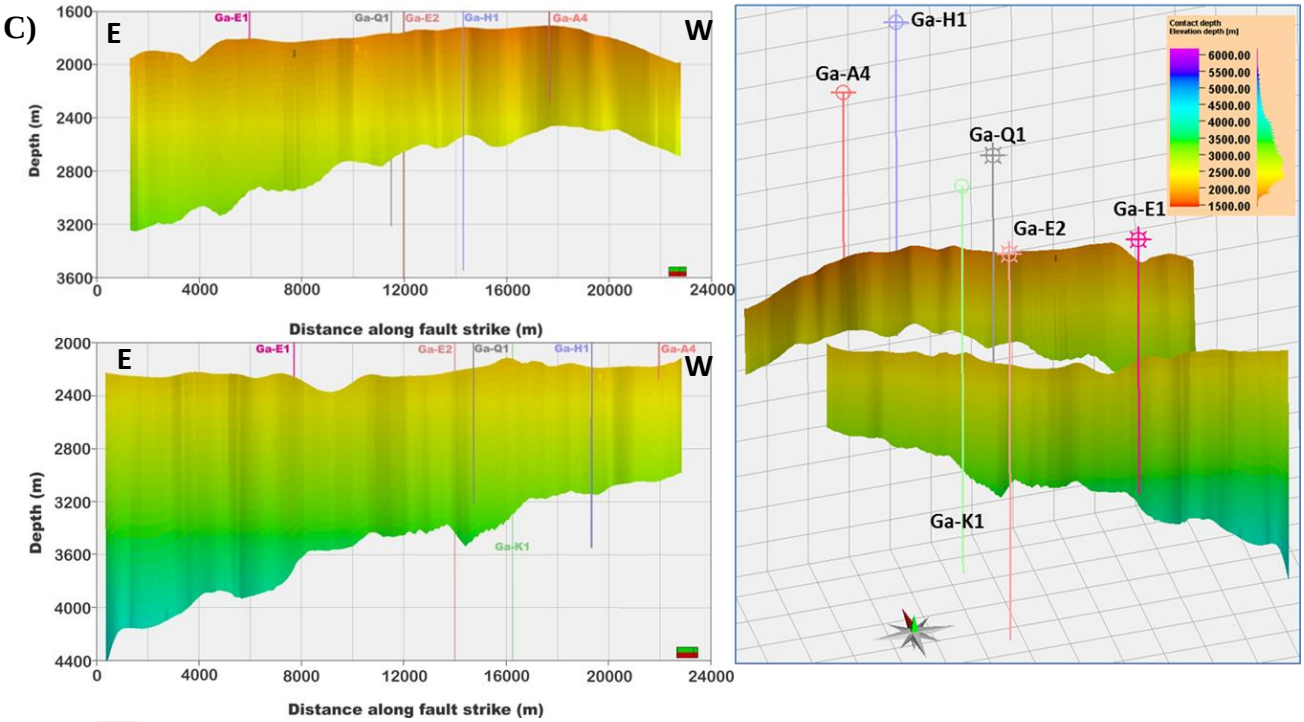

Figure 4-12: a) *calculated threshold pressures* ***b)*** *predicted hydrocarbon column heights and* ***c)*** *contact depth estimations along the fault plane.*

All threshold pressure values are slightly in excess of 1 bar (i.e. 1.030 – 1.075 bar). It is interesting to note that the highest predicted threshold pressures (indicated by colours ranging from dark blue to purple) correspond to the high SGR zones (Fig. 4-11) and the reverse is also true. Further, the potential hydrocarbon column heights range between 11.5 – 12 metres and they are seen to be lowest (blue colours) along the self-juxtaposed areas (Fig. 4-12 b) close to Ga-Q1 and Ga-K1.

The SGR property (Fig. 4-11) acted as a proxy in the estimation of the fault rock permeability, as outlined in Chapter 3. The computed permeability and thickness properties are presented in Figure 4-13 a) and b), respectively. It can be observed in Figure 4-13 a) that the predicted fault rock permeability has a strong correlation with the fault clay content (with higher clay contents corresponding to low lognormal permeabilities).

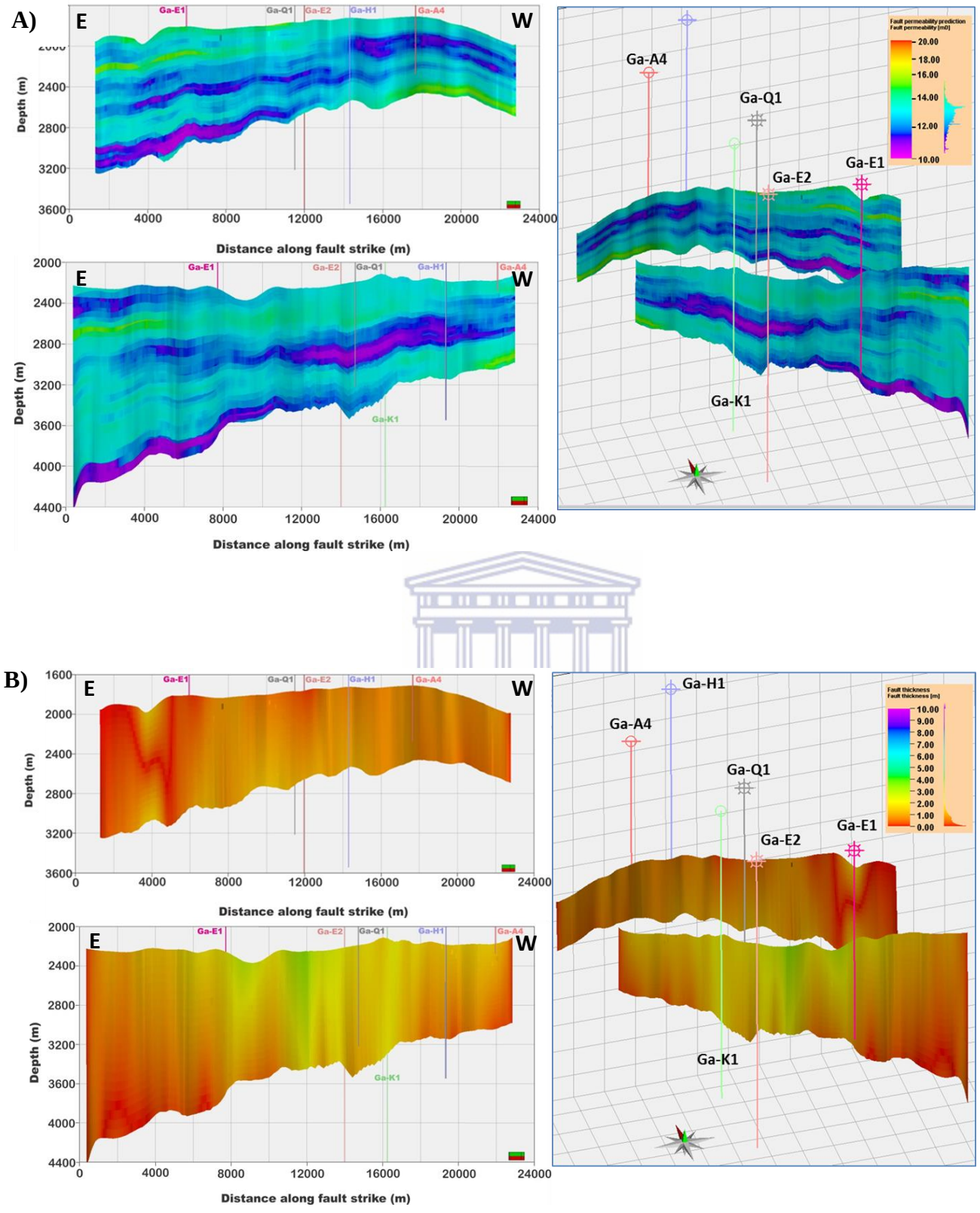

Figure 4-13: a) *Interpolation of fault rock permeability across the fault plane* ***b)*** *Fault thickness estimation (from fault displacement).*

Figure 4-14 shows the assignment of fault transmissibility multipliers (TMs). The TM values displayed on the Figure were based on the combination of fault rock permeabilities and thicknesses (Fig. 4-13 a) and b)) coupled with the grid cell sizes of the geo-cellular model. Red colours indicate fault transmissibility values of zero – completely sealing zones; green colours indicate transmissibility values of one – no impact on fluid flow. Note that some TM values are above 1, as indicated by the blue colours (close to the well). This implies that the fault rock has a greater permeability than the host rock at those particular zones.

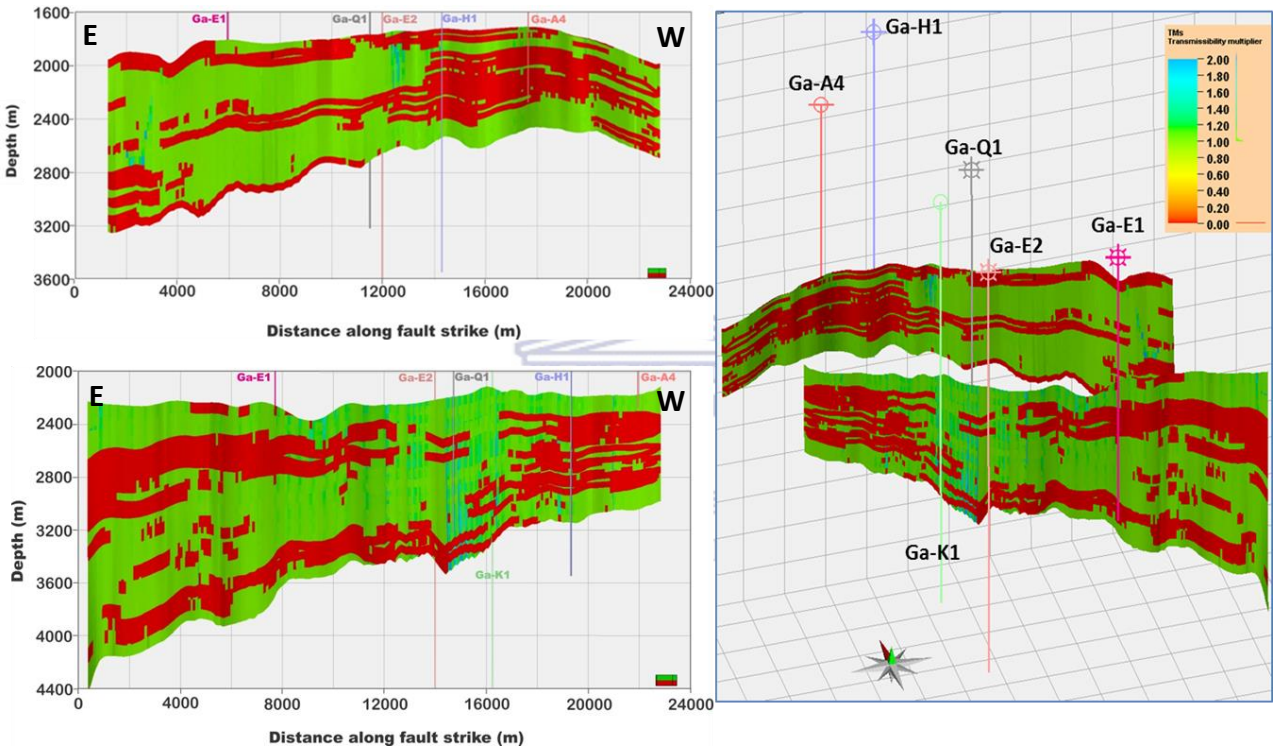

Figure 4-14: *Computed fault transmissibility multipliers across the fault.*

Based on Figure 4-11 and Figure 4-14, the relationship between the computed TM values and the SGR is complicated; there is no clear link between the SGR value and the predicted TM value. To provide a more suitable means of assessing the variation in likely cross-fault fluid flux, the Effective Cross-Fault Permeability (ECFP) and Effective Cross-Fault Transmissibility (ECFT) are presented in Figure 4-15.

The ECFP generally mimics the trends observed in the TMs, with the lowest permeability values corresponding to TM values of zero. The ECFP has a range of values from ~0.0001 mD (purple) to ~ 10 mD (red) on a logarithmic scale. Similarly, the ECFT is high at these zones. Notably, the ECFP and ECFT can be closely correlated with each other.

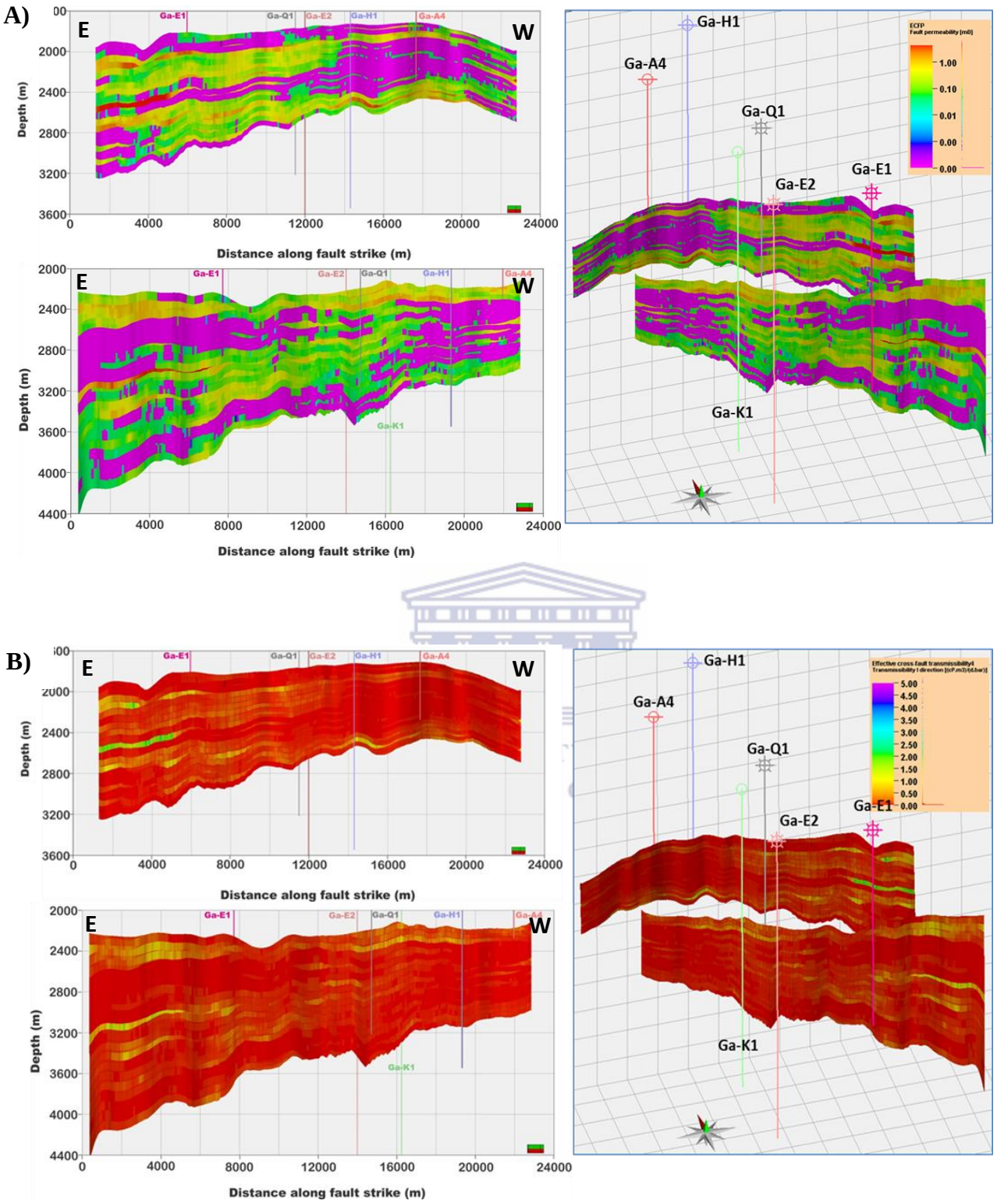

Figure 4-15: *Cross-fault fluid flow properties;* ***a)*** *Effective cross-fault permeability (ECFP) and* ***b)*** *Effective cross-fault transmissibility (ECFT) in cP.m^3/day/bar units.*

4.4.3. Burial History Models

The model was calibrated using Static Bottom Hole Temperatures. Success of calibration was tested through a reasonable match between computed and present-day measured well temperatures (Fig. 4-16).

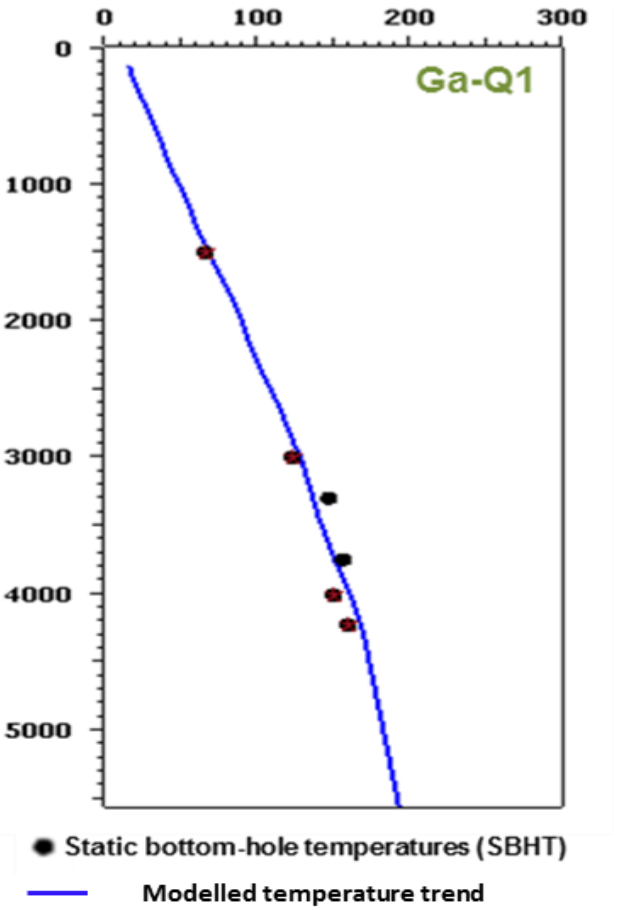

Figure 4-16: *A comparison between the modelled/calculated (blue line) and the measured (circles) SBHT measured during logging.*

The geo-history diagram (Fig. 4-17) illustrates that there have been several burial and subsequent uplift-erosion episodes since the Late Jurassic. Of the most relevance to the study is the recent Miocene uplift at ~10Ma. Furthermore, the fluctuations in paleo-temperatures are observed to have occurred due to these events. The highest paleo-temperatures are seen to have occurred between the early Lower Cretaceous and late Upper Cretaceous (Campanian). This can be attributed to the combination of increased sedimentation rates and the basal heat flow due to the commencement of drifting in the basin and the Shona-Buvet hotspot event, respectively (Davies, 1997; Fig. 4-17). Temperatures at the base of the 1At1 interval reached values of up to 160 ^{0}C and a maximum burial depth of 3600m.

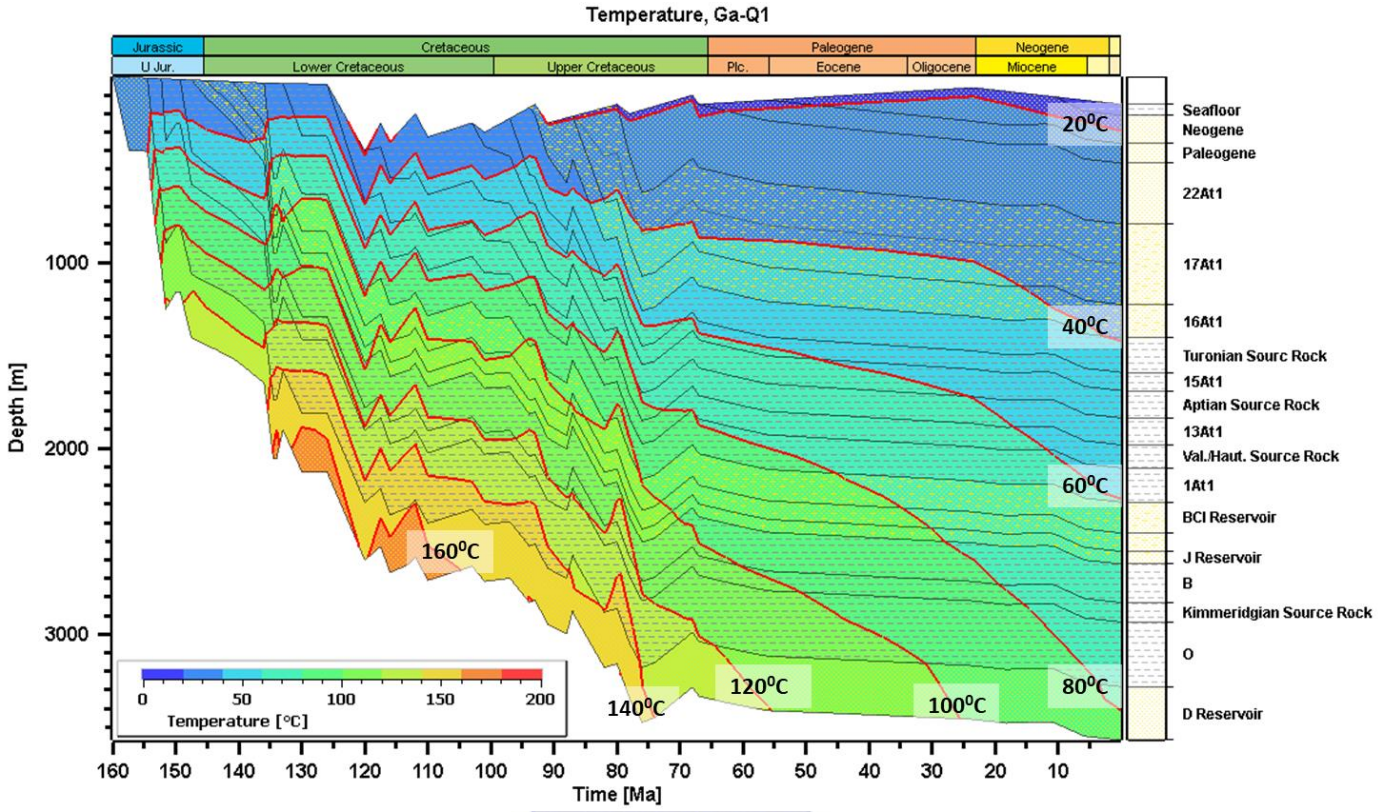

Figure 4-17: *Geo-history plot superimposed using the calculated temperature history obtained from the 1D-modelling of the geological evolution of the Ga-Q1 well within the southern Pletmos Basin. The red lines indicate the main temperature isolines (20, 40, 60 ^{0}C etc.). The simulation began at 160 Ma and continued until present-day.*

Figure 4-18 exemplifies the effects of confining pressure (overburden) on the porosity. With increasing overburden, the effective porosities for the assigned lithologies show a reduction. Generally, the shale facies ('source rocks') show a greater reduction in the porosities compared to the sand facies ('reservoirs'). The highest present-day porosity for the 1At1-D interval ranges between 19.04 – 23.80 % and is recorded in the reservoir sands around 2300 m.

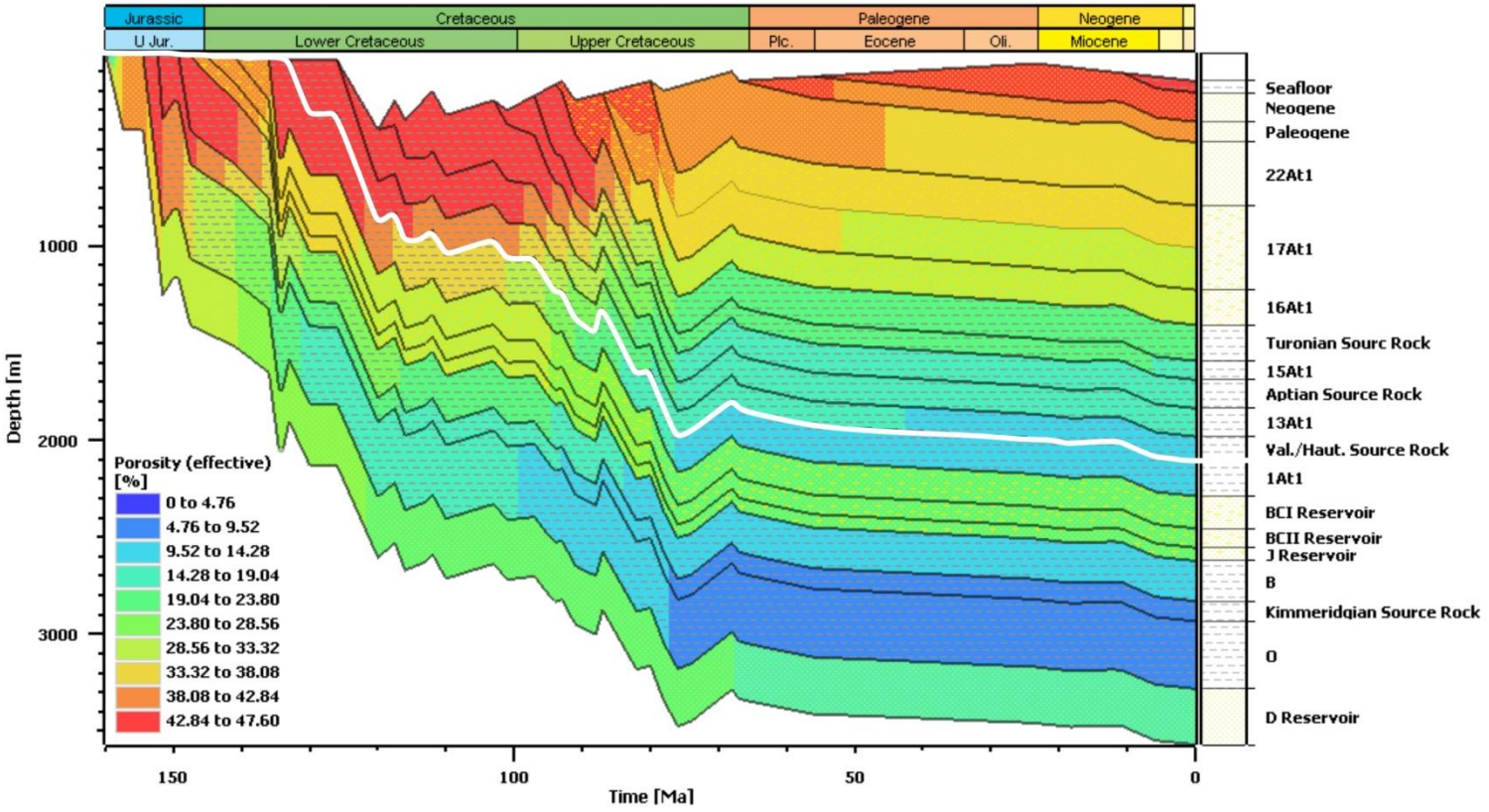

Figure 4-18: *Porosity evolution of the assigned lithologies as function of geologic time (proxy for stress history).*

5

Discussion

5.1. INTRODUCTION

This study has set out to assess the impact of faulting within the main reservoir interval in the southern Pletmos Basin. Identification of the leakage (or seal) points along major prospect-bounding faults is a vital tool for future play and prospect assessments and may improve the current understanding of hydrocarbon migration and entrapment in the basin. In this study, a multidisciplinary approach was employed to construct a comprehensive three-dimensional geo-cellular model. Through a combination of juxtaposition and fault-rock property analyses, the sealing nature of the faults has been systematically analysed. Well Ga-Q1, Ga-K1 and Fault F1 and F2 provided the focal point for illustrating the findings.

5.2. GEO-CELLULAR MODEL DESCRIPTION

The 3D geo-cellular model developed and presented in this thesis illustrated that sandstone facies within the reservoir interval are characteristically impure with high clay contents (VSh > 30%). Moreover, most porosity values are not high enough for the sands to qualify as clean sands (Fig. 4-6). When faulted such impure sandstones are likely to develop phyllosilicate framework fault rocks or clay smears (Knipe *et al.*, 1997; Fisher and Knipe, 1998; Fig. 2-10), and are likely to impact on sealing behaviour in a way that prevents fluid flow across fault zones (Knai and Knipe, 1998). Since permeability assignment for the model layers was based on log derived porosity-permeability transforms, it is not surprising that the permeability values are mostly on the lower end of the spectrum with the highest modelled permeability values corresponding to sand facies (Fig. 4-7). Surprisingly, the lowest interpolated permeability values do not necessarily correspond to shale facies. This may be attributed to the sparse core data used in the computation of the permeability curves.

5.3. FAULT SEAL POTENTIAL

The seal potential of the faults was predicted using 1) triangle juxtaposition diagrams (Knipe, 1997), 2) fault plane sections that depict the juxtaposition of lithologies on both sides of each fault (also called Allan maps; Allan, 1989), and 3) a proxy algorithm Shale Gouge Ratio (Yielding *et al.*, 1997).

The results of the triangle juxtaposition analysis revealed six possible juxtaposition types based on the stratigraphy. Of these, three are important unless other factors come into play. These are: sand-sand (open to flow), shale-sand (totally sealed), and sand-silt (partially sealing/flow baffling). It is evident on these diagrams that the range of leak points, particularly for Ga-Q1, is extremely small. This is further supported by the extracted fault plane sand-sand juxtaposition windows along F1 which were deterministically identified (i.e. depict a single stratigraphy that is presumed to correctly represent the actual stacking of reservoirs and seals). Notably, the stratigraphy was derived from well Ga-Q1.

Furthermore, the SGR values along the self-juxtaposed (sand on sand) zones were found to exceed 0.35. SGR values in excess of 0.3 (30%) across sand on sand windows along the faults suggest that they have a high probability of being sealed by shale gouge in the fault zone (Hock and Schulte, 2012). Thus, the SGR property significantly reduces the likely leak points along the faults. Intuitively, one would expect a higher likelihood of seal as high SGRs would theoretically mean that the fault would be sealing over geologic time (millions of years) and is capable of trapping considerable columns of hydrocarbons. However, despite the high SGRs, the fault can only be sealing for pressure differences up to the threshold pressure across the fault plane as suggested by Ottesen Ellevset *et al.* (1998) and Bretan *et al.* (2003).

5.4. FAULT SEAL CAPACITY

This process involved the calculation of some of the most important factors that limit hydrocarbon accumulation. Having said that, the results have shown that the computed threshold pressures for the faults presented in this study are in the range of 1.030 – 1.075 bar. This implies that cross-fault pressure differences that exceed this value would cause the fault seal to fail. In other words, threshold pressures of such low magnitudes indicate that these faults have a low capacity for sealing. Further, the predicted hydrocarbon column heights are in the range of 11.5 – 12 metres. This implies that the analysed faults may only support the pressure exerted by a 12m column yet leak if the column height increases.

As mentioned in Chapter 3, the ability of faults to seal (or retard fluid flow) is controlled by the combination of the threshold pressure and the fault rock permeability and thickness. Fault-rock permeability values predicted from the fault clay content are more than 10 mD on a lognormal distribution. As suggested by Knai and Knipe (1998), primarily for a gas field a cut-off permeability value of 0.1 mD can be used as a general seal/non-seal value in the reservoir model. For oil, a permeability cut-off of 1mD is used unless unusual circumstances apply (e.g. it is a fractured reservoir). Thus, seemingly the predicted fault-rock permeability is overestimating the fault leakage potential suggesting that this approach alone is not robust enough for the analysis of fault seal capacity. This is in accordance with findings by Freeman *et al.* (2010) who concluded that the Effective Cross-Fault Permeability (ECFP) should be used instead. This property, in conjunction with the Effective Cross-Fault Transmissibility (ECFT), provided transferable parameters that can be used to infer likely cross-fault fluid flux from the static geo-cellular model.

Notably, the majority of the ECFP values are below 1 mD. The ECFT values are predominantly zero, with a few values around 1.5 $cP.m^3/day/bar$. Under production conditions, these low permeability and transmissibility zones will generally lead to the compartmentalization of pressure distribution and hydrocarbon contacts across the faults (Jolley *et al.*, 2007).

5.5. EFFECTS OF GEO-HISTORY

The great burial depth of the reservoir interval (> 3 km; T > 90 ^{0}C), the high host rock clay content within the interval (> 30%), deep burial during deformation (~0 to 1800 m) favoured enhanced shale gouge in the fault zone, and may have promoted enhanced pressure solution on fault planes compared to the host sandstones (Fisher and Knipe, 1998). Furthermore, the geo-history and petrophysical analysis has permitted the fault rocks to be classified according to the possible deformation mechanisms involved in their formation as well as their present-day properties. The classification used is based on that of Knipe *et al.* (1997) reviewed in Figure 2-10. Seals present in the modelled area include:

1) Phyllosilicate/clay smears developed from clay-rich units
2) Phyllosilicate framework fault rocks developed from impure sandstones

What the above findings mean is that based on the local host geology, developed fault rocks in the area are expected to have a high degree of seal integrity. Faults with a high seal integrity are expected to be those associated with seals whose fine-grained material remains intact or

continuous (Castillo *et al.*, 2002). This is further supported by the high paleo-temperatures which likely led to deformation mechanisms that further enhanced the sealing potential of the major faults. This discovery raises the question of what could be the possible reason for the low threshold pressures and small predicted hydrocarbon column heights.

Assuming hydrocarbon source presence and effective migration pathways, successful charge and fill of fault traps would likely be possible if the fault zone seal material acted as an impermeable barrier that prevented further migration. It is hereby proposed that at some point during the basin's evolution, the hydrocarbons breached their seals resulting in underfilled and/or empty traps. It's important to note that if the fault becomes critically stressed with respect to the ambient stress field during the charge period or after being charged, there is a high probability that the fault will slip and rupture the lateral seal; thereby increasing fault zone permeability and enabling hydrocarbons to be discharged from the reservoir (Castillo *et al.*, 2002).

6

Conclusions, Implications and Future Research

6.1. INTRODUCTION

This research has explored how the major faults in the southern Pletmos Basin may impact the prospectivity of the basin. This study is important because it provides new insights into the fault seal integrity of the major prospect-bounding faults in the basin through the integration of all available data. This approach means that conclusions have been drawn from the ground up, in this instance from core analysis results and well logs to structural and stratigraphic analyses using high definition three-dimensional seismic data. The study was highly exploratory, further study that builds upon these insights is recommended.

In this concluding chapter, the key findings and major insights from the study and the contribution that it makes to the current understanding of hydrocarbon entrapment in the basin are summarized. The chapter also discusses the limitations of the study and concludes with a discussion of the important directions for future work in the basin.

6.2. SUMMARY

Before the specific technical implications are summarized, below are the main conclusions that have emerged from the current study for the faults analysed.

- The parameter and property models constructed in this study are geologically sound, internally consistent, and generally fit all the known well and core data in the area. They enabled the determination of the likely seal characteristics of the faults within the main reservoir interval in the southern Pletmos Basin where fault seal is a critical prospect

risk. The fault seal analysis provided a basis for the risking of future prospects in the area.

- Initial in-place fault seal integrity was excellent; this was given by a combination of favourable across-fault juxtaposition of sand against an impermeable lithology and/or adequately well-developed shale gouge over likely leak points to retain significant hydrocarbon columns. Moreover, both sand-sand juxtaposition risk and leak by fault-rock properties tend to have a certain degree of covariance (i.e. both decrease with decreasing sand in an interval).
- Despite the initial development of good fault seal integrity, the permeability indicates that there may be open and permeable fracture networks within the fault zone.
- The situation is exacerbated by low threshold pressures and calculated hydrocarbon column heights. The results suggest that the predicted hydrocarbon columns are too small for the retention of significant hydrocarbon volumes at present-day. It is therefore possible that the predicted column heights explain the ubiquity of residual hydrocarbon shows in the syn-rift sands as observed at well Ga-Q1. Likewise, the computed threshold pressures are also in accordance with low lateral capillary sealing capacity.

6.3. IMPLICATIONS FOR HYDROCARBON ENTRAPMENT

Though the extant literature leads to the conclusion that charge is clearly adequate in the area as similar tilted fault blocks (e.g. Ga-A gas field) are known to have been filled with commercial volumes of gas that migrated from the same source areas, this study has revealed that it is very likely that there has been post-charge breach of fault seal of the Ga-K and Ga-Q fault-related traps. As revealed in Chapter 2, Davies (1997) and Roux and Davids (2009) suggested two phases of charge: primarily in the Palaeocene (~60 – 50Ma) and the Late Plio-Pleistocene (0 – 10Ma). Hence post-charge seal breach can be considered likely to have occurred within the last ~50Ma which may have led to remigration of previously trapped hydrocarbons towards the Ga-A area. Perhaps this was instigated during the recent (~10Ma) uplift as indicated in Chapter 2 possibly resulting in fault reactivation and the subsequent weakening of the fault seal integrity. This is in accordance with results from geochemical analyses and petroleum systems modelling by Roux and Davids (2009) (Chapter 2).

In conclusion, not only did this study call into question the fault seal potential, it also pointed out the importance of the assessment of fault seal capacity. Thus, to answer the research questions posed in the first chapter, it can be said that initially the faults were barriers to fluid

flow. While this is true, they are hereby construed to have a low trap integrity at present-day with fault-dependent leak points predominantly concentrated on the upper parts of the interval of interest as indicated by the predicted fault parameters (Fig. 4-10; Section 4.4.1.). Based on the low computed ECFT and ECFP, the analysed faults may exhibit dynamic sealing behaviours during hydrocarbon production; however, since these two parameters are relatively unconstrained in the present study due to limited data, caution should be taken not to overinterpret the results. Given that the analyses of ECFT and ECFP in this study are not exhaustive for production-related fault seal analyses, it is therefore suggested that other studies should use dynamic simulation models to test out these parameters and to draw out additional insights into this conclusion.

Nonetheless, this work has taken this research area as far as it can be taken without access to more fault-seal calibration datasets. Therefore, the above conclusions provide considerable insights on the current sealing properties of the major prospect-bounding faults in the basin. Thus, regardless of the petrophysical property distribution within the syn-rift interval, fault seal failure did contribute to the failed exploration efforts in the study area. Therefore, this study brings to the fore information that does not warrant further exploration of the Ga-K prospect.

6.4. LIMITATIONS AND UNCERTAINTY

Despite the best efforts to minimise all limitations that might ensue, there were certain constrains within which the research was completed. These are discussed below;

Considering the stratigraphic uncertainty in the field due to poor seismic resolution of the reservoir zones in the interval of interest, the existence of interbedded shales and the limited wells completed in the interval, there is significant uncertainty in the computed stratigraphic juxtapositions across the faults, especially away from well control. In these cases, what may give the impression of a shale smear seal may in fact be a juxtaposition seal of reservoir against non-reservoir facies. Differences in cross-fault fluid characteristics would then not be attributed to the fault rock itself, but rather the presence of an impermeable lithology. Further, this study has modelled each fault as a single plane as there were no cored fault rocks available.

There is no criterion as to what level of uncertainty is tolerable, but fields with a moderate to high degree of uncertainty in the structural and/or stratigraphic models require that care be taken in making conclusive statements regarding fault seal.

6.5. FUTURE DIRECTIONS

The more precise the structural and stratigraphic models are for the study area, the higher the level of confidence one can place on the resulting juxtaposition and SGR results. If uncertainty in the model warrants for more than one probable set of stratigraphic juxtapositions across the modelled faults or more than one volume of shale property for individual units, the range of all likely scenarios should be explored to ascertain the effect of different models and to better quantify heterogeneity in the models. The degree of structural and stratigraphic uncertainty in the study area was found to be acceptable near well locations; hence the conclusions drawn herewith strictly present the implications of results for these zones. This subject can be investigated, and the analysis improved in the future when better-quality seismic data and additional well data are available to better constrain the geo-cellular models. This would necessitate that the new data offer undisputable evidence supporting one stratigraphic and structural model.

Moreover, the exact impact of the recent uplift on the sealing capacity of the faults is yet to be determined with certainty in the study area. So detailed petroleum systems analysis and the assessment of in-situ stress would assist in clarifying this issue.

7

Literature Cited

Allan, U.S., 1989, 'Model for hydrocarbon migration and entrapment within faulted structures', *American Association of Petroleum Geologists Bulletin*, **73**(7), 803-811.

Anggraini, J. and Puspa, M.A., 2008, 'Supervised and unsupervised neural networks technique in facies classification and interpretation', *Proceedings: Indonesian Petroleum Association,* Thirty-Second Annual Convention & Exhibition.

Bate, K.J. and Malan, J.A., 1992, 'Tectonostratigraphic evolution of the Algoa, Gamtoos and Pletmos Basins, offshore South Africa'. In: M.J. de Wit and I.G.D. Ransome (Eds.), 'Inversion Tectonics of the Cape Fold Belt, Karoo and Cretaceous Basins of Southern Africa'. *Balkema*, Rotterdam, 66-76.

Beaumont, E.A. and Foster, N.H., 1999, 'Exploring for Oil and Gas Traps', Treatise of Petroleum Geology, *Handbook of Petroleum Geology*.

Berg, R.R., 1975, 'Capillary pressures in stratigraphic traps', *American Association of Petroleum Geologists Bulletin*, **59**(6), 939-956.

Bolas, H.M., Hermanrund, C. and Teige, M.G., 2005, 'Seal capacity estimation from subsurface pore pressures', *Basin Research*, **17**, 583–599.

Bouvier, J.D., Kaarssijpesteijn, C. H., Kluesner, D. F., Onyejekwe, C. C. and Vanderpal, R. C., 1989, 'Three-dimensional seismic interpretation and fault sealing investigations, Nun River Field, Nigeria', *American Association of Petroleum Geologists Bulletin*, **73**(11), 1397-1414.

Bretan, P., Yielding, G. and Jones, H. 2003, 'Using calibrated shale gouge ratio to estimate hydrocarbon column heights', *American Association of Petroleum Geologists Bulletin*, **87**, 397–413.

Bridger, T., Leahy, G. and Kråkenes, T. 2013, 'Benefits operators expect from their reservoir models, creating the perfect reservoir model and how can it improve your decision-making', *Roxar Software Solutions*, a division of Emerson Process Management.

Brink, G.J., Brown, L.F., Jr. and Keenan, J.H.G., 1994, 'Deposition of fourth-order post-rift Lower Cretaceous sequences and sequence sets (Lower Valanginian to Mid-Aptian),

Pletmos Basin, southern Offshore, South Africa*'*. In: P. Weimer and H. Posamentier (Eds.), 'Siliciclastic Sequence Stratigraphy; Recent advances and applications'. *American Association of Petroleum Geologists Memoir*, **58**, 43-69.

Broad, D.S., Jungslager, E.H.A., Mclachlan, I.R. and Roux, J., 2006, 'Geology of the offshore Mesozoic Basins*'*. In: M. R. Johnson *et al.* (Eds.*)*, 'The geology of South Africa', *Geological Society of South Africa*, Pretoria, 553–571.

Brown, L.F., Jr., Benson, J.M., Brink, G.J., Doherty, S., Jollands, A., Jungslager, E.H.A., Keenan, J.H.G., Muntingh, A. and van Wyk, N.J.S., 1996, 'Sequence stratigraphy in offshore South African divergent basins: an atlas on exploration for Cretaceous lowstand traps by Soekor (Pty) Ltd*'*, *American Association of Petroleum Geologists Studies in Geology*, **41**, 184 p.

Caers, J., 2005, 'Petroleum Geostatistics', *Society of Petroleum Engineers*, Richardson, 96 p.

Castillo, D.A., Bishop, D.J. and de Ruig, M., 2002, 'Fault Seal Integrity in the Timor Sea Area: Prediction of trap failure using well-constrained stress tensors and fault surfaces interpreted from 3D seismic', *28th Annual Convention Proceedings*, **1**, 261-288.

Cerveny, K., Davies, R., Dudley, G., Fox, R., Kaufman, P., Knipe, R. J. and Krantz, B., 2004, 'Reducing uncertainty with Fault-Seal Analysis', *Oilfield Review*, **16**(4), 38-51.

Childs, C., Walsh, J. J., Manzocchi, T., Strand, J., Nicol, A., Tomasso, M., Schöpfer, M. P. J. and Aplin, A. C., 2007, 'Definition of a fault permeability predictor from outcrop studies of a faulted turbidite sequence, Taranaki, New Zealand', *Geological Society, London, Special Publications*, **292**(1), 235-258.

Clapp, F.G., 1929, 'The role of geologic structure in the accumulation of petroleum'. In: S. Powers, S. (Ed.), 'Structure of typical American oil fields II: Tulsa', *American Association of Petroleum Geologists*, 667–716.

Crawford, B.R., 1998, 'Experimental fault sealing: shear band permeability dependency on cataclastic fault gouge characteristics', *Geological Society*, London, Special Publications**,** **127**(1), 27–47.

Davies, C.P.N., 1997, 'Hydrocarbon evolution of the Bredasdorp Basin, Offshore South Africa: From source to reservoir' [PhD Thesis]: University of Stellenbosch, 286 p.

Deutsch, C.V., 2002, 'Geostatistical Reservoir Modeling', *Oxford University Press*, New York, 376 p.

Dingle, R.V., Siesser, W.G. and Newton, A.R., 1983, 'Mesozoic and Tertiary geology of Southern Africa', *A.A. Balkema*, Rotterdam, 375 p.

Fisher, Q.J. and Knipe, R.J., 1998, 'Fault sealing processes in siliciclastic sediments' *Geological Society*, London, Special Publications, **147**, 117-134.

Fisher, Q.J. and Knipe, R.J., 2001, 'The permeability of faults within siliciclastic petroleum reservoirs of the North Sea and Norwegian Continental Shelf', *Marine and Petroleum Geology*, **18**(10), 1063-1081.

Fisher, Q.J., Knipe, R.J. and Worden, R.H., 2009, 'Microstructures of deformed and non-deformed sandstones from the North Sea: Implications for the origins of quartz cement in sandstones'. In; Worden, R. H. and Morad, S. (Eds.), 'Quartz cementation in sandstones, *Blackwell Publishing Ltd*., Oxford, UK, **14**, 129-146.

Fossen, H., 2010, 'Structural geology', *Cambridge: Cambridge University Press*, 480 p.

Foxford, K.A., Walsh, J. J. and Watterson, J., 1998, 'Structure and content of the Moab Fault Zone, Utah, USA, and its implications for fault seal prediction'. In: Jones, G., Fisher, Q. J. & Knipe, R. J. (Eds.), 'Faulting, Fault Sealing and Fluid Flow in Hydrocarbon Reservoirs', *Geological Society*, London, Special Publications, **147**, 87-103.

Freeman, S.R., Harris, S.D. and Knipe, R.J., 2010, 'Cross-fault sealing, baffling and fluid flow in 3D geological models: tools for analysis, visualization and interpretation'. In: Jolley, S. J., Fisher, Q. J., Ainsworth, R. B., Vrolijk, P. J. & Delisle, S. J. (Eds.), 'Reservoir Compartmentalization', *Geological Society*, London, Special Publications, **347**, 257–282.

Fulljames, J.R., Zijerveld, L.J.J. and Franssen, R.C.M.W., 1997, 'Fault seal processes: systematic analysis of fault seals over geological and production time scales'. In: Møller-Pedersen, P., and Koestler, A. G. (Eds.), *Norwegian Petroleum Society Special Publications*, **7**, 51-59.

Gomes, J.S., Ribeiro, M.T., El Deeb, M., Silva, F.P. and Bockel-Rebelle, R.F., 2004, 'Lessons learned from Static Reservoir Modelling on Complex Carbonate Fields, Onshore UAE', SPE 88780, Presented at the 11th Abu Dhabi International Petroleum Exhibition and Conference held in in Abu Dhabi, U.A.E, 10-13 October, 2004.

Goutorbe, B., Lucazeau, F. and Bonneville, A., 2008, 'The thermal regime of South African continental margins', *Earth Planet, Science Letters*, **267**, 256–265.

Handin, J., Hager Jr, R.V., Friedman, M. and Feather, J.N., 1963, 'Experimental deformation of sedimentary rocks under confining pressure: pore pressure tests', *American Association of Petroleum Geologists Bulletin*, **47**(5), 717-755.

Hock, T.C. and Schulte, L., 2012, 'Fault seal prediction and uncertainty estimation of a water wet fault', Presented at the AAPG International Convention and Exhibition, Singapore, 16-19 September, 2012.

Hull, J., 1988, 'Thickness-displacement relationships for deformation zone', *Journal of Structural Geology*, **10**, 431-435.

Haq, B.U., Hardenbol, J. and Vail, P.R., 1988, 'Mesozoic and Cenozoic chronostratigraphy and eustatic cycles of sea level change'. In: Wilgus, C.K. *et al.* (Eds.), 'Sea Level Change:

An Integrated Approach', *Special Publication Society of Economic Palaeontologists and Mineralogists*, **42**, 71 - 108.

IHS Basin Monitor, 2010, 'International Exploration & Production Database, Outeniqua Basin, South Africa', viewed 20 October 2016 from https://www.ihs.com/products/oil-gas-basin-monitors.html.

International Union of Geological Sciences (IUGS), 2015, 'The International Chronostratigraphic Chart, viewed 13 June 2016 from http://www.stratigraphy.org/index.php/ics-chart-timescale.

Jolley, S.J., Dijk, H., Lamens, J.H., Fisher, Q.J., Manzocchi, T., Eikmans, H. and Huang, Y., 2007, 'Faulting and fault sealing in production simulation models: Brent Province, northern North Sea', *Petroleum Geoscience*, **13**(4), 321-340.

Jolley, S.J., Fisher, Q.J. and Ainsworth, R.B., 2010, 'Reservoir Compartmentalization: An introduction'. In; Jolley, S. J., Fisher, Q. J., Ainsworth, R. B., Vrolijk, P. J. & Delisle, S. D. (Eds.), 'Reservoir Compartmentalization', *Geological Society*, London, Special Publications, **347,** 1-8.

Jungslager, E.H.A., 1999, 'Petroleum habitats of the Atlantic margin of South Africa', *Geological Society*, London, Special Publications, **153**, 153-168.

Knai, T.A. and Knipe, R.J., 1998, 'The impact of faults on fluid flow in the Heidrun Field', *Geological Society*, London, Special Publications, **147**(1), 269-282.

Knipe, R.J., 1992a, 'Faulting processes and fault seal'. In: Larsen, R. M., Brekke, H., Larsen, B. T., and Talleraas, E. (Eds.), *Norwegian Petroleum Society Special Publications*, **1**, 325-342.

Knipe, R.J., 1992b, 'Faulting processes, seal evolution, and reservoir discontinuities: An integrated analysis of the ULA Field, Central Graben, North Sea', Abstracts of the Petroleum Group meeting on collaborative research programme in petroleum geoscience between UK Higher Education Institutes and the Petroleum Industry, *Geological Society*, London, Special Publications.

Knipe, R.J., 1997, 'Juxtaposition and seal diagrams to help analyze fault seals in hydrocarbon reservoirs', *American Association of Petroleum Geologists Bulletin*, **81**(2), 187-195.

Knipe, R.J., Fisher, R.J., Jones, G., Clennell, M.R., Farmer, A.B., Harrison, A., Kidd, B., McAllister, E.R.P.J. and White, E.A., 1997, 'Fault seal analysis: successful methodologies, application and future directions', *Norwegian Petroleum Society Special Publications*, **7**, 15-40.

Knipe, R.J., Jones, G., and Fisher, Q.J., 1998, 'Faulting, fault sealing and fluid flow in hydrocarbon reservoirs: an introduction', *Geological Society*, London, Special Publications, **147**(1), vii-xxi.

Knott, S.D., 1993, 'Fault seal analysis in the North-Sea', *American Association of Petroleum Geologists Bulletin*, **77**(5), 778-792.

Knott, S.D., Beach, A., Brockbank, P.J., Lawson Brown, J., McCallum, J.E. and Welbon, A.I., 1996, 'Spatial and mechanical controls on normal fault populations', *Journal of Structural Geology*, **18**, 359-372.

Lindsay, N.G., Murphy, F.C., Walsh, J.J. and Watterson, J., 1993, 'Outcrop studies of shale smears on fault surface, the geological modelling of hydrocarbon reservoirs and outcrop analogues, *Blackwell Publishing Ltd*., 113-123.

Maier, J.J., 1990, 'The complexities of the sedimentary and reservoir models in the Superior structure, Abstract: Geocongress 90, *Geological Society of South Africa*, 69-72.

Manzocchi, T., Walsh, J.J., Nell, P. and Yielding, G., 1999, 'Fault transmissibility multipliers for flow simulation models', *Petroleum Geoscience*, **5**, 53-63.

Manzocchi, T., Childs, C. and Walsh, J.J. 2010, 'Faults and fault properties in hydrocarbon flow models', *Geofluids*, **10**, 94–113.

McKenzie D., 1978, 'Some remarks on the development of sedimentary basins', *Earth and Planetary Science Letters*, **40**, 25–32.

Mcleannan, J.A. and Deutsch, C.V, 2006, 'Best practice reservoir characterization for the Alberta oil sands', Paper 2006-096, Presented at the Petroleum Society's 7th Canadian international Petroleum Conference (57th Annual Technical Meeting), Calgary, Alberta, Canada, June 13-15.

McMillan, I.K., Brink, G.J., Broad, D.S. and Maier, J.J., 1997, 'Late Mesozoic sedimentary basins off the South Coast of South Africa'. In: Selly, R.C. (Ed.), African Basins: Sedimentary Basins of the World, *Elsevier*, Amsterdam, 319–376.

Ottesen Ellevset, S., Knipe, R.J., Svava Olsen, T., Fisher, Q. J. and Jones, G., 1998, 'Fault controlled communication in the Sleipner Vest Field, Norwegian Continental Shelf; detailed, quantitative input for reservoir simulation and well planning', *Geological Society*, London, Special Publications, **147**(1), 283-297.

Sneider, R.M., Sneider, J.S., Bolger, G.W. and Neasham, J.W., 1997, 'Comparison of seal capacity determinations: conventional cores vs. cuttings', *American Association of Petroleum Geologists Memoirs*, **67**, 1-12.

Sperrevik, S., Gillespie, P.A., Fisher, Q.J., Halvorsen, T. and Knipe, R.J. 2002, 'Empirical estimation of fault rock properties. In: Koestler, A. G. & Hunsdale, R. (Eds.), 'Hydrocarbon Seal Quantification', *Norwegian Petroleum Society*, Special Publication, Elsevier, Singapore, **11**, 109–125.

Pei, Y., Paton, D., Knipe, R. and Wu, K., 2015, 'A Review of fault sealing behaviour and its evaluation in siliciclastic rocks', *Earth-Science Reviews*, **150**, 121-138.

Porter, J.R., Knipe, R.J., Fisher, Q.J., Farmer, A.B., Allin, N.S., Jones, L.S., Palfrey, A.J., Garrett S.W. and Lewis G., 2000, 'Deformation processes in the Britannia Field, UKCS', *Petroleum Geoscience*, **6**, 241-254.

Robertson, E.C.,1983, 'Relationship of fault displacement to gouge and breccia thickness', *American Institute of Mining Engineers Transactions*, **274**, 1426-1432.

Roux, J., 1997, 'Exploration and production: potential outlined in southern Outeniqua Basin offshore South Africa, Soekor (Pty) Ltd., *Oil and Gas Journal*, July 21.

Roux, J. and Davids, A., 2009, 'Barremian basin floor fan complex: an untested gas play within the Northern Pletmos Basin'. In: *AAPG International Conference and Exhibition*, Rio de Janeiro, Brazil, 2009, AAPG Search and Discover Article # 10234.

Rushing, J., Newsham, K., Lasswell, P., Cox, J., Blasingame, T., 2004, 'Klinkenberg-corrected permeability measurements in tight gas sands: steady-state versus unsteady-state techniques', *SPE Annual Technical Conference and Exhibition*, SPE 89867.

Schowalter, T.T., 1979, 'Mechanics of secondary hydrocarbon migration and entrapment', *American Association of Petroleum Geologists Bulletin*, **63**(5), 723-760.

Scott, T.E. and Nielsen, K.C., 1991, 'The effects of porosity on the brittle-ductile transition in sandstones', *Journal of Geophysical Research*, **96**(B1), 405-414.

Van Der Merwe, R. and Fouché J., 1992, 'Inversion tectonics in the Bredasdorp Basin, offshore South Africa'. In: De Wit, M.J. and Ransome, I.G.D. (Eds.), 'Inversion tectonics of the Cape Fold Belt, Karoo and Cretaceous basins of Southern Africa', *Balkema*, Rotterdam, 49 -59.

Viljoen, J.H.A., Stapelberg, F.D.J. and Cloete, M. 2010, 'Technical report on the geological storage of Carbon Dioxide in South Africa', *Council for Geoscience*, Pretoria, pp. 238.

Walderhaug, O., 1996, 'Kinetic modelling of quartz cementation and porosity loss in deeply buried sandstone reservoirs', *American Association of Petroleum Geologists Bulletin*, **80**(5), 731-745.

Walsh, J.J., Watterson, J., Heath, A.E. and Childs, C. 1998, 'Representation and scaling of faults in fluid flow models', *Petroleum Geoscience*, **4**, 241–251.

Watts, N.L., 1987, 'Theoretical aspects of cap-rock and fault seals for single and two-phase hydrocarbon columns', *Marine and Petroleum Geology*, **4**(4), 274-307.

Wiprut, D.J. and Zoback, M.D., 2000, 'Fault reactivation and fluid flow along a previously dormant normal fault in the northern North Sea', *Geology*, **28**(7), 595-598.

Wygrala, B.P., 1989, 'Integrated study of an oil field in the southern Po Basin, Northern Italy' [PhD thesis]: University of Cologne, Germany.

Yielding, G., Freeman, B. and Needham, D.T., 1997, 'Quantitative fault seal prediction', *American Association of Petroleum Geologists Bulletin*, **81** (6), 897-917.

APPENDICES

APPENDIX A: WELL DATA

Table A1: General well information

Well Name	*Ga-A4*	*Ga-E1*	*Ga-E2*	*Ga-H1*	*Ga-Q1*
Well Type	Appraisal	Exploration (Wildcat)	Appraisal	Exploration (Wildcat)	Exploration (Wildcat)
Latitude	$34^0$33’36.07” S	$34^0$42’03.13” S	$34^0$41’13.55” S	$34^0$31’03.96” S	$34^0$37’11.50” S
Longitude	$23^0$43’17.05” E	$23^0$49’56.60” E	$23^0$46’06.74” E	$23^0$45’46.13” E	$23^0$46’52.90” E
Water Depth	118.5 m	130.5 m	126.8 m	120 m	124 m
KB Elevation	26 m	30 m	30 m	26 m	26 m
KB - SL	144.5 m	160.5 m	156.8 m	146 m	150 m
TD	2302 m	2898 m	4396 m	3575 m	3243 m
Final Status	Potential commercial gas well	Dry well with gas shows	Dry well with gas shows	Non-commercial gas rates	Dry well with gas shows
	Temporally Suspended	Plugged and Abandoned	Plugged and Abandoned	Plugged and Abandoned	Plugged and Abandoned

Figure A1: Establishing the stratigraphy and paleo-environment conditions using the two wells that best represent the complete stratigraphic succession

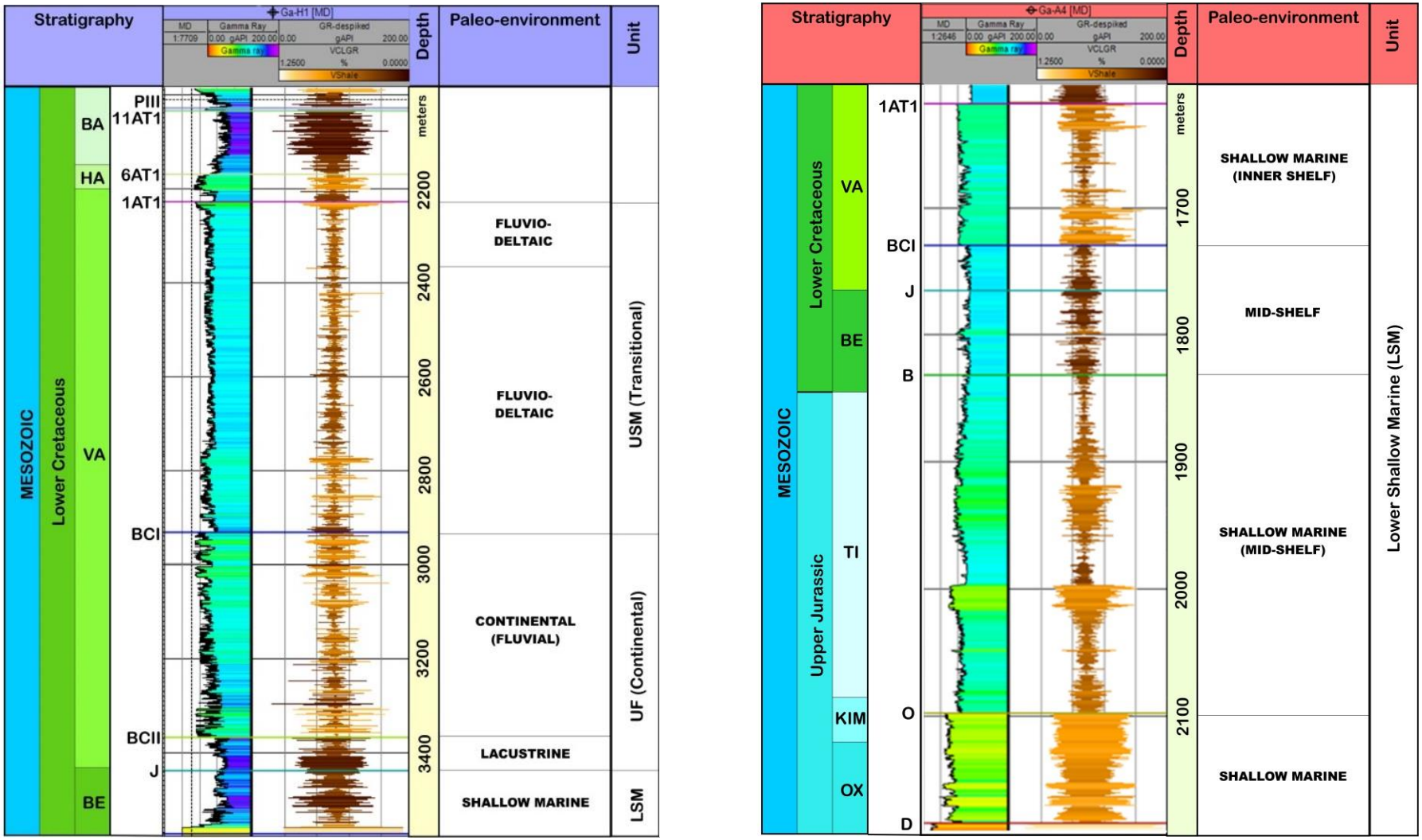

Figure A2: Regional structural well correlation

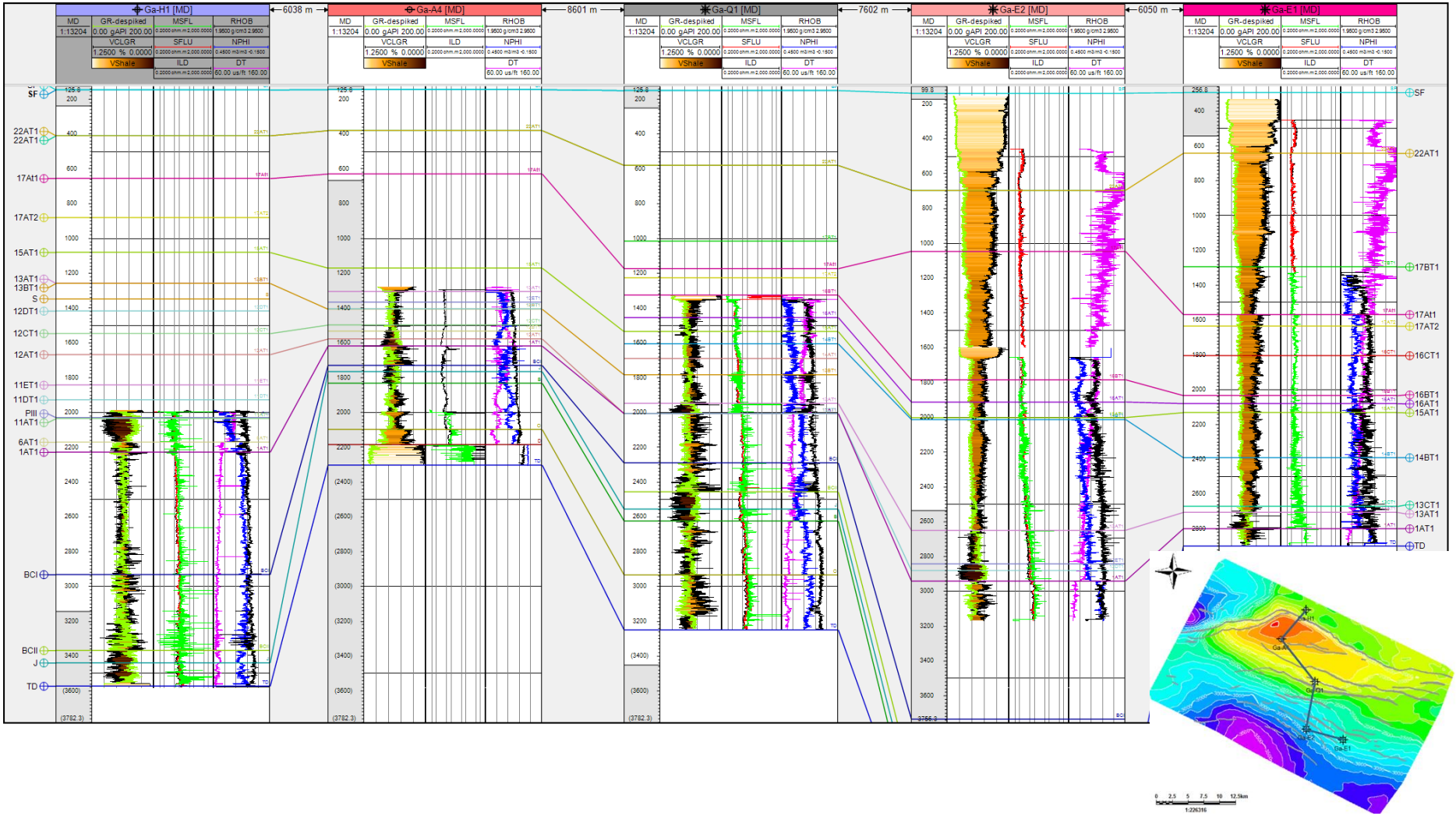

Figure A3: Regional chronostratigraphic correlation (flattened at 1At1)

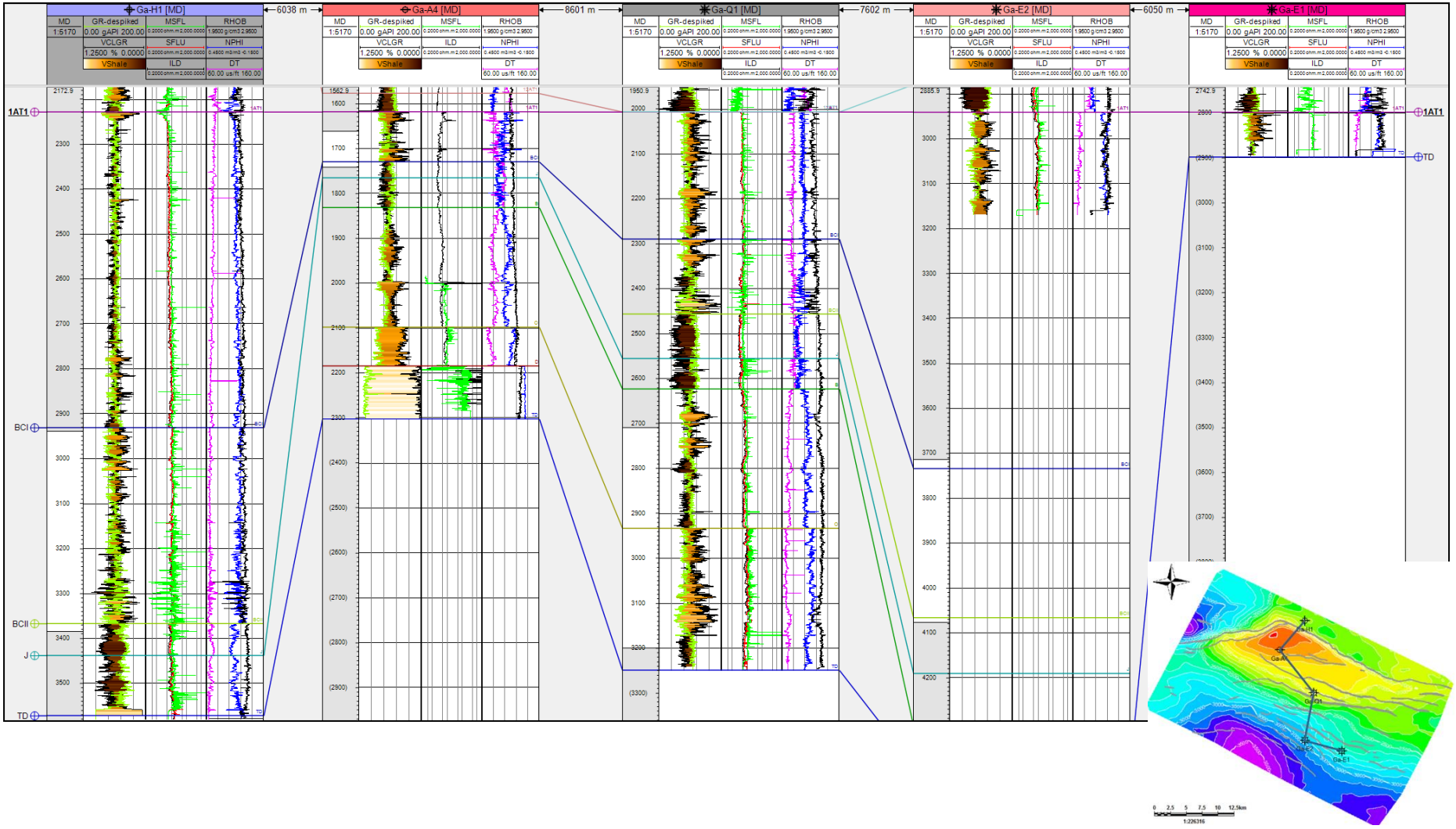

APPENDIX B: DOMAIN CONVERSION

Figure B1: a) The resultant Time-Depth Relationship (TDR) curve from the synthetic generation process and a) the advanced velocity modelling process utilized in the study

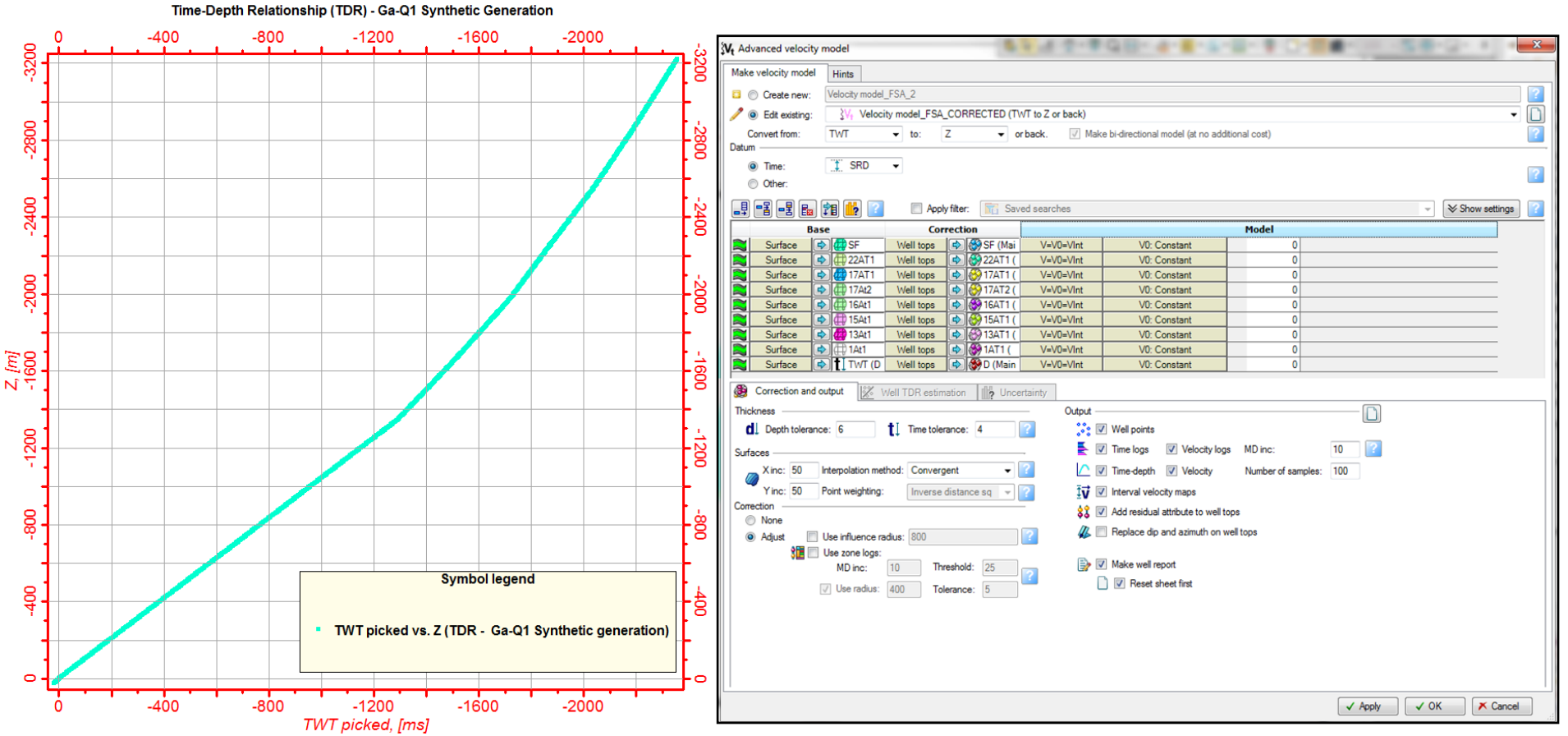

APPENDIX C: JUXTAPOSITION TRIANGLE

Figure C1: Meaning of the different colours of the juxtaposition triangle